# Wind Engineering and Dispersion

## Contents



Other posts with a Wind Engineering and Dispersion connection can be found in the Train Aerodynamics collation.

# Crop lodging

January 24, 2020

In this blog post I want to introduce the work that I, together with a number of colleagues, are carrying out on the phenomenon known as crop lodging. First I guess it is actually necessary to define what the word "lodging" means. In simple terms, lodging is the failure of crops due to stem breakage or uprooting during periods of high winds and/ or heavy rainfall. I need to make the point very firmly right at the start that it has got absolutely nothing at all to do with crop circles! It does however have significant economic consequences, with yield losses in winter wheat resulting in costs to growers of the order of £100m in the UK in a high lodging season. Some pictures of lodging are given in figure 1 below.

**Figure 1. Lodging in cereal crops**

Our work on this issue goes back in one form or another over a period of 30 years. It all began in in 1987 when I was an academic at the University of Nottingham. After the Great Storm of that year wreaked havoc with the tree stock in the south of the country, I still remember a colleague (Andrew Dawson) putting his head around the door of my office and saying "I have an idea for a research grant….". This led to a grant from the Science Research Council to investigate the

aerodynamics of urban trees – and we thoroughly enjoyed ourselves making measurements of the mechanical and aerodynamic properties of trees on and around the University campus, evolving an experimental technique that we named tree-twanging – pulling trees with a winch and then releasing them to measure the frequency of the oscillations. One of the less successful parts of that work was the initial development of a mechanical model of trees in high winds, which tried to represent trees in engineering terms. At the time this didn't progress very far, but a few years later, in the early 1990s, I was approached by a colleague from the University School of Agriculture at the Sutton Bonnington Campus (Prof. Keith Scott) to help with a project that was investigating the lodging of winter wheat, and in particular to help supervise the PhD research of two students – John Griffin and Pete Berry. Perhaps the most challenging part of this work, both for me and staff and students at Sutton Bonnington was the need to learn to speak the vocabulary of anther discipline. This collaboration led to me doing some serious work on analytical model development that produced a reasonably robust description of the mechanical behavior of plants, and in particular winter wheat, in high winds and heavy rainfall.

The next phase of this work began in 1998, when we (myself and colleagues at Sutton Bonnington and ADAS) obtained a grant from the Biology and Biotechology Research Council (BBSRC) to investigate lodging of winter wheat in some detail, to identify those plant characteristics that resulted in an increase in lodging risk. This date also coincided with my move from Nottingham to the University of Birmingham. This work involved an extensive series of field trials at ADAS to measure characteristics of plants relevant to the lodging process, and we at Birmingham were responsible for developing a model of the lodging process and for carrying out experiments to calibrate the model. By this time (Dr.) Pete Berry was working for ADAS, so the collaboration with him thus continued. The Research Fellow appointed at Birmingham for this work was Dr. Mark Sterling, who had recently graduated from there with a PhD in open channel flow. We built the lodging model on the basis of the earlier modeling work, but needed a variety of aerodynamic information to calibrate this. Normally in engineering terms, this would have been obtained through wind tunnel tests – it is however not easy to put a representative section of a wheat field into a wind tunnel. The solution was to take a wind tunnel into the field – see the picture below. This proved to be more than a little challenging, but during the course of the experiments we were able to obtain the very first video footage of lodging actually taking place – this usually occurs in high winds and heavy rain and more often than not in the middle of the night, so the use of a portable wind tunnel, difficult as it was, was actually the most straightforward way of doing this. I am told by Mark that fixing strain gauges to wheat stems in the field to measure the displacement was one of the most entertaining tasks that he has ever been faced with.

Overall the project was very successful and enabled us to learn a great deal about the mechanics of root and stem lodging, to provide solid scientific information that cut through much of the hearsay that was around in the industry at the time about lodging, and to provide

robust agronomical advice for farmers for techniques to avoid lodging. The collaboration between the University and ADAS was vital in this regard.

Over the next few years, work continued at a lower level, with the production of a few collaborative review papers, and the application of the lodging model to barley. However by the start of the current decade it was becoming clear that the model as it stood, whilst perfectly acceptable for wheat crops where the plants were essentially isolated throughout the growing season, was not really applicable to a range of crops for which, late in their growing season, individual plants interlocked to produce a much denser canopy. Thus we (myself, Pete Berry and Mark Sterling, by now the Head of Civil Engineering at Birmingham and thus my boss) began work on the development of a generalized lodging model that could allow for plant interlocking. Whilst the modeling was quite complex, it resulted in the relatively simple pictorial representation shown below in figure 2, where regions of stem lodging and root lodging were defined in terms of the daily rainfall rate and the hourly wind speed. The various velocities and rainfalls shown on this figure are all (rather complex) functions of plant and soil parameters and can, once the model is calibrated, be fairly easily specified. In principle this graph can be used with a representation of wind and rainfall probabilities to determine the risk of lodging occurring for any set of plant and soil parameters, and mitigation methods taken if this risk is deemed to be too high. In the peer review process, one of the reviewers of the paper acknowledged the elegance of the model, but made the comment that it would never find a practical outcome. We were to prove him wrong!

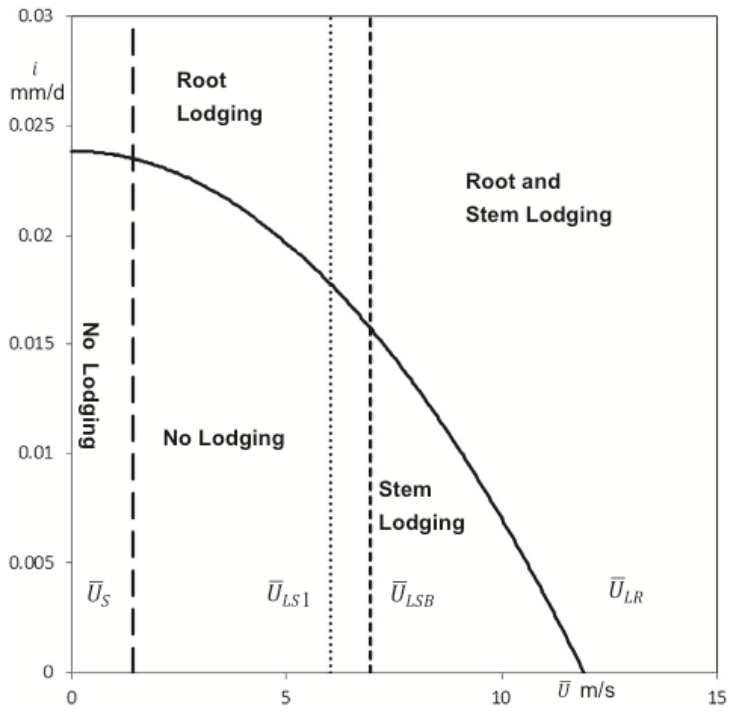


**Figure 2. Lodging regions in the rainfall / windspeed plane**

Over the last few years the work on lodging has grown very significantly, and we now have three projects underway. The first was funded by Teagasc in Ireland, to investigate methods to

reduce oat lodging. We used the model described above and the work included a series of experiments in Ireland to measure, the behaviour of oats in high winds.. The second project was funded by BBSRC under the SARIC (Sustainable Agriculture Research and Innovation Club) scheme, with myself and Mark, working again with Pete at ADAS. This used the same set of techniques to investigate the lodging of Oil Seed Rape. The unique aspect of this project however was a collaboration with Dr. Alan Blackburn and his colleagues at the University of Lancaster who are experts in Earth Observation and Remote Sensing, and the local modeling of lodging is being embedded in a much wider scheme to integrate spatial, topographic and meteorological data sets to predict the risk of lodging for individual crops and fields, and to identify those soil, plant and weather characteristics that cause lodging. The final project was also funded by BBSRC, but this time through the Global Challenges Research Fund which directs research funds to the problems of developing countries. We used a similar approach to the SARIC project, but this time directed towards maize and rice, working again with ADAS and Lancaster University, and also with colleagues at the Chinese Agricultural University and with CIMYTT in Mexico, who work in a large range of countries in the developing world. The potential significance of this project is huge – lodging causes yield losses of up to 40% in rice and maize, reduces grain quality, increases time to harvest, increases grain drying costs and increases health damaging micro-organisms on grain. It is estimated that lodging in rice and maize reduces crop production in China and Mexico alone by $1500 million per year.

All this research has all developed from a chance conversation and some early blue-sky research on trees over 30 years ago – and now has the possibility of producing results that will have a major effect on crop productivity around the world. In these days when funding for such fundamental research is under increasing pressure, this is perhaps worth remembering. But for now, these are exciting times – watch this space for future updates.

# Specifying accident windspeed risk

March 9, 2020

*This post is intended to start a discussion – and ideally identify what data might be available to address this problem further. The analysis presented is preliminary in nature, and could almost certainly be refined. I would really value a discussion of this with colleagues who read it.*

**Accident risk**

In studies of road and rail vehicles in cross winds, some estimate of the risk of an accident is often required. If the critical accident wind speed for a particular vehicle is known, then my approach in the past has been to use the probability distribution for the hourly mean wind speed (assumed to be a Weibull distribution) and the probability distribution for the turbulence fluctuations around this average (assumed to be a normal distribution) to calculate the percentage of time that this critical value is exceeded, through a convolution of the two distributions. Additionally, when wind-warning systems are being developed, the question often arises as to what would be an appropriate mean wind speed at which to limit vehicle movements. This can be derived by calculating the percentage of time that the critical wind speed is exceeded from the probability distributions for turbulence fluctuations, for a range of mean wind speeds, and then choosing a value that has an acceptable level of risk.

In some recent work that I have carried out for a particular client, it has become clear to me that this approach is not really adequate – an example of practical reality not always conforming with attractive theoretical approaches! Both road and rail vehicles require a gust to be above the critical value *for a specific period of time* before an accident occurs. This period of time is usually between 0.5s and 3s, the time it takes for a vehicle to actually blow over. Thus in determining the risk of an accident what is really required is some idea of the number of times the critical wind speed is exceeded, $N$, for more than (say) $T$ seconds for a particular mean wind speed $U$. This is not the same as the proportion of time for which the critical wind speed is exceeded, as some these exceedances will often last for less than $T$ seconds. If the probability of $N$ for any particular $U$ is known, then this can be convoluted with the probability distribution for $U$ to calculate the overall risk, or used to determine an appropriate value of $U$ for wind warning systems.

To the best of my knowledge, the specification of the number of gusts $N$ lasting greater than a specific time $T$ for a particular mean wind speed has not been investigated in the past – but if any reader knows of such work, I would be glad to hear of it. In this post, I present the results of a preliminary investigation into this problem.

**The data**

In what follows, I will use two experimental wind datasets as follows.

- Data from that late 1990s obtained at the Wind Engineering field site at Silsoe Research Institute, and in particular two one-hour datasets (Silsoe 1 and Silsoe 2) with wind velocities measured at 10Hz at 3, 6 and 10m above the ground, for 10m wind speeds of 9.7 and 10.5m/s.
- Data from Storm Ophelia in 2017, obtained from measurements at the top of the Muirhead Tower at the University of Birmingham, 72m above the ground, measured at 10Hz, for mean hourly wind speeds of 10.4, 12.5 and 13.8m/s (Birmingham 1, Birmingham 2 and Birmingham 3). *With thanks to Dr Mike Jesson of the University of Birmingham for making this data available*

The basic statistics for each hour of data is given in table 1.

| Location | Dataset | Mean velocity m/s | Standard deviation of velocity (m/s) | Turbulence intensity | Skew of probability distribution | Surface roughness length (m) |
|---|---|---|---|---|---|---|
| Silsoe Research Institute | Silsoe 1 3m | 8.32 | 1.75 | 0.210 | 0.378 | 0.0052 |
| | Silsoe 1 6m | 9.09 | 1.79 | 0.199 | 0.393 | |
| | Silsoe 1 10m | 9.68 | 1.82 | 0.188 | 0.385 | |
| | Silsoe 2 3m | 9.00 | 1.84 | 0.203 | 0.292 | 0.0057 |
| | Silsoe 2 6m | 9.90 | 1.84 | 0.185 | 0.350 | |
| | Silsoe 2 10m | 10.53 | 1.88 | 0.178 | 0.356 | |
| University of Birmingham | Birmingham 1 72m | 10.36 | 2.13 | 0.205 | -0.14 | - |
| | Birmingham 2 72m | 12.54 | 3.02 | 0.240 | -0.07 | |
| | Birmingham 3 72m | 13.84 | 3.31 | 0.239 | 0.06 | |

**Table 1. Wind characteristics**

From this table it can be seen that the Silsoe site has a surface roughness length (determined from velocity profiles) typical of smooth rural environments (0.005m), with turbulence intensities (standard deviation / mean values) that are consistent with such an environment and which fall slightly with height. The Birmingham data was obtained at one point high above a suburban environments, and thus the surface roughness length cannot be determined from a velocity profile, but can be expected to be an order of magnitude or more higher than at the

Silsoe site. The turbulence intensity is similar to that measured at Silsoe, although the measurements were made at a much greater height above the ground. For the Silsoe data the probability distributions of the data all show a positive skew, whilst the Birmingham data show both positive and negative skew values that are much closer to zero. Typical examples of such distributions are shown in figure 1. The Silsoe near-ground distribution has a significantly longer upper tail, than the Birmingham values high above the ground, i.e. a significant skew towards the higher velocities. This may well be because of individual sweep events in the atmospheric boundary layer being more significant near to ground level. The normal distribution, which I have assumed in the past for my calculations, does not fit either dataset particularly well.

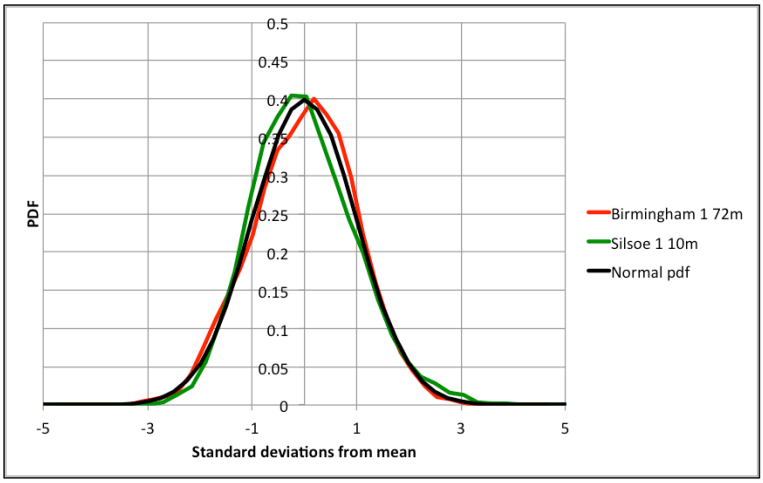


**Figure 1 Wind Probability distribution**

**Analysis of exceedances**

The approach to using this data has been to find, for each dataset, the number of exceedances *N* for *T*= 0.5s, 1s and 3s gusts above a range of velocity levels above the mean. To enable comparison between the different datasets, these velocities are expressed in terms of standard deviations above the mean, denoted by *X*. The results are shown in figure 2 for the Silsoe data and figure 3 for the University of Birmingham data. The following comments can be made.

- *N* falls as *T* increases, which is only to be expected.
- The value of *X* at which *N* falls to zero falls as *T* increases, as again is to be expected. This value is around 3 to 3.5 for the Silsoe data, and 2.5 to 3 for the Birmingham data, reflecting the form of the tail of the probability distributions discussed above.
- For the Silsoe data, the results for the two datasets are very similar and there is an indication that *N* varies with height above the ground.
- The Birmingham datasets also have similar results, and there is no discernible effect of wind speed in the data when plotted in this way.

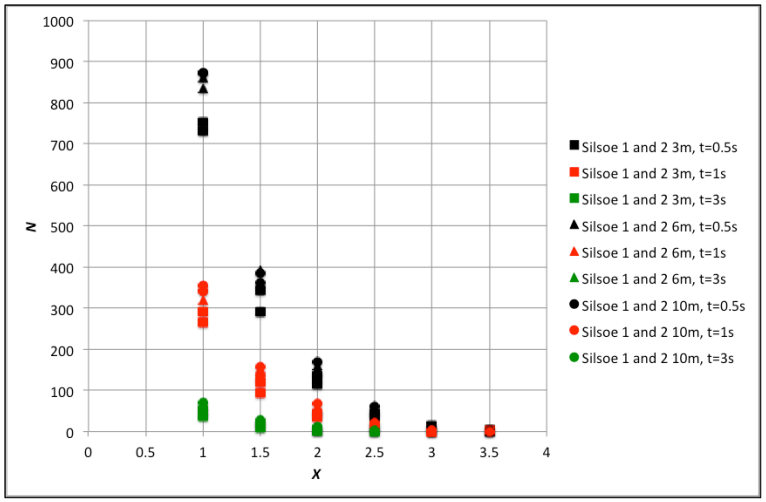


**Figure 2 Number of exceedances (Silsoe data)**

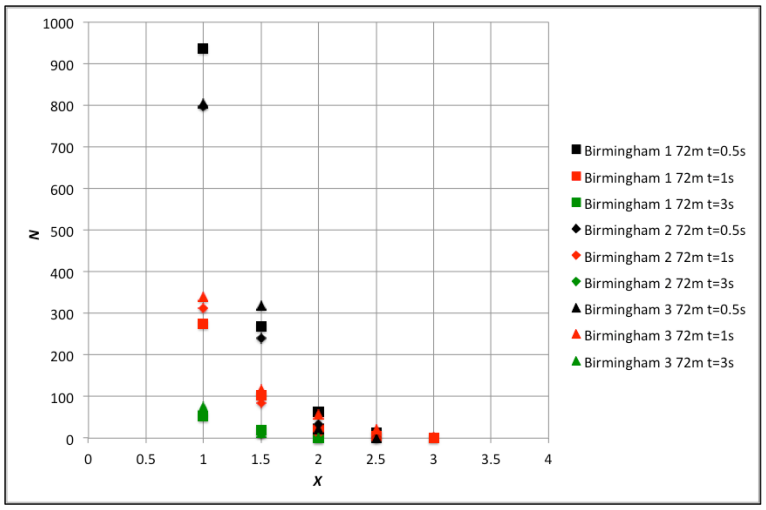


**Figure 3 Number of exceedances (Birmingham data)**

Clearly the distributions of $N$ have an upper limit. This can be characterized in two ways.

- By the value of $X$ for which the probability of the wind speed exceed $T/3600$, $X_1$
- By the highest value of $X$ for which $N>0$, $X_2$

Both these values of $X$ are shown in table 2 for the various datasets. It can be seen that there is some variability in the results, which is inevitable as we are dealing with the tails of the distribution where data becomes discontinuous. In general the values for $X_1$ are higher than those for $X_2$, particularly for the near ground Silsoe data, suggesting that the use of simple probabilities rather than gust numbers may well significantly overestimate vehicle overturning risk. Both values fall as the time period $T$ increases as would be expected, and the values for the Silsoe data are significantly higher than for the Birmingham data, which again follows from the difference in probability distributions. The equivalent values for $X_1$ for a normal probability distribution are 3.64, 3.45 and 3.14, for $T$= 0.5, 1 and 3s respectively. It can thus be seen from

Table 2 that the Silsoe values lie above the normal distribution values, and the Birmingham values lie significantly below them.

| Dataset | Data Item | $X_1$ | | | $X_2$ | | |
|---|---|---|---|---|---|---|---|
| | | $T$=0.5s | $T$=1s | $T$=3s | $T$=0.5s | $T$=1s | $T$=3s |
| Silsoe Research Institute | Silsoe 1 3m | 4.33 | 4.08 | 3.63 | 3.9 | 3.8 | 2.9 |
| | Silsoe 1 6m | 4.19 | 3.82 | 3.52 | 3.6 | 3.1 | 2.8 |
| | Silsoe 1 10m | 4.05 | 3.97 | 3.56 | 3.9 | 3.7 | 2.6 |
| | Silsoe 2 3m | 3.95 | 3.78 | 3.41 | 3.3 | 3.2 | 2.4 |
| | Silsoe 2 6m | 3.66 | 3.55 | 3.23 | 3.5 | 3.4 | 2.4 |
| | Silsoe 2 10m | 3.58 | 3.49 | 3.36 | 3.5 | 3.2 | 2.6 |
| | | 4.1 | 3.9 | 3.5 | 3.8 | 3.3 | 2.6 |
| University of Birmingham | Birmingham 1 60m | 2.91 | 2.78 | 2.44 | 2.9 | 2.8 | 2.4 |
| | Birmingham 2 60m | 2.69 | 2.56 | 2.27 | 2.7 | 2.5 | 1.7 |
| | Birmingham 3 60m | 2.86 | 2.76 | 2.46 | 2.7 | 2.7 | 2.1 |
| Average | | 2.82 | 2.7 | 2.39 | 2.77 | 2.67 | 2.07 |

**Table 2. Upper limits of X**

The data from figures 2 and 3 thus appears to be consistent and sensible, but the question then arises as to how this data can be parameterized to enable it to be used easily in calculations. After some trial and error analysis it was found that all the data for each site could be made to collapse around a single curve by plotting the combined variables $NT$ and $(X_1\text{-}X)/X_1$ against each other. These variables seem sensible, as both are dimensionless, with the former giving a normalised value of number of exceedances, and the latter describing being the difference between specific gust velocities, and the value at which $N$ must be zero. The results are shown in figures 4 and 5 for the Silsoe and Birmingham data respectively, using the measured values of $X_1$ for each dataset. It can be seen there is much scatter, but the data collapse is reasonably good. The two sets of data do not however coincide, indicating the effects of the underlying shape of the probability distribution, and in particular the upper tails.

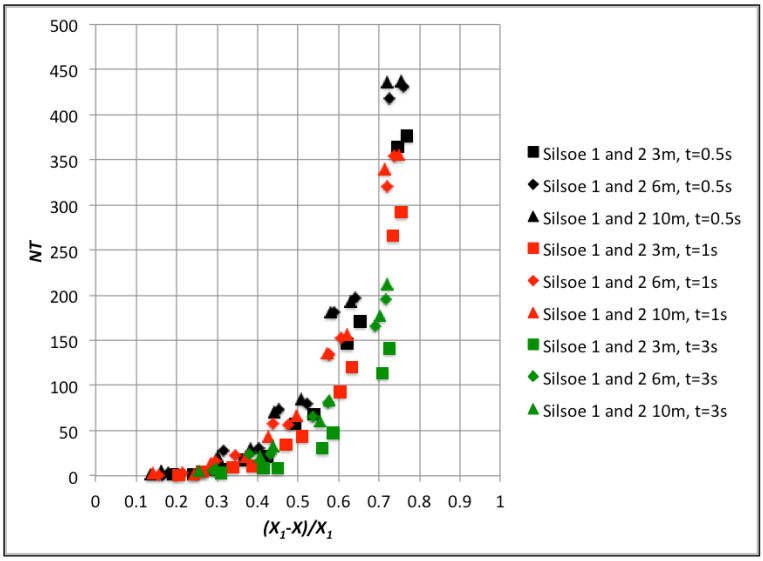


**Figure 4. Analysis of Silsoe exceedance data**

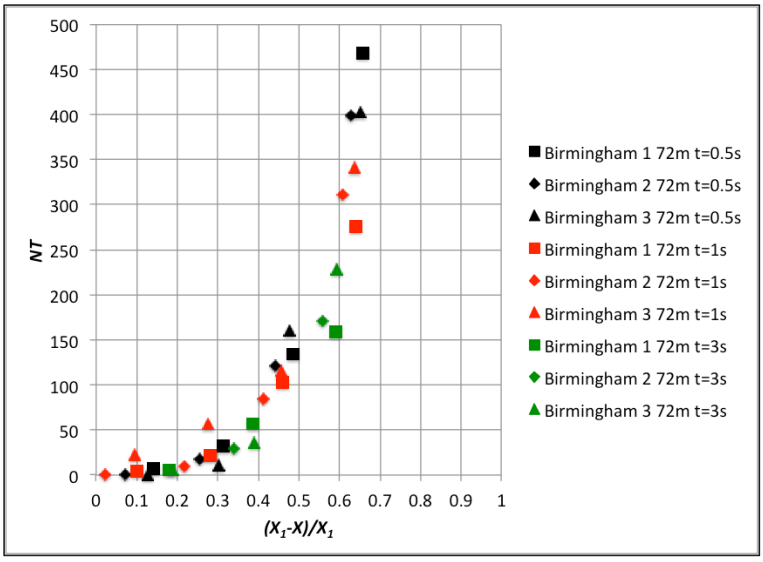


**Figure 5. Analysis of Birmingham exceedance data**

The region of most practical interest on these data collation is for a low number of events, since these represent conditions where the risk might be tolerable. Thus figures 6 and 7 thus show expanded versions of figures 4 and 5 for $NT<50$. It would quite possible to fit lines or curves to this data, although the best fit values would be different between the Birmingham and Silsoe datasets.

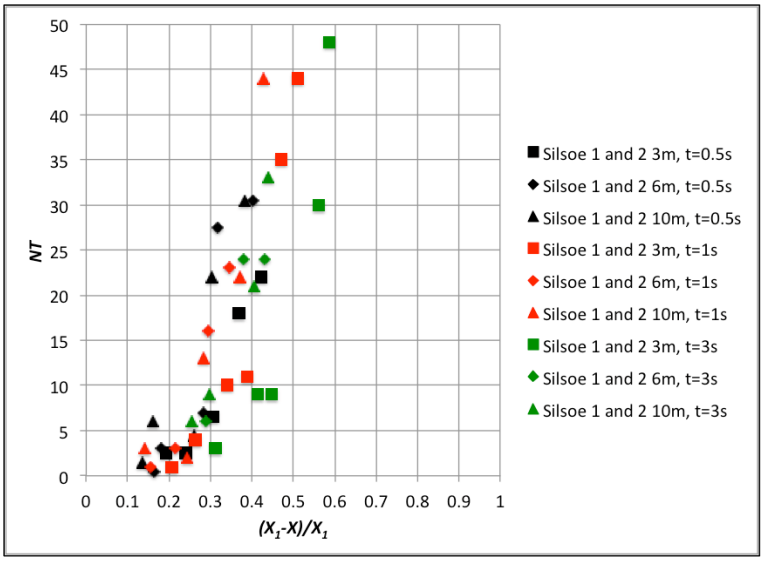


**Figure 6. Expansion of figure 4 for low NT values**

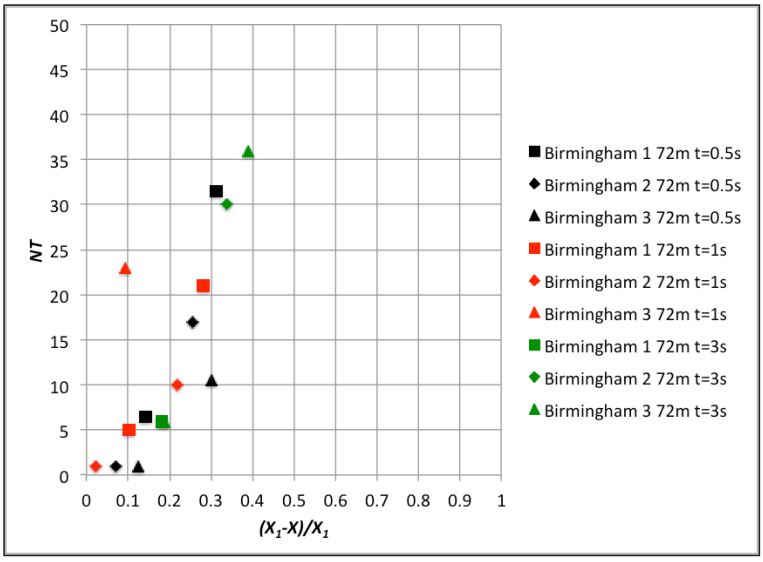


**Figure 7. Expansion of figure 5 for low NT values**

It would seem that if this method is to become useful in a predictive, rather more detailed information on near ground probability distributions is required for a variety of ground roughness conditions / heights above the ground etc., so that the variation in the exceedance curves of figures 4 to 7 can be more fully understood and an overall data collation be achieved. If any reader knows of systematic data for wind probability distributions, please let me know.

# Vehicle restrictions during windy conditions on long span bridges

March 16, 2020

**The Bridges**

Around the UK, there area number of relatively long and high bridges across river estuaries, that all operate some sort of traffic restriction protocol in high wind conditions, to limit the risk of vehicle accidents. In this post, I will attempt to collate publicly available information on these traffic restriction protocols to assess their similarities and differences. It will be seen (surprisingly in my view) that this information is not at all easy to find and sometimes does not seem to be in the public domain. .

The bridges that will be considered are shown in Table 1, which gives name, location, construction type and length. Pictures of them are given in figure 1. It can be seen that, with the exceptions of the Cleddau Bridge in South Wales and the Skye Bridge in Scotland, these are all over a kilometre long. The construction types vary, from concrete boxes on large numbers of concrete piers to long span suspension and cable stay structures. Only two bridges in the table have protection for vehicles against cross winds – the Prince of Wales (Second Severn) Bridge and the Queensferry Bridge in Edinburgh. All the bridges in the table have Wikipedia entries, which give further details of planning, construction and operation.

| | Location | Type | Length (m) |
|---|---|---|---|
| Cleddau | Pembrokeshire | Box Girder | 820 |
| Severn | Gloucestershire / Monmouthshire | Suspension | 1600 |
| Prince of Wales (Second Severn) | Gloucestershire / Monmouthshire | Cable Stayed, Concrete multi-span | 5128 |
| Queen Elizabeth II (Dartford) | Kent / Essex | Cable Stayed | 2872 |
| Orwell | Suffolk | Box Girder | 1000 |
| Humber | Lincolnshire / Yorkshire | Suspension | 2220 |
| Erskine | Dumbartonshire / Renfrewshire | Cable Stayed | 1322 |
| Forth Road | Edinburgh / Fife | Suspension | 2512 |
| Clackmannanshire | Falkirk / Fife | Concrete multi-span | 1200 |
| Skye | Skye / Highland | Concrete multi-span | 500 |
| Kessock | Inverness | Cable Stayed | 1065 |
| Tay Road | Fife / Dundee | Concrete multi-span | 2250 |
| Queensferry | Edinburgh / Fife | Cable Stayed | 2700 |

**Table 1 The Bridges**

**Cleddau**

**Severn**

**Prince of Wales (Second Severn)**

**Queen Elizabeth II (Dartford)**

**Orwell**

**Humber**

**Erskine**

**Forth Road**

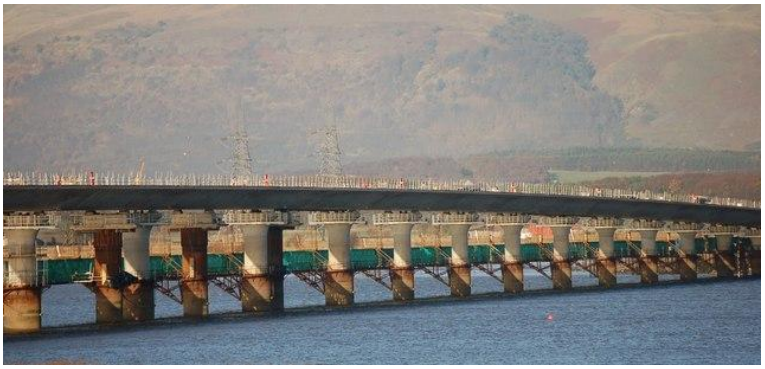

**Clackmannanshire**

**Skye**

**Kessock**

**Tay Road**

**Queensferry**

**Figure 1. The Bridges (photos from Wikipedia, Creative Commons licenses)**

**Vehicle restrictions**

The data for wind speed restrictions was found from a variety of sources – official documents, FOI releases, newspapers etc. The information that has been obtained is shown in Table 2. Most have a similar form, with different levels of restriction being used as the gust wind speed increases – vehicle speed limits, lane closures, restrictions to various classes of vehicles, and total closure. Most seem to base the wind speed values on local anemometers, although it is usually not clear where these are sited, and neither is the period of the gust given. Thus the values that are given are not strictly comparable with each other in absolute terms.

| | Warning | Speed limit (30mh or 40mph) | Windward land closure | Restriction - double deck buses | Restriction – high sided | Restriction - Motorcycles | Restrictions – cycles | Restrictions - pedestrians | Closure |
|---|---|---|---|---|---|---|---|---|---|
| Cleddau | | | | 55 | 55 | 55 | 55 | 70 | 70 |
| Severn | | | | 45* | 45* | 45* | 45* | 70* | 70* |
| Prince of Wales | | | | | | | | | |
| Queen Elizabeth II | | 50(C) 60(H) | 55(C) 65(H) | 60(C) 70(H) | 60(C) 70(H) | 60(C) 70(H) | 60(C) 70(H) | 60(C) 70(H) | 60(C) 70(H) |
| Orwell | | | | 50(C) 60(H) | 50(C) 60(H) | 50(C) 60(H) | 50(C) 60(H) | 50(C) 60(H) | 50(C) 60(H) |
| Humber | | | | | | | | | |
| Erskine | 35 | | | 45(C) 60(H) | 45(C) 60(H) | 70 | 70 | 70 | 70 |
| Forth Road | | 35 | | 45 | 45 | 50 | 50 | 50 | 65 |
| Clackmannanshire | | 35 | | 50 | 50 | 75 | 75 | 75 | 75 |
| Skye | | 35 | | 50 | 50 | 75 | 75 | 75 | 75 |
| Kessock | | | | | | | | | |
| Tay Road | | | | 45 | 60 | 60 | 60 | 60 | 80 |
| Queensferry | | 50 | | 60 | 70 | 70 | 90 | 90 | 100 |

**Table 2 Wind speed restrictions**

(H- Headwind, C – Crosswind, * values are given in mph in table, but equivalent values in knots are used in practice)

From table 2 it can be seen that no data could be obtained for the Kessock Bridge, the Humber Bridge or the Prince of Wales (Second Severn) Bridge. With regard to the latter, vehicles crossing the bridge are shielded by wind fences and the bridge has not had to impose restrictions on traffic during its lifetime. Kessock probably has the same sort of traffic restriction strategy as the other Scottish bridges, as Transport Scotland operates a common approach. From press reports it seems that Humber has some sort of vehicle speed limit and high-sided vehicle restriction strategy, although it has not been possible to determine the wind speeds at which the different measures are put into place. . Also note that Queensferry has much higher values of wind speed for restrictions than the other bridges, again due to the fact that vehicles are protected by wind fences.

For the other bridges, there seems to be a general consistency in the information shown, with vehicle speed limits of either 30mph or 40mph imposed when the wind gusts over 35 to 50mph. Vehicle restrictions begin at gusts of around 45mph to 60mph, with double deck buses

and high sided vehicles being restricted at the lower gust speeds. Further restrictions may be imposed on vehicles of different types, before overall bridge closure at wind speeds of 65 to 80mph. Some bridges use different gust speeds for cross winds and for headwinds. Orwell Bridge for example applies the crosswind criterion if the wind gust direction is from a sixty degree segment centred on the direction normal to the bridge. The Queen Elizabeth II Bridge at Dartford uses similar strategies to inform speed limits, lane closures, vehicle restrictions and bridge closure.

The restriction strategies depend very much on the nature of the traffic over the bridge and its location. For example, if only some vehicles are to be restricted, then some method of filtering them out and diverting them is required, which needs to take place at some distance from the bridge. Such procedures are in operation at Severn, Erskine, Humber and the Queen Elizabeth Bridges amongst others. Clearly ease of identification of vulnerable vehicles is required – see figure 2 for the Humber Bridge. Other bridges simply base their protocols on vehicle height eg 1.9m for Cleddau and 2.1m for Severn.

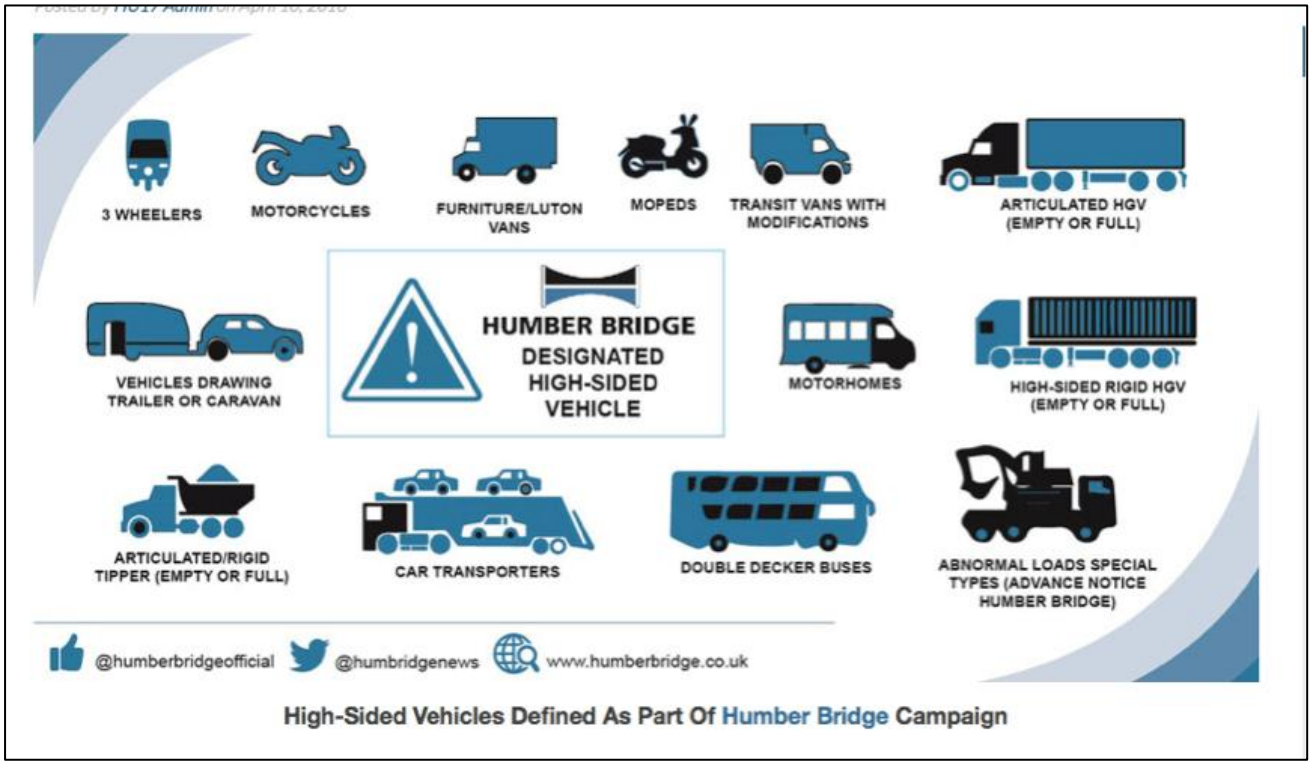


**Figure 2 Humber Bridge High sided Definition**

Orwell Bridge operates a very simple strategy, with different gust speed triggers for crosswinds and headwinds, leading to complete closure, without any restrictions for, say, high sided vehicles at lower wind speeds. This arises because of the urban nature of its surroundings, which makes vehicle filtering difficult. This has led to a considerable number of closures in recent years, and much public concern. Recently both numerical and wind tunnel studies have been carried out to investigate ways in which this strategy can be modified, perhaps through the use of speed limits, lane restrictions or barriers. The details of these studies have not been

released to date but may prove of some interest. Studies to relax the restrictions on Skye Bridge have also been recently carried out following frequent closures and public complaints.

As can be seen, the various restriction strategies are in general quite simple and easy to operate. This inevitably means that they are conservative and largely based on the most vulnerable vehicle – usually unladen high sided vehicles. There are in fact methods available for discriminating between vehicle types and vehicle weights – see the recent paper by Baker and Soper (2019) for example. This gives a method for determining a curve of accident wind speed against vehicle speed for specific vehicle type and weight, based on which restrictions strategies for any particular vehicle can be determined. However operational constraints make the full utilisation of such methods difficult. Until such time as vehicle type and vehicle weight can be automatically determined by (say) remote visualisation techniques and dynamic weight determination, and vulnerable vehicles can be suitably diverted, then the use of simple methods such as those currently adopted will remain the best that can be achieved.

# Measuring the behaviour of pedestrians in high winds

June 8, 2020

*This post outlines some of the results from the project "The safety of pedestrians, cyclists and motor vehicles in highly turbulent urban wind flows" funded by the UK Engineering and Physical Sciences Research Council. The work that is described below involved a number of colleagues, whose contribution to the project was significantly greater than mine, particularly Dr Zhenru Shu, Dr Mike Jesson, Dr Andrew Quinn, and Prof Mark Sterling. Their contribution is gratefully acknowledged.*

**1. Introduction**

The assessment of wind conditions around new buildings has become standard practice over recent years, either by wind tunnel testing or through the use of CFD calculations. The assessments usually concentrate on two aspects – the effect of wind conditions on human comfort and thus the usability of the area around the building; and the effect of high wind conditions on human safety and stability. It is with the latter that this paper is concerned. In general the criterion for assessing a site for pedestrian safety is based on a gust wind speed of a specified magnitude with a specified probability of occurring, that is deemed to be at the

safety limit. Current UK practice is illustrated in Figure 1 below. There is a great deal of variability in the specification of this windspeed and the specification is usually based on largely subjective data from questionnaires etc. Following a fatality caused by high winds around a new building in the city of Leeds, a major research project was funded by the UK Engineering and Science Research Council to enable the University of Birmingham to investigate the safety of vehicles and pedestrians around high-rise buildings. This included full-scale wind measurements and the assessment of the ability of different wind tunnel and CFD techniques to replicate these measurements. In addition tests were carried out to make quantitative measurements of human response in gusty winds, using instrumentation mounted on volunteers. As will be appreciated by any reader who has tried to make full scale wind measurements of any type, the setting up of the experimental apparatus usually guarantees that strong winds will not occur, and the same phenomenon was observed for these tests. The two winter seasons that were available for these measurements had relatively few storms, and only two trials could be carried out. As a result, although some very interesting results were obtained and will be presented in what follows, they must be regarded as provisional and tentative. More work is required to obtain a fuller dataset of human response measurements of the type that are presented here.

| Lawson (2001) | | LDDC | |
|---|---|---|---|
| Sitting | 5.60m/s , 1% (5) | Pedestrian sitting | 4m/s, 5% |
| Entrance doors | 5.6m/s, 6% (6) | | |
| Pedestrian standing | 5.6m/s, 6% (6) | Pedestrian standing | 6m/s, 5% |
| Pedestrian walk through | 8.25m/s, 4% (8) | Pedestrian walking | 8m/s, 5% |
| People around buildings | 10.95m/s, 2% (9) | | |
| Roads and car parks | 10.95, 6% (10) | Business walking | 10m/s, 5% |
| Distress | 14.1m/s, 0.01% | Distress | 15m/s, 0.025% |

**Figure 1 Current UK practice for specifying wind comfort and safety (Values given are for mean wind speed and percentage of time exceeded)**

## 2. The trials

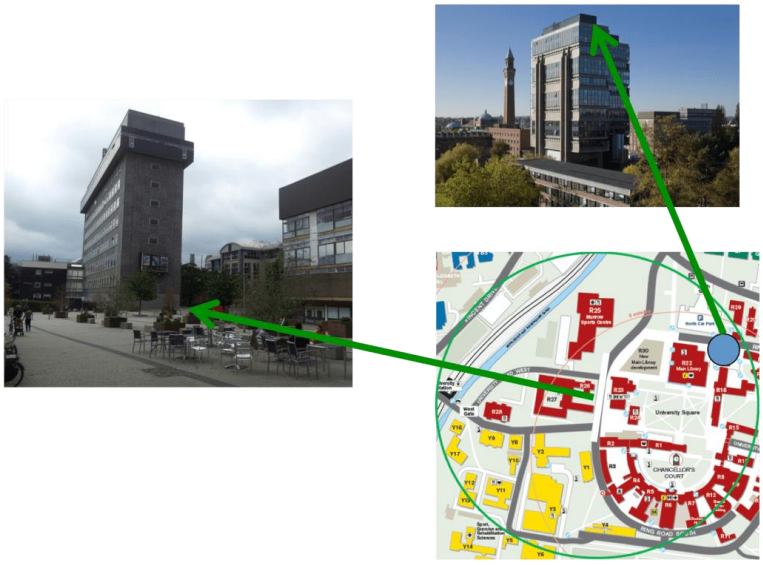

**Figure 2. The test site showing the walking route along the Biosciences building and the reference anemometer site on the Moorhead Tower**

The trials on the response of pedestrians to high winds were carried out on the campus of the University of Birmingham (figure 2). A walking route of length 63m was set up in the centre of the campus. Eight sonic anemometers were placed 2m above the ground at 9m intervals along the route. A reference anemometer was installed at the top of the nearby high rise Muirhead Tower. A reference anemometer was mounted at the top of the Moorhead Tower. All the anemometers sampled at 10 samples / sec, and data was recorded on an AntiLog data logger. Human response was measured using GaitUp Physilog (combined accelerometer and gyroscope) sensors. Sensors were attached to both feet of the subjects, and provided details of walking speed and stride parameters every second through GaitUp's proprietary software. A third sensor was placed on the back of a safety jacket worn by the subjects and thus gave details of upper body acceleration.

Two trials were carried out – October 2017 during Storm Ophelia, and in February 2019 (figure 3. In total there were 15 subjects, with weights ranging from 54 to 110kg, and ages between 28 and 75. Each subject was asked to walk along the test route 10 times in each direction during which the gait and acceleration information was measured.

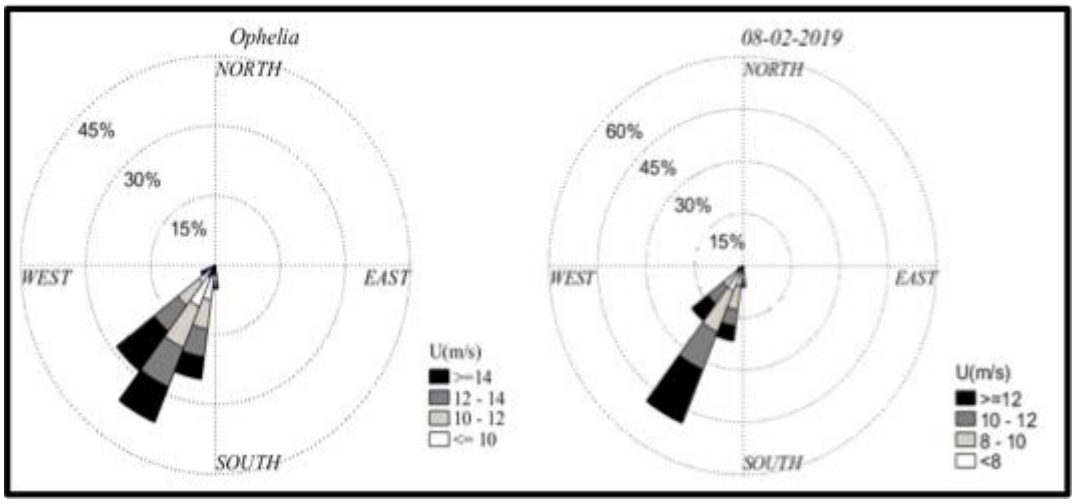


**Figure 3 Wind conditions during the trials**

### 3. Analysis

The overall wind conditions at the reference site on the Muirhead Tower are shown in figure 3 for the two test periods. It can be seen that in each case the wind is from the South-West (shown in longer term analysis to strongly be the prevailing wind direction), with gust speeds up to 18m/s

Before the data could be analysed, some data preparation was required. Firstly the gait data and accelerometer time series had to be synchronized with the anemometer time series of velocities and the raw accelerometer data was transformed into horizontal and vertical co-ordinates. The time series of velocity and direction relative to the subjects were then derived form the stationary anemometer data as the subject walked along the route. A histogram of gust speed distribution, as experienced by the volunteers, for the two trials is shown in figure 4.

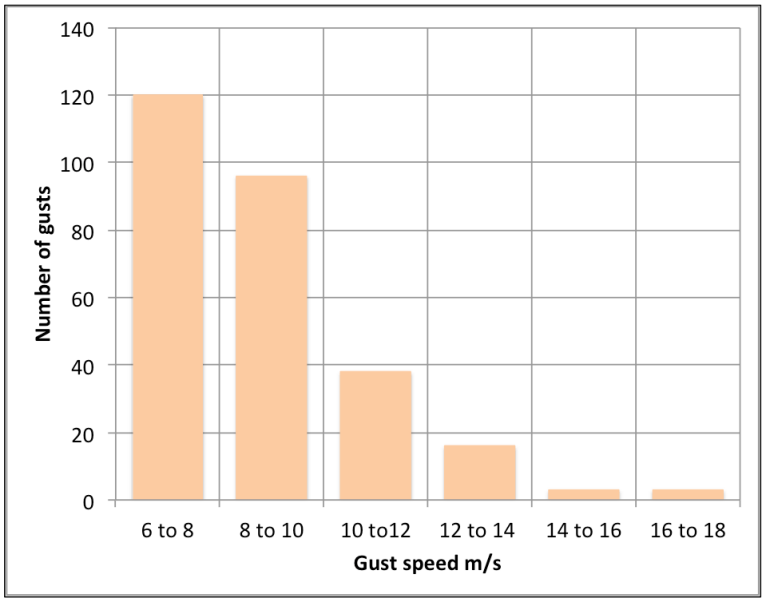


**Figure 4 Histogram of gust velocities**

Initial inspection of the data showed that there was very significant variability between each recorded walk along the track. This was in part due to the normal variation in wind conditions with higher gust speeds on some walks than on other, but it also seemed that the reaction of subjects varied both with time and between subjects. A typical set of results is shown in figure 5. The direction of travel of the subject is from 0 to 63m. The wind speed relative to the subject can be seen to have a maximum of around 12 m/s in this case (associated with the corner flow from an adjacent building). The horizontal and vertical accelerometer data show slight oscillations around the gust position gust with the former having an average value of zero, and the latter an average value of 1.0. Most of the gait measurements (cycle time, stride length, stride speed) revealed little change in behaviour as the subjects walked along the route, all remaining approximately constant along the walk in most conditions. The one parameter that did show variation was the swing width – the lateral variation of the foot during a stride cycle. In particular rapid changes in swing width were sometimes (but not always) observed as the subjects encountered gusts – see the graph for swing width gradient.

At the highest gust speeds that were recorded, there were three events where the subject became unstable to a variable extent. Figure 6 shows the experimental data for one such case. Here it can be seen that at the gust position there are significant vertical and horizontal acceleration responses, and all the gait parameters show a response at the event. The swing width response is again the most noticeable.

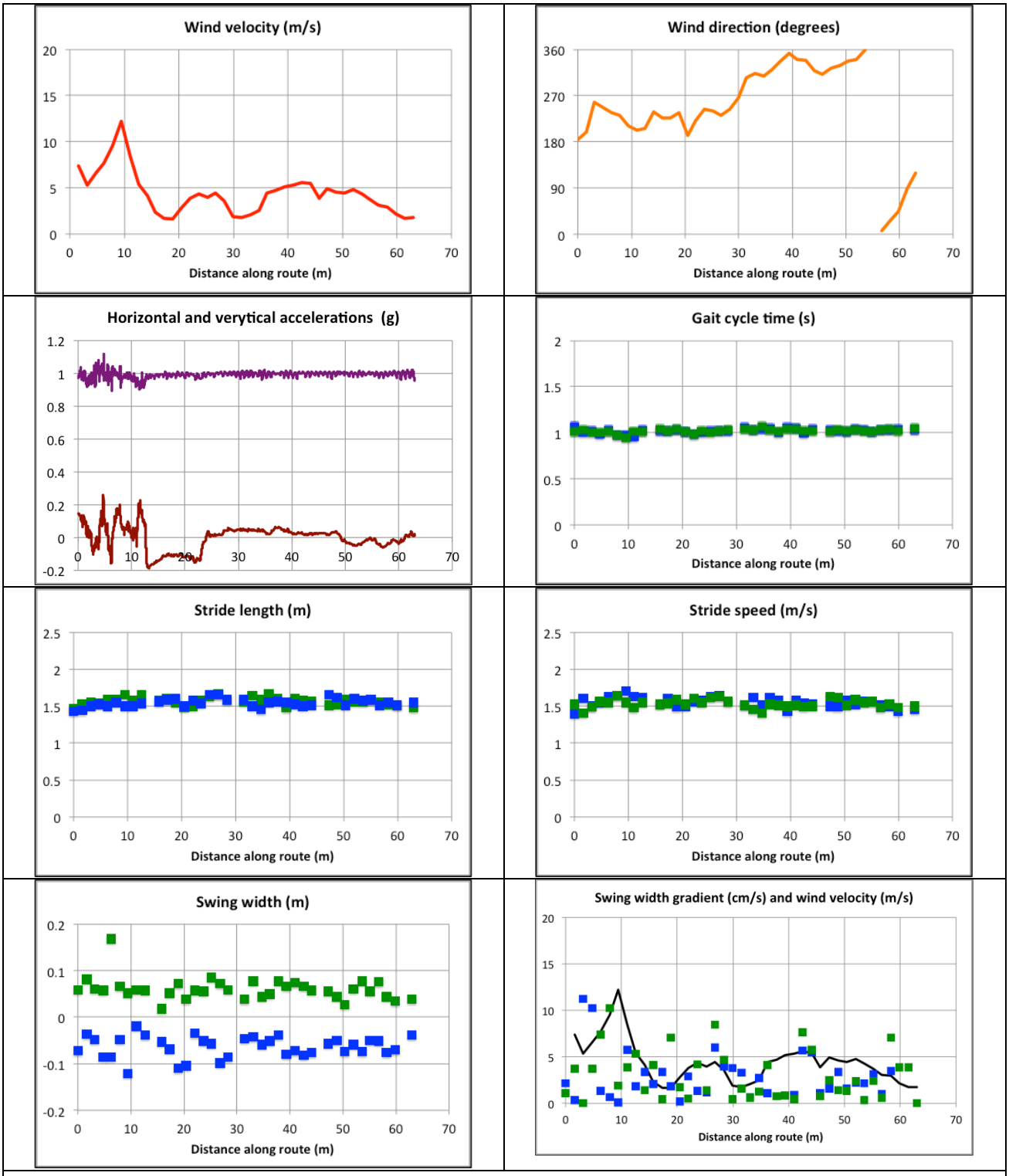


**Figure 5 Wind, acceleration and gait parameters for typical gust (green symbols indicate left foot, blue symbols indicate right foot)**

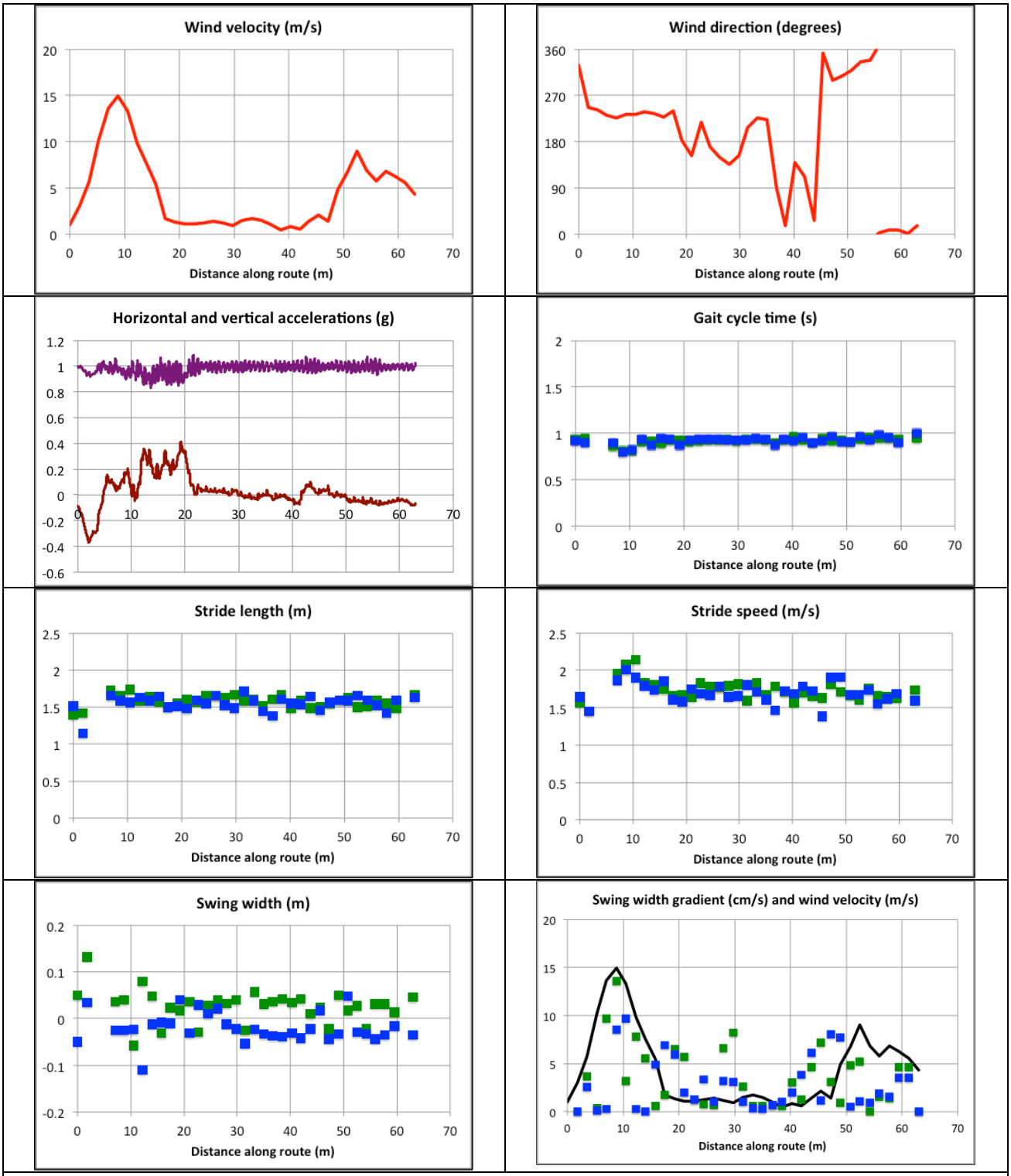


**Figure 6 Wind, acceleration and gait parameters for strong gust (green symbols indicate left foot, blue symbols indicate right foot)**

A somewhat more quantitative approach to the data is possible by looking at the various responses statistically. In what follows we consider the results from both trials, for all subjects, as one dataset. Figure 7 shows the percentage of such gusts in which the subjects showed a swing width response (with either the left or right swing width changing by more than 0.06m in one second) and acceleration response (where an acceleration response greater than 0.05g could be detected) or an instability response (with an acceleration response greater than 0.4g). In considering these results the low number of gust events in the upper velocity bands need to be considered, as does the subjectivity of the response limits used. These points being made, it can be seen that for even low speed gusts of magnitude less than 10m/s, around 50% of the gusts result in a swing width response (which are mostly unconscious responses not registered by the subject). The frequency of such responses rise rapidly for gust speeds above 10 m/s, and all gusts over 14 m /s show such a response. Acceleration responses become significant at gust speeds of about 10m/s, and are observed for all gusts above 16m/s. Instability responses begin to occur at gust speeds over 14m/s, although it should be noted here that only a very small number of such events (3) were observed.

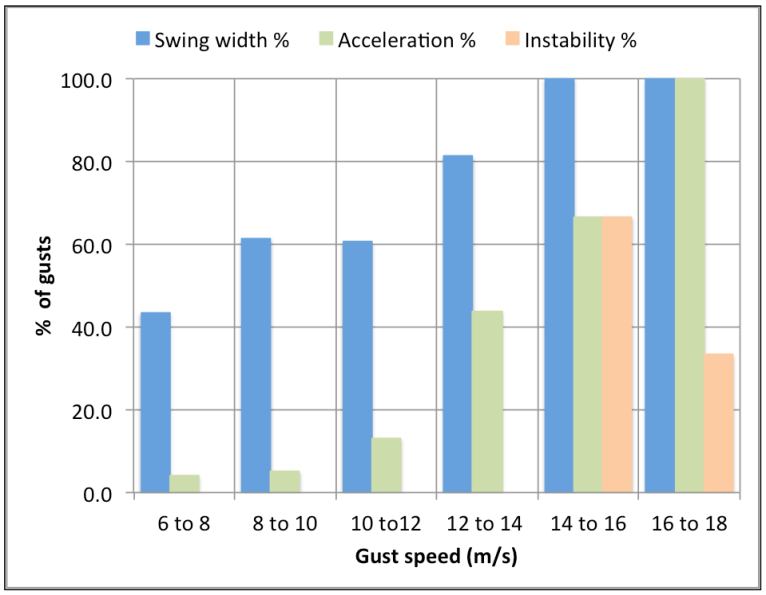


**Figure 7 Frequency of different types of response**

## 4. Concluding remarks

The results for human response in gusts presented here suggest that three levels of response can be identified – swing width response , upper body acceleration response and instability response, with the frequency of each such response increasing with wind speed. However it must be emphasised once more that the number of bot high speed gust events and the number of subjects was too small for a valid statistical analysis to be carried out, and more data is required before firmer conclusions can be drawn.

**Measurement of pedestrian behaviour in high winds**
**October 14 2020**

# Some musings on tornado vortex models

June 30, 2020

From Wikipedia

Recently I have been considering the fundamental nature of a range of analytical models of tornado like vortices, and have written up my musings as an extended essay that can be read at Appendix 2. In the essay I look at the class of tornado models that are solutions of the Navier-Stokes or Euler equations. It is clear that they all share a common analytical basis based on the assumption, either implicit or explicit, that the three velocity components (radial, vertical and circumferential) can each be specified by the multiple of two functions – one a function of radius only, and one a function of height only. Assumptions are made concerning the nature of one particular velocity component, and this assumption then allows the other components to be calculated from the continuity and momentum equations via the method of separating the variables. The recognition of this commonality allows a common analytical formulation to be developed that underlies all the models.

Those models that are solutions of the full Navier-Stokes equations (the Burgers-Rott, Sullivan and Vasistas et al models) derive velocity component formulae that are functions of Reynolds number. In the context of a full-scale tornado, this is a Reynolds number based on turbulence eddy viscosity rather than molecular viscosity. The assumptions required to obtain analytical solutions result in vertical velocities that are unbound with height and in some cases radial velocities that are unbound with distance from the vortex centre.

Those models that are solutions of the Euler equations (two by Baker and Sterling and two new models A and B) have, on the whole, rather more realistic formulations of the velocity components and, with one exception, all components for these models are bound in the vertical and radial directions. Instead of the Reynolds number, the velocity components are functions of constants of integration that relate to the Swirl ratio – the ratio of the maximum

circumferential to radial velocities. As the circumferential velocity profiles in these models fall to zero at ground level in a reasonably realistic way, the boundary layer at the bottom of the tornado is modeled to some extent. The common analytical framework of these models allows, in principle, the derivation of a large number of different models, provided that they are of a form that allows the solutions to be obtained through simple integrations. However the drawback of such models is that the pressure is zero at the ground for all distances from the vortex core and thus the dip in pressure at the centre of tornadoes is not modeled. This is broadly a consequence of viscous effects not being properly modeled near the ground.

Whilst most of the models represent single cell tornado vortices, two of them – those of Sullivan and new model B – give solutions for two cell vortices. The essay shows that the Sullivan model, based on the Navier-Stokes equations, has a more general form than that given in the original paper and can model one-cell and two-cell vortices and the transition between them. New model B, based on the Euler equations is also able to model both sorts of vortex.

The essay concludes that further work is required in two areas. Firstly there is a need to develop methods that do not rely on the assumption that the velocity components are multiples of two functions – one of radius and one of height – as recent experimental data suggests that the vortex radius can vary significantly with height. Secondly, the tornado boundary layer needs to be modeled in a more satisfactory way than at present, and the essay suggest that this might be done through matching a viscous solution of the Navier-Stokes equation near the ground, with an inviscid solution from the Euler solution away from the ground. I may have more to say on this in the future.

# Air pollution in Railway Stations

**August 1 2020**

# Modelling of extreme wind gusts

September 5, 2020

**Nomenclature**

*This post addresses the issue of the use of what has become known as the "Chinese Hat" gust model. The use of this title has become increasingly problematic over recent years for obvious reasons, and I will no longer use it, but will instead refer to the "CEN extreme gust model" in what follows.*

**The CEN extreme gust model**

In a number of situations in wind engineering, some sort of deterministic (as opposed to stochastic) gust model is required in order to determine structural response. One such case is in the determination of the risk of overturning of road or rail vehicles in high winds. A methodology of this type is set out in CEN (2018), where an extreme gust model is described. This model was originally developed in wind loading studies for wind turbines as a time dependent gust to be applied to calculate wind turbine loading at one fixed location (Bierbooms and Cheng, 2002). As such, it is perfectly adequate and a good representation of an average extreme gust in high wind conditions. In the methodology of CEN however, it is re-interpreted as a stationary spatially varying gust. This must be regarded as a very significant assumption for which, in my view, there is little justification. Nonetheless the formulation has proved useful practically and we begin by considering it in a little more detail.

For a wind normal to the track, the extreme gust formulation is given by equation (1) on Box 1. Note that the "characteristic frequency" of the gust is calculated from standard wind engineering methods for temporally, rather than spatially, varying gusts. Equation (1) is a generalised form of that given in CEN (2018) to remove some of the constants that tie the expression to a particular location and topography through specific values of peak factor and the turbulence intensity (the ratio of the standard deviation to the mean velocity). The time dependence is recovered through the passage of the train passing through this gust at a speed $v = xt$ to give equation (2). It can be seen that the gust thus has a maximum value of (1+ peak factor x turbulence intensity) when $t = 0$ and decreases to unity for small and large times. It is symmetrical about $t = 0$. The velocity relative to the train is then found by the vector addition of this gust velocity with the vehicle velocity to give a time varying value.

To enable the gust profile to be specified, the characteristic frequency $f$ is required. This is specified in equations (3) to (5). These equations are again in a more generalized form than given in CEN (2018), where a value of the upper limit of integration is fixed at 1 Hz, together with an implicit value of the turbulence length scale of around 75m. The genesis of the 4.18 factor is however not clear to me. Equation (3) shows that the calculation of the characteristic frequency is thus based on the calculation of the zero-crossing rate of temporal fluctuations through the use of the velocity spectrum. Again, note that these parameters describe a time

varying rather than a spatially varying velocity, and their use is not formally consistent with a spatially varying gust. From equations (3) to (5), it can be seen that the normalized characteristic frequency is a function of the normalized upper limit of integration. A numerical solution of these equations was carried out and the following empirical line fitted to the results for a value of the latter greater than 1.5 (which is the realistic range) – equation (6). From equations (2) and (6) we thus obtain equation (7). Although the overall methodology cannot be regarded as wholly sound, equation (7) does (in principal) significantly simplify its use and also allows the implicit wind parameters in the method to be explicitly defined.

| | |
|---|---|
| Equation (1) $\frac{u}{\bar{u}} = 1 + g\left(\frac{\sigma_u}{\bar{u}}\right) e^{-16\left\|\frac{fx}{\bar{u}}\right\|}$ | $f$ - "characteristic frequency" of the gust<br>$g$ - peak factor<br>$L$ -integral length scale of the wind normal to the track<br>$n'$ - normalization of frequency $n$<br>$n_m^{'}$ - normalisation of upper limit of integration $n_m$<br>$S'$ - normalization of spectral density $S$<br>$u$ - the wind velocity at a point $x$ or time t along the track<br>$\bar{u}$ - mean wind velocity<br>$v$ - train speed<br>$\sigma_u$ - standard deviation of wind speed |
| Equation (2) $\frac{u}{\bar{u}} = 1 + g\left(\frac{\sigma_u}{\bar{u}}\right) e^{-16\left\|\frac{fvt}{\bar{u}}\right\|}$ | |
| Equation (3) $\frac{fL}{\bar{u}} = \frac{1}{4.18}\left(\int_0^{n_m^{'}} n'S'dn'\right)^{-0.5}$ | |
| Equation (4) $n^{'} = \frac{nL}{\bar{u}}$ | |
| Equation (5) $S^{'} = \frac{nS}{{\sigma_u}^2} = \frac{4n^{'}}{\left(1+70.8{n^{'}}^2\right)^{5/6}}$ | |
| Equation (6) $\frac{fL}{\bar{u}} = 0.028\left(\frac{n_m L}{\bar{u}}\right) + 0.056$ | |
| Equation (7) $\frac{u}{\bar{u}} = 1 + g\left(\frac{\sigma_u}{\bar{u}}\right) e^{-16\left\|\frac{vt}{L}\right\|\left(0.028\left(\frac{n_m L}{\bar{u}}\right)+0.056\right)}$ | |

**Box 1 Equations 1 to 7**

**Is there a better methodology?**

It can be seen from the above that the CEN methodology thus does not fully describe a typical gust as seen by a moving train, which would vary both spatially and temporally, and can at best be regarded as an approximation, although its practical utility must be acknowledged. Ideally, if such an approach is to be used, a gust that varies both in space and time is really required. Such a gust was used in the SNCF route assessment method of Cleon and Jourdain (2001), where the shape of the gust is appropriately described as a rugby ball. This method was however for very specific wind characteristics and does not seem to have found widespread use. Thus in this post, we investigate the possibility of developing a spatially and temporally varying gust, that can be expressed in a simple form (ideally similar to equation (2)) for practical use.

**Towards a new model**

In this section we will draw on experimental results for extreme gust characteristics in both temporal and spatial terms to construct a simple, if empirical model, that fulfils the function of the CEN (2018) model without the theoretical drawbacks.

We consider first the full-scale experimental data analysed by Sterling et al (2006) which used conditional sampling to determine the average 99.5$^{th}$ percentile gust profile for four anemometers on a vertical mast with heights between 1m and 10m. These results thus give the time variation in gust speed as the gust passes the anemometers. They showed that the gust profiles could be well approximated by the formula shown in equation (8) (Box 2). The parameter $G$ in this equation is the equivalent of the peak factor multiplied by the turbulence intensity in equation (2) and for these measurements was 0.786. $n$ was -0.096, and the value of $m$ depended upon whether $t$ was greater or less than zero. For $t < 0$, i.e. on the rising limb, $m$ was 0.1, whilst for $t > 0$, on the falling limb, $m$ was 0.2. The gust shape was thus asymmetric with a maximum at $t = 0$. This curve was a good fit to all the gust profiles throughout the height range. In what follows we will use a rather different curve fit expression to the same data, more consistent with that used in CEN (2018) – equation (9). It was found that the best fit value of $b$ was equal to 0.5 for all $t$, whilst the best fit values of $a$ were 0.49 for the rising gust and 0.37 for the falling gust. This expression thus describes the temporal variation of wind speed as a gust passes through the measuring point

To describe the lateral spatial variation of the gust profile, we use the data of Baker (2001) who presents conditionally sampled peak events for pressure coefficients along a 2m high horizontal wall. This data allows the lateral extent of the gusts to be determined, from the variation of the time varying pressure coefficient divided by the mean value of the coefficient and then assuming that the gust velocity variation can be found from equation (10). The spatial variations of velocity were then fitted by a curve of the form of equation (11). g was found to be 6.16 and d was found to be 0.7.

On the basis of the above expressions one can thus write the expression of equation (12), which describes the variation of the gust velocity in both space and time. The movement of the train through the gust can again be allowed for by letting $x = vt$ (equation (13)).

| | |
|---|---|
| Equation (8) $\frac{u}{\overline{u}} = (1+G)\left[\frac{\lvert t\rvert}{m}+1\right]^{n}$ | $C_p$ - Pressure coefficient<br>$\overline{C_p}$ - Mean pressure coefficient<br>$G$ - Peak factor x turbulence intensity<br>$n$ - curve fit parameter<br>$m$ - curve fit parameter<br>$\alpha$ - curve fit parameter<br>$\beta$ - curve fit parameter<br>$\gamma$ - curve fit parameter<br>$\delta$ - curve fit parameter |
| Equation (9) $\frac{u}{\overline{u}} = 1 + g\left(\frac{\sigma_u}{\overline{u}}\right)e^{-\alpha\left(\left\lvert\frac{\overline{u}t}{L}\right\rvert\right)^{\beta}}$ | |
| Equation (10) $\frac{u}{\overline{u}} = \left(\frac{C_p}{\overline{C_p}}\right)^{0.5}$ | |
| Equation (11) $\frac{u}{\overline{u}} = 1 + g\left(\frac{\sigma_u}{\overline{u}}\right)e^{-\gamma\left(\left\lvert\frac{x}{L}\right\rvert\right)^{\delta}}$ | |
| Equation (12) $\frac{u}{\overline{u}} = 1 + g\left(\frac{\sigma_u}{\overline{u}}\right)e^{-\alpha\left(\left\lvert\frac{\overline{u}t}{L}\right\rvert\right)^{\beta}-\gamma\left(\left\lvert\frac{x}{L}\right\rvert\right)^{\delta}}$ | |
| Equation (13) $\frac{u}{\overline{u}} = 1 + g\left(\frac{\sigma_u}{\overline{u}}\right)e^{-\gamma\left(\left\lvert\frac{vt}{L}\right\rvert\right)^{\delta}\left(1+\frac{\alpha}{\gamma}\left(\frac{\overline{u}}{v}\right)^{\beta}\left(\left\lvert\frac{vt}{L}\right\rvert\right)^{\beta-\delta}\right)}$ | |

**Box 2 Equations 8 to 13**

**Model comparison**

Box 3 sets out the formulations of the CEN extreme gust model and the model derived here. In some ways they are similar in form, with an exponential formula that is primarily a function of normalized time. Whilst the CEN model is symmetric around $t = 0$, the new model has a degree of asymmetry because of the different values of the curve fit parameters for $t < 0$ and $t > 0$. However an examination of the new model suggest that the asymmetric term may be small, and thus Box 3 also shows an approximate version of the new model where this term is neglected.

| | |
|---|---|
| CEN (2018) modified - equation (7) | $\frac{u}{\overline{u}} = 1 + g\left(\frac{\sigma_u}{\overline{u}}\right)e^{-16\left\lvert\frac{vt}{L}\right\rvert\left(0.028\left(\frac{n_m L}{\overline{u}}\right)+0.056\right)}$ |
| New model from empirical curve fit - equation (13) | $\frac{u}{\overline{u}} = 1 + g\left(\frac{\sigma_u}{\overline{u}}\right)e^{-6.16\left(\left\lvert\frac{vt}{L}\right\rvert\right)^{0.7}\left(1+0.079\left(\frac{\overline{u}}{v}\right)^{0.5}\left(\left\lvert\frac{vt}{L}\right\rvert\right)^{-0.2}\right)}$ for t<0<br>$\frac{u}{\overline{u}} = 1 + g\left(\frac{\sigma_u}{\overline{u}}\right)e^{-6.16\left(\left\lvert\frac{vt}{L}\right\rvert\right)^{0.7}\left(1+0.060\left(\frac{\overline{u}}{v}\right)^{0.5}\left(\left\lvert\frac{vt}{L}\right\rvert\right)^{-0.2}\right)}$ for t>0 |
| Approximate version of equation (13) | $\frac{u}{\overline{u}} = 1 + g\left(\frac{\sigma_u}{\overline{u}}\right)e^{-6.16\left(\left\lvert\frac{vt}{L}\right\rvert\right)^{0.7}}$ |

**Box 3 Model Summary**

Figure 1 shows a comparison of these three models for the following parameter values – peak factor = 3.0; turbulence intensity = 0.25; train speed = 75m/s; mean wind speed = 25m/s;

turbulence length scale = 75m, upper frequency of integration = 1.0Hz. It can be all three models are similar in form, showing a sharp peak at $t = 0$. The full and approximate forms of the new model are almost indistinguishable, showing that the approximation suggested above is valid. The main difference is that the CEN model has a much greater spread in time than the new model. This difference persists whatever input parameters are chosen.

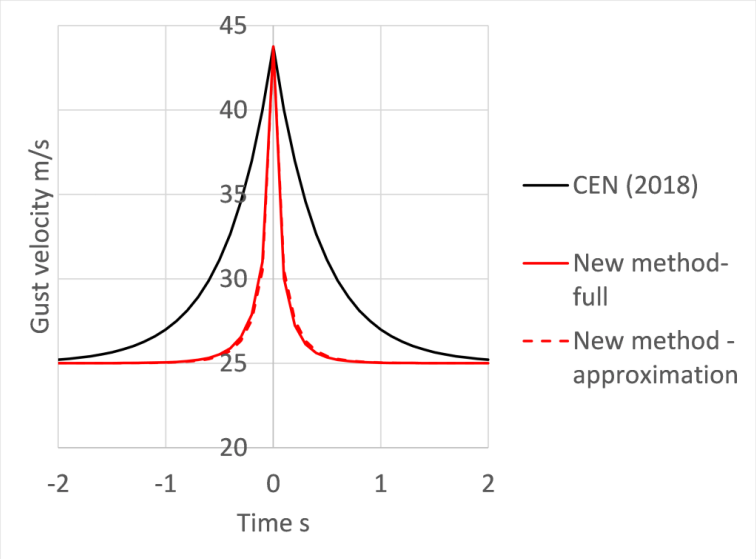


**Figure 1 Model Comparison**

At this point it is necessary to consider again the genesis of the models – the CEN model resulted from an application of a time varying gust model as a spatially varying gust model, whilst the new model was developed based on measured temporal and spatial gust values. As such, I would expect the latter to be more accurate. The broad spread of the CEN gust may result from an application of the time varying along wind statistics to a cross wind spatial gust. Since it is known that that longitudinal integral scale is several times larger than the lateral integral scale, this would result in a wider spread of the gust than would be realistic. This is to some extent confirmed by the period of the two gusts – around 2s for the CEN gust and around 0.8s for the new model. For a train speed of 75m/s, this corresponds to gust widths of 150m and 60m – roughly approximating to the expected the longitudinal and lateral turbulence integral scales.

**Concluding remarks**

In this post I have looked again at the CEN extreme gust method and raised concerns about its fundamental assumptions. I have also developed an equivalent, but perhaps more rigorous, methodology based on experimental data for wind conditions at ground level. This strongly suggests that the CEN gusts are spatially larger than they should be, which suggests its long term use should be reviewed. However, when used to compare the crosswind behaviour of individual trains, rather than in an absolute sense, it is probably quite adequate.

**References**

Baker C J, 2001, Unsteady wind loading on a wall, Wind and Structures 4, 5, 413-440. http://dx.doi.org/10.12989/was.2001.4.5.413

Bierbooms, W., Cheng, P.-W., 2002. Stochastic gust model for design calculations of wind turbines. Journal of Wind Engineering and Industrial Aerodynamics 90 (11), 1237e1251. https://doi.org/10.1016/S0167-6105(02)00255-6.

CEN, 2018. Railway Applications d Aerodynamics d Part 6: Requirements and Test Procedures for Cross Wind Assessment. EN 14067-6:2018.

Cleon, L., Jourdain, A., 2001. Protection of line LN5 against cross winds. In: World Congress on Rail Research, Köln, Germany.

Sterling M, Baker C, Quinn A, Hoxey R, Richards P, 2006, An investigation of the wind statistics and extreme gust events at a rural site, Wind and Structures 9, 3, 193-216, http://dx.doi.org/10.12989/was.2006.9.3.193

# Pollution, Covid and Trains

November 11, 2020

**Voyager at Birmingham New Street**

There has been a significant amount of research recently to investigate the air quality in railway stations. Perhaps the major study, with which I was very much involved, involved extensive measurements of the air quality at Birmingham New Street by colleagues at the University of Birmingham (Figure 1). Measurements were made of the oxides of nitrogen (NOX) and particulate matter (PM) and concentrations were measured that were considerably in excess of Environmental Health limits. Typical daily average results are shown in Figure 2. This work informed the efforts by Network Rail to improve the air quality at the station through an improved ventilation system. Further work was carried out by Kings College London and Edinburgh University, under an RSSB contract, to measure NOX and PM at Kings Cross in London and Edinburgh Waverley. Typical results are shown in figure 3 and although these results are not as extreme as the Birmingham measurements, do show some exceedances of environmental health limits. Between them, these three investigations have given a great deal of information on station air quality and informed methods for alleviating the worst of the effects.


**Figure 1. Air quality measurements at Birmingham New Street**

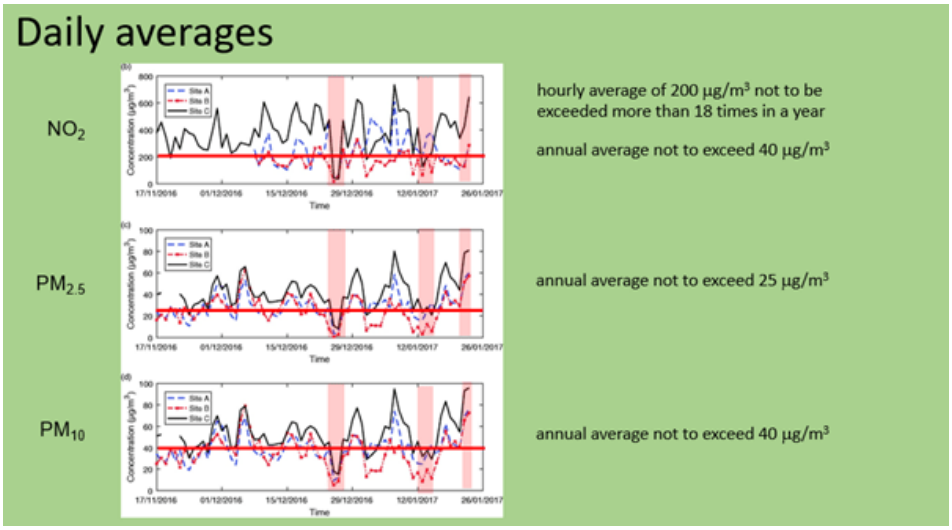


**Figure 2. Daily pollutant levels at Birmingham New Street (red lines show EU limits)**

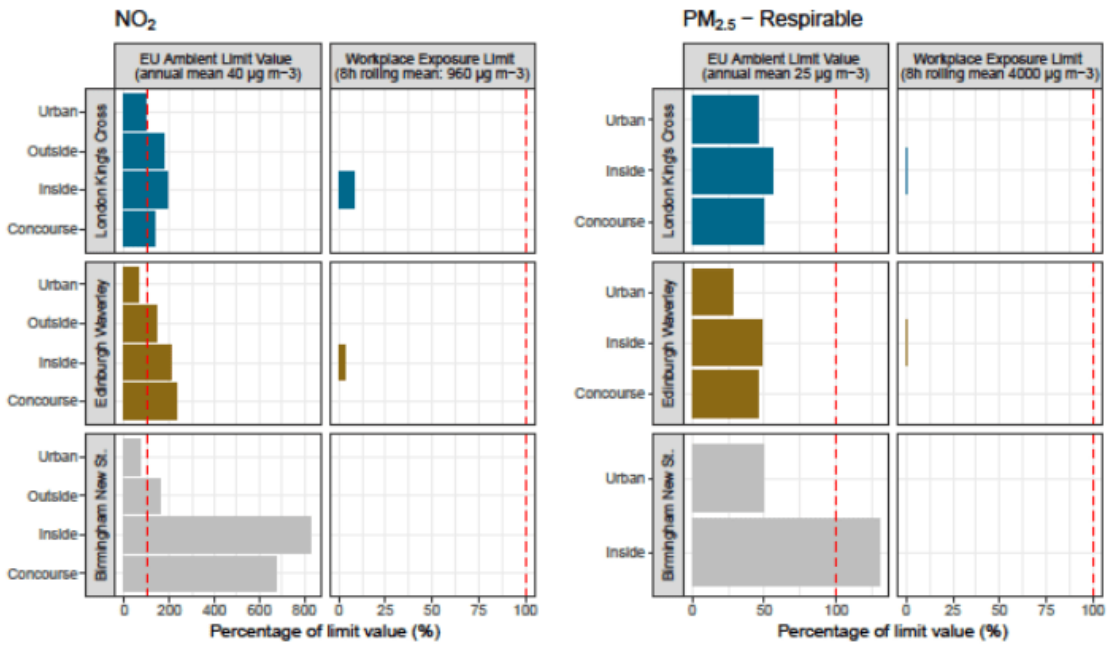


**Figure 3 Comparison of pollutant levels at New Street, Kings Cross and Edinburgh Waverley**

However, that is not the whole story. There are growing indications that air quality ON trains is also very poor. A study on diesel commuter stock in Canada has shown high levels of ultrafine particles and black carbon within the passenger cabins (Figure 4). In 2016 the BBC reported the measurements made by their reporter Tim Johns as he commuted into London, which again showed high particulate levels on diesel commuter trains, although not as high as in Black Cabs (Figure 5). Similarly, the BBC in 2019 reported a study by the Committee on the Medical Effects of Air Pollutants which showed very high levels of particulates on the London underground (Figure 6) which resulted in a strong response from the rail unions. These high levels are presumably due to two sources – diesel particulate emissions from trains being ingested into air conditioning systems, and also from ambient particulates in the dirty tunnels of the underground. The levels of particulates measured have significant implications for human health, particularly for those with respiratory conditions.

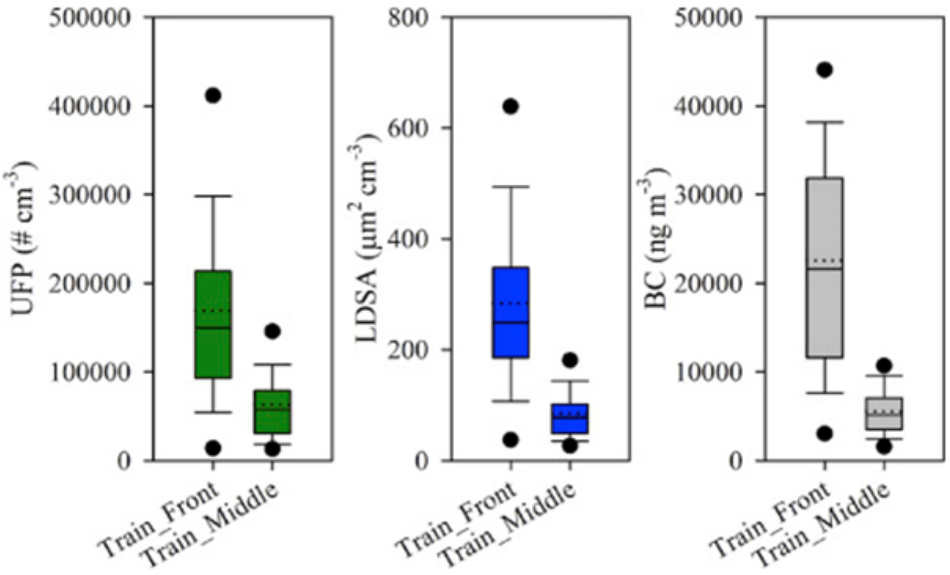


**Figure 4. Air Quality measurements on Canadian trains**

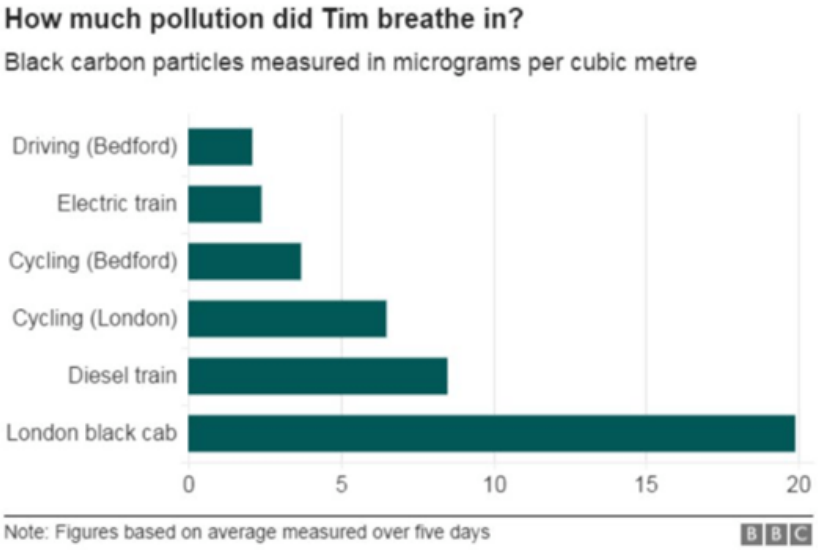


**Figure 5. Particulate measurements by BBC Reporter**


**Figure 6. BBC report on Underground particulate levels**

Similarly, some work has been recently reported from Greece that shows elevated levels of both gaseous pollutants and particulate pollutants on diesel trains, both in excess of EU limits (Figure 7). Again this is presumably due to ingestion of diesel emissions by ventilation systems. Hopefully in the near future we will see the results of more quantitative investigations for the UK of on train NOX and particulate concentrations, and of work to investigate the ingestion of external pollutants, both from diesel emissions and dirty environments, by ventilation systems. However current indications are, that, care should be taken in using ventilations systems that draw external air into the train without the use of extensive filtering of the input.

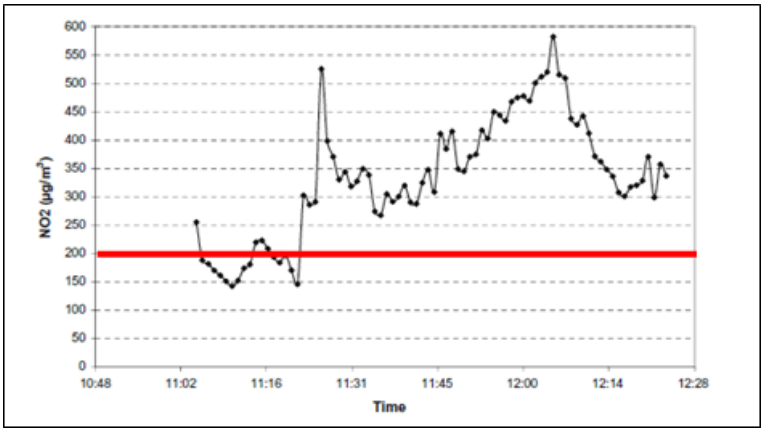


**Figure 7. NOX measurements on Greek train (red line is EU limit)**

And then along comes Covid-19. The importance of high levels of ventilation on reducing pathogen concentrations and thus the risk of infection is becoming clear – se for example the recent seminar organized by the University of Birmingham. Ideally, very high (airline) levels of air exchange with the outside are required in internal environments, including trains and buses. An interesting illustration of this is provided by the publicity material in figure 8

produced by SNCF in France. I have seen nothing similar for the UK. There is an obvious dichotomy here between the need to reduce external air intake to minimize NOX and PPM ingestion and to keep internal levels of NOX and particulates at an acceptable level, and the need to increase ventilation rates to decrease pathogen levels. Both could be achieved by aggressive filtration of the air drawn through the train. However, this is likely to require major modification to existing trains in Britain, that won't be cheap. I suspect train ventilation is going to become a major issue in the near future.

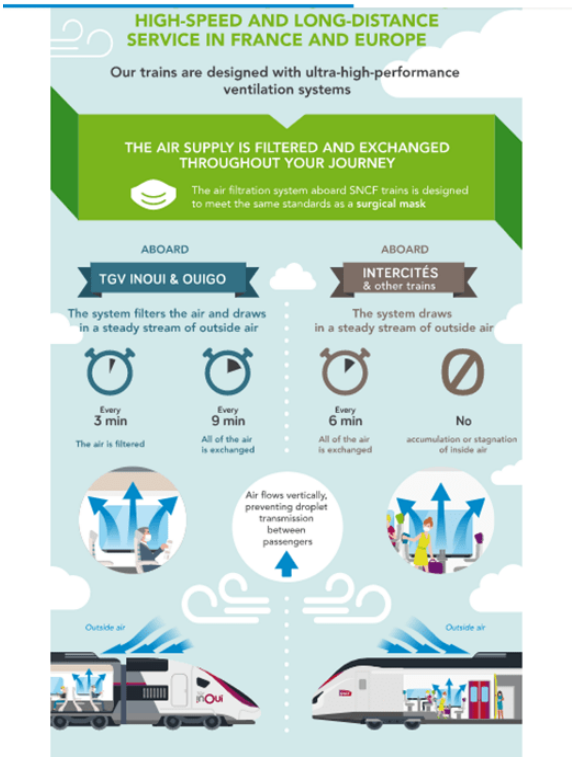


**Figure 8. SNCF publicity material**

# Some thoughts on ventilation and pathogen concentration build up

November 13, 2020

**Introduction**

Up till recently most attention had been focused on the spread of Covid-19 by near field transmission – being in close proximity to an infected person for a certain amount of time, and rather *ad hoc* social distancing rules have been imposed to attempt to reduce transmission. However, there is another aspect of transmission – the gradual build up of pathogen concentrations in the far field in enclosed spaces due to inadequate ventilation. The importance of this mode of transmission is beginning to be recognised The main tool that seems to have been used for both near and far field dispersion is Computational Fluid Dynamics (CFD) – see the graphic above from the University of Minnesota for example. Now whilst such methods are powerful and can produce detailed information, they are very much situation specific and not always easy to generalise. This post therefore develops a simple (one could even say simplistic) method for looking at the far field build up of pathogens in an enclosed space, in a very general way, to try to obtain a basic understanding of the issues involved and arrive at very general conclusions.

**The model**

We begin with equation (1) below. This is a simple differential equation that relates the rate of change of concentration of pathogen in an enclosed volume to the pathogen emitted from one or more individuals via respiration and the pathogen removed by a ventilation system. This assumes that the pathogen is well mixed in the volume and is a simple statement of conservation of volume.

$$\frac{dc}{dt}V = \delta q - Qc \qquad \text{equation (1)}$$

$c$ is the concentration, $V$ is the volume, $q$ is the respiration rate, $\delta$ is the concentration of the emitted pathogen, $t$ is time, and $Q$ is the flow rate of the ventilation system.

From the point of view of an individual, the important parameter is the pathogen dose. This is given by equation (2) and is the volume of pathogen ingested over time through respiration. The respiration rate here is assumed to be the same as that of the infected individual.

$$d = q\int_0^t c\,dt \qquad \text{equation (2)}$$

$d$ is the dose

Equations (1) and (2) can be expressed in the normalised form of equations (3) and (4) and simply solved to give equations (5) and (6).

$$\frac{d\bar{c}}{d\bar{t}} = 1 - \bar{c} \qquad \text{equation (3)}$$

$$\bar{d} = \int_0^t \bar{c}\,d\bar{t} \qquad \text{equation (4)}$$

$$\bar{c} = \frac{Qc}{q\delta} \qquad \bar{t} = \frac{Vt}{Q} \qquad \bar{d} = \frac{Q^2 d}{q^2 \delta V}$$

$$\bar{c} = 1 - (1 - \bar{c}_0)e^{-\bar{t}} \qquad \text{equation (5)}$$

$$\bar{d} = \bar{t} - (1 - \bar{c}_0)\left(e^{-\bar{t}} - 1\right) \qquad \text{equation (6)}$$

$\bar{c} = \bar{c}_0$ when $\bar{t} = 0$

Equations (5) and (6) are plotted in figures 1 and 2. Note that an increment of 1.0 in the normalised time in this figure corresponds to one complete air change in the enclosed volume. It can be seen that after around three complete air changes the concentration of pathogen reaches an equilibrium value and the dose increases linearly, whatever the starting concentration. To the level of approximation that we are considering here we can write the relationship between normalised dose and time in the form of equation (7), which results in the non-normalised form of equation (8).

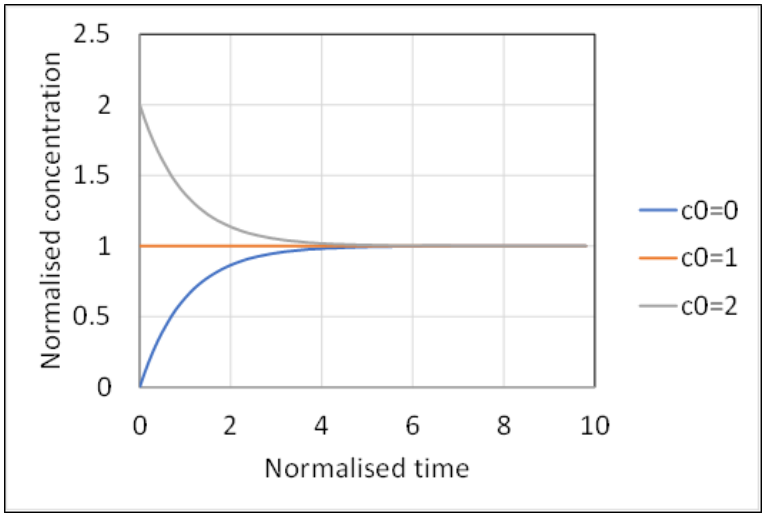


**Figure 1**

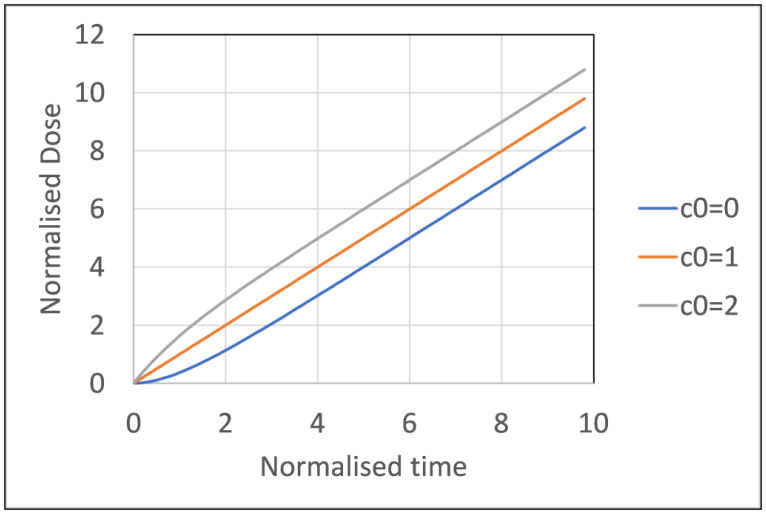


**Figure 2**

Assuming that there is a critical dose, the critical time after which this occurs is then given by equation (9).

$$\bar{d} = \bar{t} \qquad \text{equation (7)}$$

$$d = \frac{q^2 \delta t}{Q} = \frac{q^2 \delta t}{V\left(\frac{a}{3600}\right)} \qquad \text{equation (8)}$$

$a$ is the number of air changes / hour

$$t_c = \frac{d_c V\left(\frac{a}{3600}\right)}{q^2 \delta} \qquad \text{equation (9)}$$

Equation (9), although almost trivial, is of some interest. It indicates that the time required for an individual to receive acritical dose of pathogen is proportional to the volume of the enclosure and the ventilation rate. This is very reasonable – the bigger the enclosure and the higher the ventilation, the longer the time required. The critical time is inversely proportional to the concentration of the emission, which is again reasonable, but inversely proportional to the square of the respiration rate. This is quite significant and a twofold increase in respiration rate (say when taking exercise or dancing) results in the time for a critical dose being reduced by a factor of 4, or alternatively the need for ventilation rate to increase by a factor of 4 to keep the critical time constant. Similarly if there are two rather than one infected individuals in the space, then the respiration rate will double, with a reduction in the critical time by a factor of four.

**Discussion**

Now consider the implications of this equation for two specific circumstances that are of concern to me – travelling on public transport (and particularly trains) and attending church services. With regard to the former, perhaps the first thing to observe is that there is little evidence of Covid-19 transmission on trains, and calculated risks are low. In terms of the far field exposure considered here, respiration rates are likely to be low as passengers will in general be relaxed and sitting. This will increase the time to for a critical dose. On modern trains there will be an adequate ventilation system, and the time to reach a critical dose will be proportional to its performance. Nonetheless the likelihood of reaching the critical level increases with journey time – thus there is a *prima facie* need for better ventilation systems on trains that undergo longer journeys than those that are used for short journeys only. For trains without ventilation systems (such as for example the elderly Class 323 stock I use regularly on the Cross City line) has window ventilation only, and in the winter these are often shut. Thus ventilation rates will be low and the time to achieve a critical dose will be small.


**Class 323 at Birmingham New Street**

Now consider the case of churches. Many church buildings are large and thus from equation (9) the critical times will be high. However most church buildings do not possess a ventilation system of any kind, and ventilation is via general leakage. Whilst for many churches this leakage this can be considerable (....the church was draughty today vicar....), some are reasonable well sealed – this will thus, from equation (9) tend to reduce the critical time. In this case too the respiration rate is important. As noted above the critical time is proportional to the respiration rate squared. As the rate increases significantly when singing, this gives a justification for the singing bans that have been imposed.

**Church interior – Wikipedia Commons**

The above analysis is a broad brush approach indeed, and in some ways merely states the obvious. However it does give something of a handle on how pathogen dose is dependent on a number of factors, that may help in the making of relevant decisions. To become really useful a critical dose and initial pathogen concentration need to be specified together with site specific values of enclosed volume, ventilation rate and expected respiration rates. This would give at least approximate values of the time taken to reach a critical dose in any specific circumstance.

# Tornadoes and debris

November 13, 2020

*The debris trajectory animations of Figures 6 to 11 were provided by Professor Mark Sterling, whose ability to use advanced EXCEL functions seems to be significantly greater than mine. His contribution is much appreciated.*

**Previous work**

In 2017 Mark Sterling and I published the paper "Modelling wind field and debris flight in tornadoes", which described the integration of a tornado wind field model and the debris flight equations to look at the pattern of compact debris movement in tornadoes of different types. Typical results for falling and flying debris are shown in figure 1 below and give an indication of the complexity of the debris trajectories that were predicted.

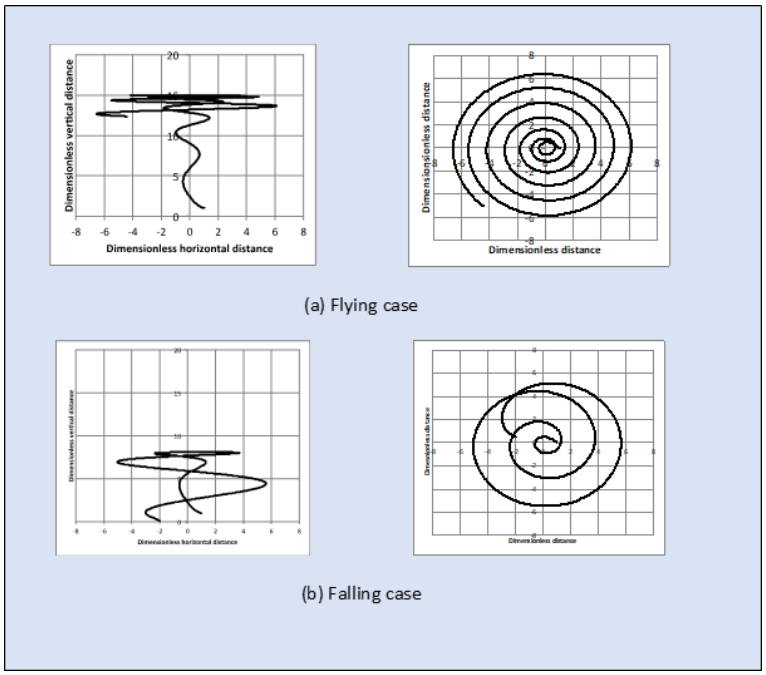


**Figure 1. Debris Trajectories from 2017 model**

Now whilst the tornado wind model that was used in the analysis was a considerable improvement over those that existed at the time, in that it gave a consistent three dimensional

velocity formulation, it did however have one major drawback. This was the fact that the vertical velocity component was unbound and increased with height, albeit quite slowly. In a more recent paper in 2020 "The lodging of crops by tornadoes", we developed an improved model, in which the vertical velocity peaked at a certain height and then decreased at greater heights. In this blog post I will briefly explore the use of this wind model to predict compact debris flight paths using the same methodology as in the first paper, and in doing so will illustrate the importance of the tornado model on debris trajectory prediction.

**The tornado wind model**

$$\bar{U} = -K \frac{\bar{r}^{\gamma-1}}{(1+\bar{r}^2)^{\gamma/2}} \frac{\bar{z}^{(\gamma-2)/2}(1-\bar{z}^2)}{(1+\bar{z}^2)^{(\gamma+2)/2}} \qquad \bar{V} = \frac{4\bar{r}\bar{z}}{(1+\bar{r}^2)(1+\bar{z}^2)}$$

$$\bar{W} = \delta K \frac{2\bar{r}^{\gamma-2}}{(1+\bar{r}^2)^{(\gamma+2)/2}} \frac{\bar{z}^{\gamma/2}}{(1+\bar{z}^2)^{\gamma/2}} \qquad K = \frac{F(\gamma)}{S}$$

**Figure 2. Velocities from 2020 model**

The expressions for the radial, circumferential and vertical velocities in the 2020 model are given in figure 2. Here the velocities are normalized by the maximum circumferential velocity and the radial and vertical distances by the radius at which the maximum velocity occurs. Note that this is different from the 2017 paper where the maximum radial velocity was used for normalization. The parameter *K* is related to what will be termed the swirl ratio *S* (the ratio of the maximum circumferential to maximum radial velocity) by a function of the parameter gamma, which is a shape parameter that affects the shape of the radial and vertical profiles. (Unfortunately this web template doesn't support Greek letters, so I have to spell them out). Figure 3 shows typical velocity profiles for different values of this parameter. It can be seen that for gamma = 2, the peak of the vertical velocity is at the vortex centre, as in a typical single cell vortex, whilst for higher values it moves away from the centre becoming more like a two cell vortex (but note there is no downflow at the vortex centre in this case.

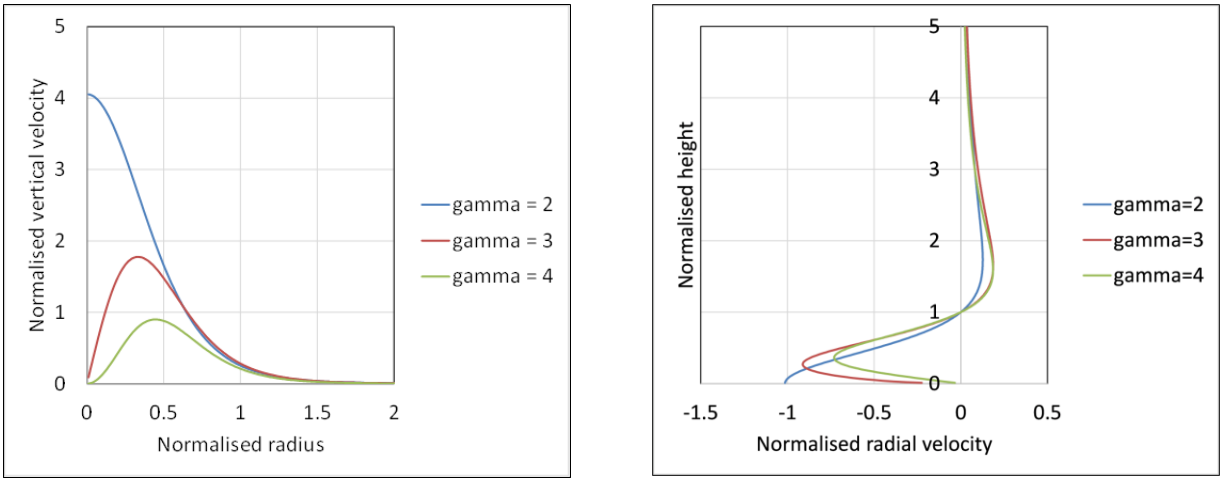


Figure 3. Velocity profiles from 2020 model (left- Normalised vertical velocity at a normalised height of 1.0; right – Normalised radial velocity profiles at a normalised radius of 1.0)

**Debris flight equations**

The equations for compact debris flight are given in figure 4. These are the same as in the 2017 paper, although expressed a little differently. The debris velocities (lowercase) in the three directions are again normalized by the maximum tangential tornado velocity. Two dimensionless parameter are identified – the Tachikawa number *Ta* that relates the flow force on the debris particle to its weight, and a tornado Froude number *Fr*. Different dimensionless parameters were used in the 2017 paper, because of the different reference velocity that was used

$$Fr\ \frac{d\bar{u}}{d\bar{t}} = Ta\ \bar{R}(\bar{U} - \bar{u}) + Fr\ \frac{\bar{v}^2}{\bar{r}}$$

$$Fr\ \frac{d\bar{v}}{d\bar{t}} = Ta\ \bar{R}(\bar{V} - \bar{v})$$

$$Fr\ \frac{d\bar{w}}{d\bar{t}} = Ta\ \bar{R}(\bar{W} - \bar{w}) - 1$$

$$\bar{R} = ((\bar{U} - \bar{u})^2 + (\bar{V} - \bar{v})^2 + (\bar{W} - \bar{w})^2)^{0.5}$$

$$\bar{t} = \frac{tV_m}{r_m} \qquad Ta = \frac{0.5\rho A V_m^2}{Mg} C_D \qquad Fr = \frac{V_m^2}{g r_m}$$

$\bar{U}, \bar{V}$ and $\bar{W}$ are the normalised wind velocity components
$\bar{u}, \bar{v}$ and $\bar{w}$ are the normalised debris velocity components
$\bar{t}$ is the normalised time
$V_m$ is the maximum tangential velocity
$r_m$ is the radius at which the tangential velocity is maximum
$M$ is the debris mass
$A$ is the debris frontal area
$C_D$ is the debris drag coefficient.

Figure 4. Debris flight equations

**Solutions**

| | | | |
|---|---|---|---|
| Tornado parameter | $S = 1$ | $\gamma = 2$ | $Fr = 1$ |
| Debris parameter | $Ta = 100$ | | |
| Starting positions | $\bar{r}_0 = 1$ | $\bar{z}_0 = 1$ | |

**Figure 5. Base case parameters**

Putting together the velocity equations in figure 2 and the particle flight equations in figure 4, it can be seen that there are four parameter that define debris trajectories – the tornado parameters S, gamma and Fr, and the debris Tachikawa number Ta. In addition any one flight trajectory will be defined, at least in its early stages by the dimensionless values of the radius and height at its release point. If these six parameters are specified then the equations of debris flight can be solved in a straightforward manner. In what follows we define a base case situation as in figure 5, and then vary each of the parameters around this base case value. We present the results in the animations of figures 6 to 11.Each animation shows four plots – the trajectories projected onto a vertical plane through the tornado centre; the trajectories projected onto a horizontal plane; the trajectories in a rotating plane in the radial and vertical directions, and a plot of the variation of particle kinetic energy with time. The latter acts as a damage indicator of debris flight, but also clearly shows whether or not the solution converges or diverges with time. Note that the dimensionless time shown in the kinetic energy plots is proportional to the time of revolution of the vortex – a time of 2 pi corresponds to one vortex revolution.

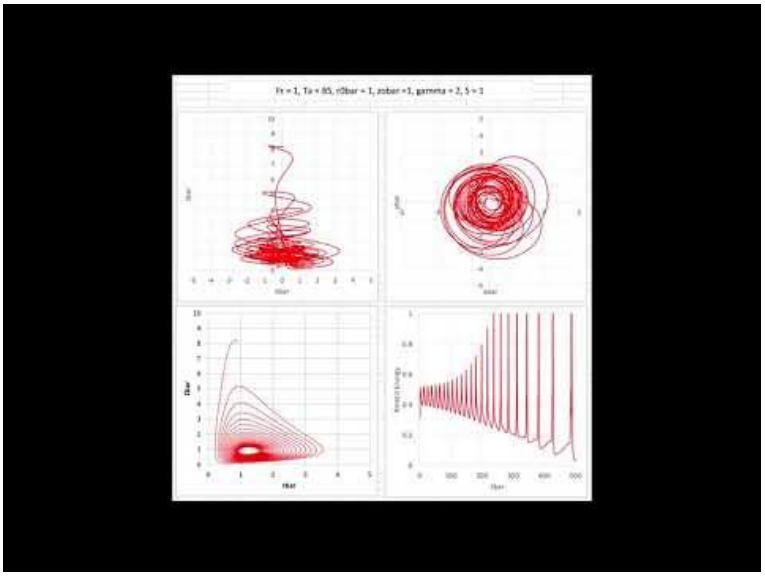

**Figure 6. Effect of variations in Tachikawa number**

First consider the effect of changing Tachikawa number, *Ta* – see Figure 6. This represents changes in the nature of the debris. A low value of Ta represents heavy debris and vice versa. It

can be seen that at low values of *Ta*, the debris tracks can reach significant heights and the debris undergoes a diverging motion when viewed in the radius / height plane, with a diverging kinetic energy oscillation. At some point in the trajectory the debris hits the ground and the energy falls to zero. The base case situation at *Ta* = 100 is still mildly diverging but the trajectory does not intersect the ground plane for the length of the calculation. As *Ta* increases further, the debris takes up a stable path in the radius / height plane travels around a small circular trajectory, with the kinetic energy converging to a stable value. This suggest that light debris can reach an equilibrium where it is held aloft by the tornado. The position around which the circular motion takes place is around a normalized radius of 1.3 and a normalized height of 0.9. The value of height is much less than calculated in the 2017 paper, reflecting the fact that the vertical velocity does not decrease indefinitely with height for the new model as it did in the old.

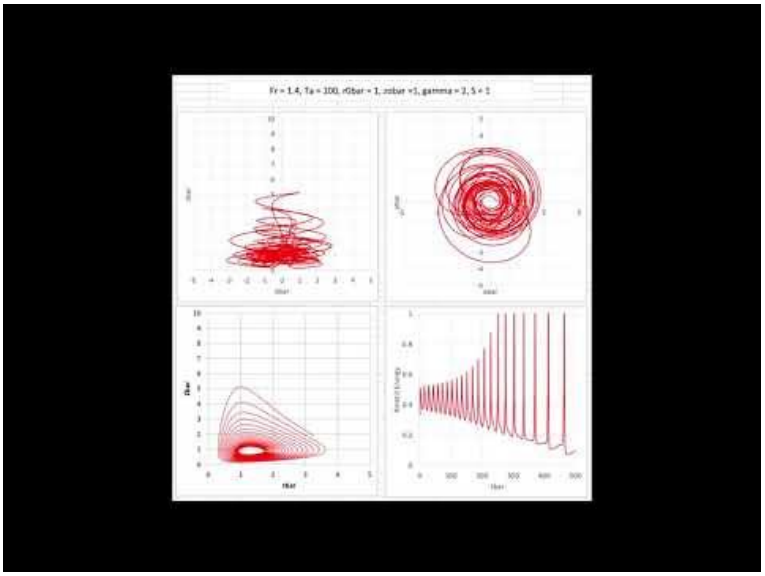

**Figure 7. Effect of variations in Froude number**

The effect of variations in Froude number is shown in Figure 7. The primary effect that increase in *Fr* has is to increase the centrifugal force on the debris. At low values, the trajectories are stable and similar to that of the base case. As the values increase above 1.0 the oscillations become larger due to the increased centrifugal forces and eventually become unstable, with the trajectories meeting the ground at high values.

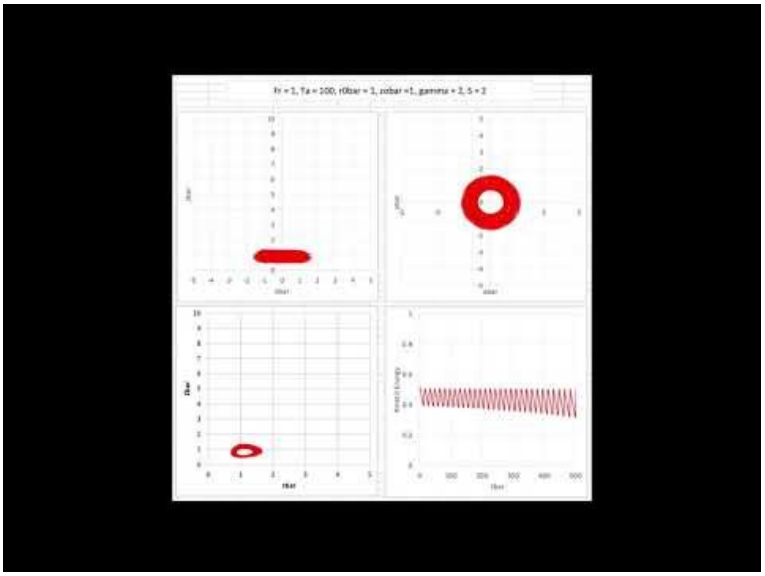

**Figure 8. Effect of variation in Swirl Ratio**

The effects of variations in the Swirl ratio shown in Figure 8 are complex, with diverging trajectories (and ground impact) at both low and high values, and a region of stable trajectories between values of around 1.0 to 1.9. At low values the trajectories are destabilized by the high values of radial velocity, and at high values are destabilized by high values of the circumferential velocity.

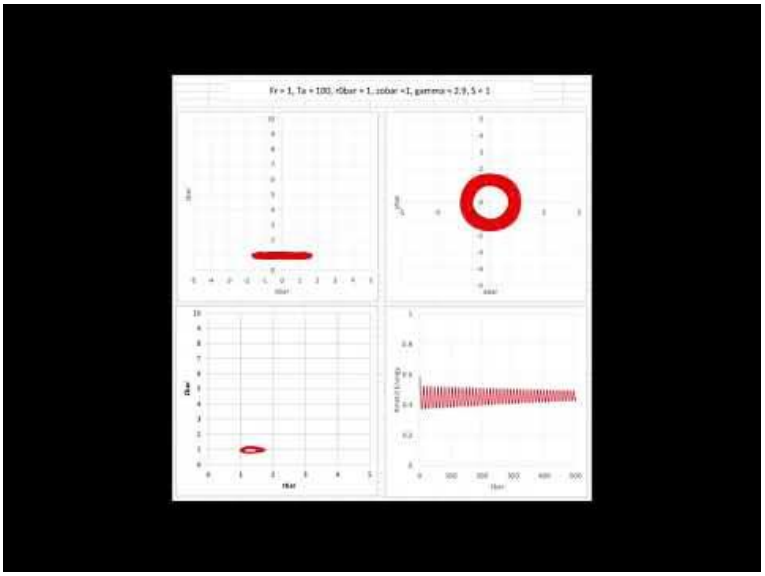

**Figure 9 Effect of variations in gamma**

The change in values of gamma from the one cell form of gamma = 2 to the quasi-two cell form of gamma = 4 shown in Figure 9 results in little change to the debris trajectories from the base case, although the oscillations in the kinetic energy fall as gamma increases.

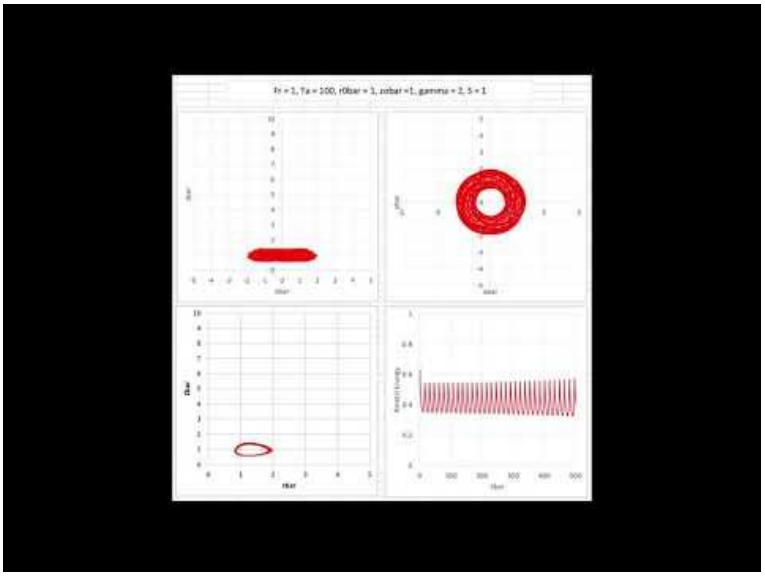

**Figure 10. Effect of variations in radial starting position**

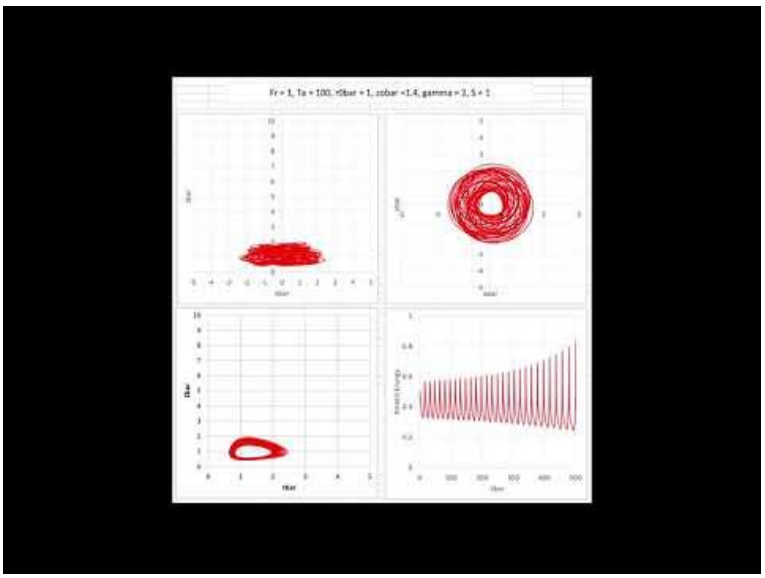

**Figure 11. Effect of variations in vertical starting position**

The debris trajectories remain stable as the normalized radius varies between 1 and 1.9 but outside those limits the trajectories diverge and intersect with the ground (Figure 10). Similarly the trajectories are only stable for normalized values for height between 0.8 and 1.2 (Figure 11). Thus the starting point window for the trajectories to ultimately attain a stable form is quite small.

**Concluding remarks**

A number of points arise from the results presented above.

- Even for the simple wind and debris flight formulation adopted, debris trajectories can be quite complex.

- A comparison of the results obtained with the old and the new wind field model show very considerable differences, due to the different vertical velocity formulation. analysis reveals that the debris trajectories can be specified by a small number of debris and tornado parameters, with the Tachikawa number and the Swirl Ratio being the most significant.
- There are regions within parameter space for which the debris trajectories become stable – i.e. the debris flies indefinitely.

# International Wind Engineering seminars 2020/21


**Purpose**

Because of the Covid19 pandemic, opportunities for the international wind engineering community to meet physically were very much restricted in 2020 and 2021. To enable the community to continue to interact with each other, at least in a virtual way, the University of Birmingham organised a series six seminars via Zoom from October 2020 to March 2021. These were sponsored by the IAWE and had a significant international audience. Each seminar lasted around an hour and a half to two hours, and consisted of a main speaker for around 30 minutes followed by further short contributions or a panel debate with opportunities for online discussion by those attending.

**Programme and Keynote speakers**

*Abstracts, biographies and in some cases discussion summaries are given in Appendix 1.*

Seminar 1. Thursday October 8th 2020 — Tornadoes – research and design (Prof Greg Kopp, University of Western Ontario)

Seminar 2. Thursday November 5th 2020 – Indoor and outdoor ventilation and dispersion (Prof Bert Blocken, Eindhoven University, The Netherlands; KU Leuven, Belgium)

Seminar 3. Thursday December 3rd 2020 – Modeling the Dynamics of Tall Buildings Under Winds: From Historical Perspective to Recent Advances and Beyond (Prof Ahsan Kareem, University of Notre Dame)

Seminar 4. Thursday January 7th 2021 – Developments in bridge aerodynamics (Prof John Owen, University of Nottingham)

Seminar 5. Thursday February 11th 2021. Wind loading code developments. (Svend Ole Hansen, Svend Ole Hansen ApS).

Seminar 6. Thursday March 4th 2021 – Wind-related Disaster Risk Reduction: Current Status and Future Prospects (Prof Yukio Tamura, Chongqing University)

## Recordings of presentations

**Seminar 1 Main Speaker**

**Seminar 1 short presentations**

**Seminar 2 Main Speaker**

**Seminar 2 short presentations**

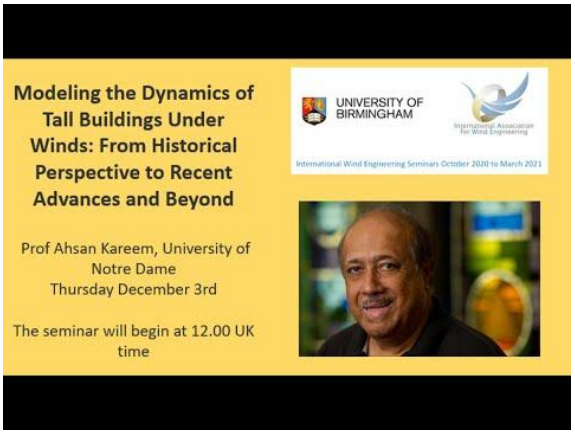


**Seminar 3 Main Speaker**

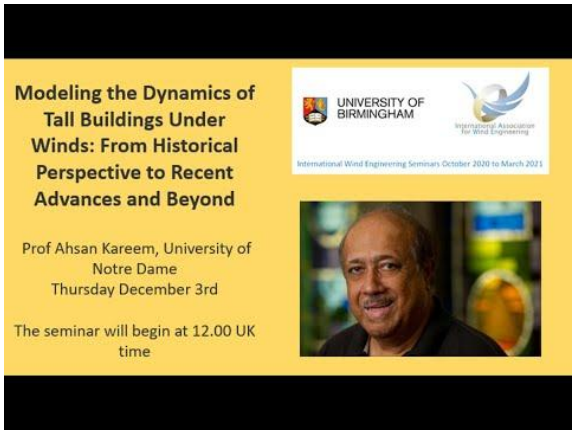


**Seminar 3 short presentations**


**Seminar 4 Main Speaker**


**Seminar 4 short presentations**


**Seminar 5 Main Speaker**


**Seminar 5 short presentations**


**Seminar 5 Questions and answers**

**Se**

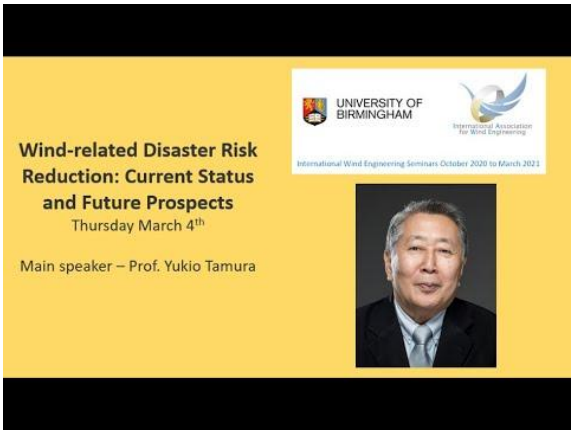


**Seminar 6 Main Speaker**

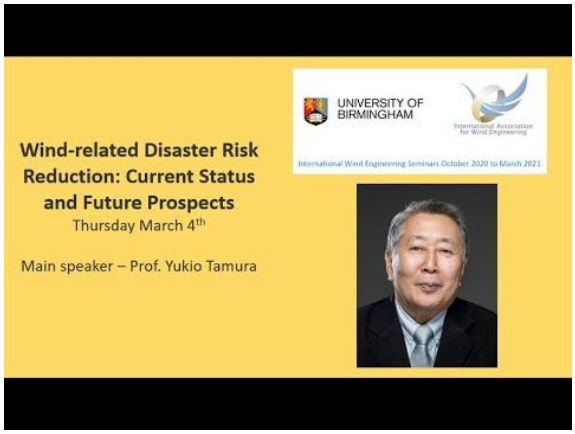


**Seminar 6 short presentations**

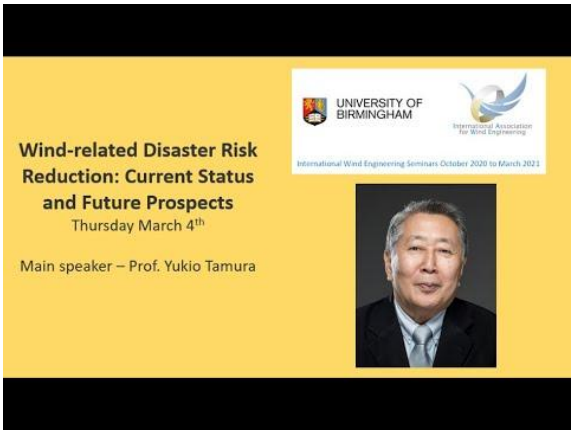


**Seminar 5 Questions and answers**

# International Wind Engineering seminars 2020/21 – some reflections

March 15, 2021

A Japanese version of this post can be found here


Between October 2020 and March 2021, I organised a series of six International Wind Engineering Seminars, through the University of Birmingham, my employer before I retired. These were sponsored by the International Association of Wind Engineering (IAWE) and delivered via Zoom. The justification for organising it was as follows.

*"Because of the Covid19 pandemic, opportunities for the international wind engineering community to meet physically have been very much restricted and are likely to remain so for at least the next year. To enable the community to continue to interact with each other, at least in a virtual way, the University of Birmingham is organizing a series of six seminars via Zoom from October 2020 to March 2021."*

In this post, I want to reflect on how these seminars were delivered and received, what lessons might be learnt, and ask some questions concerning the future.

Each seminar consisted of a main speaker, followed by either a panel discussion or between two and four shorter presentations. The dates and topics are given in table 1. As these seminars were set up in some haste in August / September 2020, I mainly called upon my circle of contacts to be the main speakers at the events, and they suggested other speakers or panel members. I am indebted to all the speakers for taking part and spending considerable time in preparation. The nature of the delivery and follow up evolved over the course of the series. After the first seminar it became clear that I could not both chair the sessions and organise the questions in Chat to put to the speakers. Thus, from seminars 2 to 6, I was assisted by Grace Yan from Missouri who collated all the questions that were put on Chat and forwarded them to me to put to the speakers. Her help was hugely appreciated. For seminars 3, 4 and 6 the presenters and panellists were also asked to provide written answers to questions, and these were posted on the web pages that were for each of the seminars. All the presentations (and for seminars 5 and 6 the questions and answers) were recorded using the Zoom Record function and these recordings were place on my YouTube site and linked to the

appropriate page. These pages also included talk abstracts and speaker biographies. After the third seminar I realised that YouTube could not be accessed from all parts of the world, so a link to the Zoom cloud versions was also given. From seminar 4 onwards, these could also be downloaded as required. The time chosen for the seminars (after the first) was 12.00 UK time, this being the best compromise for most time zones, with the exception of the west coast of the America and Australasia. I tried to institute a separate Q and A session for these time zones a day or so after the seminar, but there was insufficient take up to make it worthwhile. Thus the whole process was a considerable learning experience for me.

| Seminar date | Subject | Main Speaker | Other presenters / Panel Members |
|---|---|---|---|
| 08/10/2020 | Tornadoes – research and design | Prof Greg Kopp, University of Western Ontario | Dr Franklin T. Lombardo, University of Illinois, USA<br>Prof. Mark Sterling, University of Birmingham, UK<br>Dr Grace Yan, Missouri University of Science and Technology<br>Prof Shuyang Cao, Tongji University, China<br>Prof Chris Baker, Emeritus University of Birmingham, UK<br>Prof Fred Haan, Jr., Calvin University, Michigan, USA |
| 05/11/2020 | Indoor and outdoor ventilation and dispersion | Prof Bert Blocken, Eindhoven University, The Netherlands; KU Leuven, Belgium | Prof Ted Stathopoulos, Concordia University, Montreal, Canada<br>Prof Kenny Kwok, University of Sydney, Australia<br>Prof Yoshihide Tominaga, Niigata Institute of Technology, Japan<br>Dr. Eoghan Clifford, NUI Galway, Republic of Ireland |
| 03/12/2020 | Modelling the Dynamics of Tall Buildings Under Winds | Prof Ahsan Kareem, NatHaz Modelling Laboratory, University of Notre Dame, USA | Professor Yukio Tamura, Chongqing University, China<br>Dr. Melissa Burton, Arup, Toronto, Canada<br>Dr. Tracy Kijewski-Correa, Keough University of Notre Dame, USA<br>Dr. John Kilpatrick, RWDI, Guelph, Canada |
| 07/01/2021 | Developments in bridge aerodynamics | Dr John Owen, School of Engineering, University of Nottingham, United Kingdom | Prof Steve Cai, Louisiana State University<br>Prof Claudio Mannini, University of Florence<br>Prof Ole Andre Øiseth, Norwegian University of Science and Technology<br>Prof Luca Caracoglia, North Eastern University, Boston |
| 11/02/2021 | Wind loading code developments | Svend Ole Hansen, Svend Ole Hansen ApS | Prof Francesco Ricciardelli, University of Campania, Italy<br>Professor John Dora, Climate Sense<br>Donald Scott, PCS Structural Solutions. |
| 04/03/2021 | Wind-related Disaster Risk Reduction | Professor Yukio Tamura, School of Civil Engineering, Chongqing University, China | Professor Forrest J. Masters, University of Florida<br>Professor Chris Baker, School of Engineering, University of Birmingham |

**Table 1 Seminar dates, titles and speakers**

It must be mentioned at this point that the third seminar occurred shortly after the death of Prof Giovanni Solari, who was instrumental in the setting up of the IAWE, and the speaker, Prof Kareem, paid tribute to him in his talk.

**Prof. Giovanni Solari**

Table 2 shows the bare statistics for the seminars. The size of the distribution list for publicity grew through the series from the original 688 of the mailing list for the abortive BBAA conference to 1525 for seminar 6. By seminar 3 the size of the list became so large that my e mail account was temporarily stopped as it was thought it had been hacked and was sending out spam. Thereafter I sent the information around in smaller batches. The number of registrants varied between 279 and 616, although only around 50 to 70% of these actually connected. The number of video views was also encouraging although again one must interpret these numbers cautiously as only around 20 to 30% of the views were for more than a few minutes. Note that these statistics are up to March 14th 2021 only, and as the views continued for several months after each seminar, the number of video views for the 2021 seminars will not be the final values.

| | Circulation list | Registrants | Video views of main talk YouTube | Video views of short talks YouTube | Video views of Q and A YouTube | Video views Zoom | Video downloads Zoom |
|---|---|---|---|---|---|---|---|
| **Seminar 1** | 688 | 279 | 140 | 110 | - | - | - |
| **Seminar 2** | 839 | 360 | 586 | 232 | - | - | - |
| **Seminar 3** | 1031 | 616 | 324 | 153 | - | 134 | 4 |
| **Seminar 4** | 1374 | 392 | 140 | 134 | - | 49 | 29 |
| **Seminar 5** | 1483 | 365 | 143 | 76 | 45 | 59 | 24 |
| **Seminar 6** | 1525 | 338 | 51 | 42 | 19 | 141 | 5 |

**Table 2 Seminar statistics (up to March 14th 2021)**

Table 3 shows a breakdown of the views of the seminar web pages by month (which includes links to the videos). As expected these peak just before and just after the seminar, but all the seminars attract a significant number of views for a number of months after the event, which suggest that the subject matter is of ongoing interest. Again, note that this date only extends to the middle of March 2021,and a significant number of views could be expected for the later seminars after this date.

| | Sep-20 | Oct-20 | Nov-20 | Dec-20 | Jan-21 | Feb-21 | Mar-21 |
|---|---|---|---|---|---|---|---|
| **Seminar 1** | 288 | 459 | 52 | 47 | 19 | 38 | 5 |
| **Seminar 2** | 14 | 503 | 538 | 56 | 24 | 35 | 5 |
| **Seminar 3** | | 15 | 819 | 947 | 68 | 40 | 15 |
| **Seminar 4** | | | 15 | 317 | 509 | 86 | 14 |
| **Seminar 5** | | | | | 147 | 498 | 44 |
| **Seminar 6** | | | | | 3 | 413 | 362 |

**Table 3 Views of seminar web pages (up to March 15th 2021)**

Table 4 shows the location of those who registered, as far as could be judged from email addresses. The generic .com address contains registrants from a wide variety of countries, and this rather skews the results. Nonetheless, it can be seen that whilst those countries where wind engineering is well established are well represented, a very wide range of countries was represented overall.

| | Seminar 1 | Seminar 2 | Seminar 3 | Seminar 4 | Seminar 5 | Seminar 6 |
|---|---|---|---|---|---|---|
| .com | 70 | 120 | 282 | 168 | 154 | 145 |
| Other generic | 3 | 5 | 6 | 6 | 6 | 6 |
| Algeria | 1 | 1 | 1 | 0 | 1 | 0 |
| Australia | 3 | 9 | 16 | 4 | 8 | 5 |
| Austria | 0 | 2 | 3 | 2 | 2 | 0 |
| Belgium | 0 | 11 | 8 | 7 | 4 | 3 |
| Brazil | 0 | 0 | 0 | 0 | 2 | 1 |
| Canada | 22 | 16 | 23 | 10 | 9 | 7 |
| China | 27 | 22 | 35 | 19 | 9 | 17 |
| Croatia | 1 | 2 | 2 | 1 | 2 | 0 |
| Czechia | 0 | 0 | 0 | 1 | 0 | 0 |
| Denmark | 2 | 4 | 3 | 9 | 25 | 2 |
| Eire | 1 | 3 | 7 | 3 | 5 | 3 |
| France | 3 | 6 | 5 | 6 | 2 | 3 |
| Germany | 8 | 8 | 25 | 17 | 15 | 10 |
| Greece | 0 | 1 | 1 | 0 | 0 | 0 |
| Hong Kong | 10 | 8 | 10 | 6 | 3 | 6 |
| Iceland | 1 | 1 | 1 | 0 | 1 | 0 |
| India | 4 | 3 | 3 | 2 | 3 | 2 |
| Indonesia | 0 | 0 | 5 | 2 | 2 | 3 |
| Italy | 11 | 10 | 17 | 19 | 18 | 12 |
| Japan | 22 | 30 | 24 | 12 | 7 | 16 |
| Luxemburg | 0 | 0 | 0 | 0 | 1 | 0 |
| Macedonia | 1 | 0 | 0 | 0 | 0 | 0 |
| Malaysia | 0 | 2 | 5 | 1 | 1 | 2 |
| Mexico | 2 | 1 | 2 | 2 | 2 | 1 |
| Netherlands | 6 | 18 | 11 | 4 | 8 | 6 |
| New Zealand | 1 | 5 | 4 | 1 | 2 | 3 |
| Norway | 2 | 3 | 8 | 13 | 11 | 5 |
| Pakistan | 1 | 0 | 1 | 0 | 0 | 0 |
| Poland | 6 | 4 | 6 | 1 | 2 | 3 |
| Portugal | 3 | 3 | 3 | 2 | 1 | 0 |
| Romania | 5 | 3 | 2 | 2 | 4 | 0 |
| Saudi Arabia | 0 | 1 | 1 | 1 | 1 | 0 |
| Slovakia | 0 | 1 | 2 | 1 | 0 | 0 |
| South Korea | 2 | 0 | 3 | 11 | 0 | 2 |
| Spain | 10 | 12 | 9 | 10 | 8 | 6 |
| Switzerland | 0 | 1 | 1 | 1 | 1 | 0 |
| Turkey | 1 | 2 | 1 | 2 | 0 | 0 |
| UK | 21 | 21 | 35 | 17 | 13 | 16 |
| Uruguay | 0 | 0 | 0 | 0 | 0 | 1 |
| USA | 28 | 17 | 45 | 27 | 30 | 46 |
| Vietnam | 0 | 0 | 0 | 1 | 0 | 0 |

**Table 4 Locations of registrants**

Thus the numbers suggest that there was a significant number of wind engineers around the world who appreciated the seminar series and found them useful, and indeed that is what has been suggested by the informal feedback I have received. Again, caution is required to avoid over interpretation – the level of engagement with online seminars is likely to be much less than with in person presentations – I for one tend to do things such as checking my e mail / cricket scores when attending such virtual events – but not when I am chairing of course! But broadly the seminar series seems to have met a need. But there are needs it hasn't addressed, for example the inclusion of a social aspect for informal discussion and the inclusion of young researchers in a meaningful way etc. To address this sort of issue, other formats can be envisaged – for example I can think of the following.

- Specific discussion topics could be set, and potential attendees asked to submit short abstracts of a two minute, two slide talk, from which a balanced group of young and established researchers could be selected for a series of short presentations and a more relaxed discussion. These could be recorded and put on-line for all to see.
- Interviews (by me or others) of a range of wind engineers, talking about their careers, their successes and failures etc., which could again be recorded and put on-line.
- The use of a platform such as Gather Town, which seems to allow for multiple individual conversations within a group structure and could be used for, say, virtual poster sessions (but note I have never used this, although on the face of things it seems potentially useful.)

And there are no doubt other possibilities. The question then arises as to what should happen next. I don't intend to organise any more such seminars till September at least – amongst other things I wish to watch a number of cricket matches rather than just checking the scores, and to re-acquaint myself with a number of heritage railways in Wales. So, I put the following questions to the wind engineering community.

- Should something similar be organised for next winter as I suspect international travel won't resume in any real sense until Summer 2022 at best? Note that I am not necessarily implying that should something felt to be necessary, then I would be the one to organise it!
- If so, what should the format be – just one speaker, or more than one speaker, or something completely different?
- Are there any suggestions for topics and speakers?
- Are there any other suggestions for possible related activities, such as I mention above.

There is also a larger question of course about the future of the four year cycle of Wind Engineering conferences and whether such a cycle is still sustainable – see for example the initiative of Glasgow University which is urging academics to reduce overseas travel as part of

the greening of its activities. But that is a discussion for others to have within the IAWE committee.

# Giovanni Solari 1953-2020

April 19, 2021


*On April 19th 2021 an online memorial event was held to celebrate the life of Prof Giovanni Solari of the University of Genoa who died five months previously. His career is well described in a memorial article in the Journal of Wind Engineering that can be found here. I was one of over 20 friends and colleagues who spoke at the event. My short contribution is given below.*

Giovanni Solari has left us a very considerable legacy, and I would like to briefly consider three aspects of this. The first is his legacy to the wind engineering community. He was the first President of the International Association of Wind Engineering and held that role from 2003 to 2007. But that role involved much more than a ceremonial aspect. He was instrumental in turning the IAWE from a very loose association that met for an extended supper every four years at the major conferences to a legally organised society with a properly formulated constitution, member organisations and a functioning secretariat. This involved much work with lawyers (an unenviable task) and much travelling and discussion. In a real way the existence of an international wind engineering community is one of Giovanni's major legacies.

The second aspect I want to mention is his intellectual legacy. Giovanni had the gift of being able to take a complex physical or engineering problem, often in the field of structural dynamics, and to express this problem mathematically in such a way that he could obtain closed form solutions for the engineering parameters of interest. These were often complex but allowed a proper appreciation of the role of different material and loading properties to be understood and generalised. Giovanni was the master of the closed form solution. In these days, when it is so easy simply to throw computer power at a difficult problem through complex CFD of FE analysis, the need for such closed form solution becomes all the greater to inform calculations and to actually understand the issues in depth. Giovanni's intellectual legacy, of doing the hard thinking and analysis before resorting to numerical calculation, is a very important one to keep hold of.

The third of the legacies I want to mention is a personal one. I believe I first met Giovanni at the first European Conference on Wind Engineering in the early 1990s. Certainly we began to correspond after that (and remember those were the days before the instant gratification of

emails) and I paid a memorable visit to Genoa around that time where the highlight for me was the ability to spend some hours in the library, which was much better resourced in wind engineering terms than that of my own institution. I was received with courtesy and kindness and Giovanni spent time showing me around the city that he clearly loved. Over the years that same courtesy and kindness has been shown by Giovanni to numerous people – from research students at the very start of their careers to the more senior of us. And that is how many of us, myself included, who remember him – for his personal legacy as much as for his undoubted scholarship, organisational and intellectual legacies, as the kindest and most courteous of friends and colleagues. He will be very much missed by many in the community.

Giovanni – Requiescat in pace

# Covid-19 and train ventilation

May 9, 2021


Recently the Rail Delivery Group has issued a short video animation of which the above is a screenshot. This addresses, for the first time, the need for good ventilation to decrease the risk of Covid infection on trains. Aerosol transmission is now regarded as the primary mode of pathogen transmission and infection is much more likely via this route than from surface transmission, despite the emphasis that has been given to the latter. So this little video is to be welcomed. But in telling us that train ventilation systems change the air every 6 to 9 minutes, giving the number of air changes per hour (ACH) of between 7 and 10, it rather begs the question as to what actually is an adequate ventilation rate to minimize infection risk. In a blog of November 2020, I addressed this issue in a rather simplistic way and came up with the expression shown below. This simple formula says that the time for a critical pathogen dose increases with increases in the value of the critical dose and in the number of air changes per hour, but decreases with increases in the respiration rate of infected individuals and the initial concentration of the pathogen. This all seems very reasonable, but precise values depend crucially on the values of critical dose, respiration rate and initial concentration. I would guess such values are available (or at least arrange of them) but I don't have easy access to them.

$$t_c = \frac{d_c V(\frac{a}{3600})}{q^2 \delta}$$

$t_c$ is the time for a passenger to receive acritical dose of pathogen.

$a$ is the number of air changes per hour.

$V$ is the volume of the carriage.

$d_c$ is the critical dose of pathogen.

$q$ is the respiration rate of an infected individual.

$\delta$ is the concentration of the emitted pathogen from the infected person.

But let us assume for the sake of argument that the current air exchange rates on trains are adequate to keep the risk of infection low (but note that they are significantly less than in aircraft, where 25 to 30 ACH seem to be common). This only applies of course to trains with air conditioning systems, but there are trains that rely on window opening for ventilation – not

least the Class 323s on the Cross City line in Birmingham – the trains that I travel on most frequently. How does the ventilation of these trains compare with that for air-conditioned trains.?

For such trains the ventilation mechanism will be what can be referred to as shear layer ventilation – the flow in and out of the train windows and doors due to the relative air movement when the train is moving, or due to wind effects when the train is stationary. In some work from about 20 years ago, a research student and myself derived the simple expression shown below for shear layer ventilation for wind passing across an opening in a large box structure.

$Q = kAv$

$Q$ is the ventialtion rate.

$A$ is the opening area.

$V$ is the velocity across the opening.

$k$ is a constant of the order of 0.05.

$ACH = 3600\ Q/V$

The application of this method to train ventilation is a bit of a stretch, and one would not expect any great accuracy. For the Class 323, we the assume the following: 22 windows/carriage, area of window opening window of 0.02m$^2$, giving a total opening area of 0.44m$^2$; 2 open doors per carriage with an opening area of 4m$^2$ giving a total opening area of 8m$^2$; a carriage volume of 80m$^3$. We also assume that for both doors and windows, the coefficient k=0.05. The train speed when moving is taken as 20m/s, and the wind speed when the train is stationary is taken as 1m/s. In operation we assume that the train is moving for 90% of the time and stationary for 10% of the time. Based on these figures we can calculate the number of air changes per hour for when the train is moving and when it is stationary. For the former we get an ACH of 3600(20*0.44*0.05*0.9) /80= 17.8, and for the latter an ACH of 3600(1*8*0.05*0.1) /80= 1.8.

The simplicity of this method needs to be emphasised and the results should only be regarded as approximations. Nonetheless they are of interest. Firstly the figures suggest that with all windows open, the ventilation of the Class 323 is twice as high as on a typical air conditioned system. This ties in with my personal experience – when the windows are open to this extent in the summer, there is a strong (and if the weather is hot, pleasant) draft through the carriage. If only half the windows are open, the overall ventilation is equivalent to an air conditioned system. Secondly, the amount of ventilation due to doors opening in stations is small in comparison to the maximum window ventilation. This leads to the third point – if all the windows are shut (as would be the case in the winter) the overall ventilation is well below the air-conditioned case. ***It is perhaps for such vehicles in such conditions that we should look for the critical case of pathogen transmission on trains.***

# The calculation of Covid-19 infection rates on GB trains

June 16, 2021


**Preamble**

In a recent post I looked at the ventilation rate of trains without air conditioning and compared them with the ventilation rate of airconditioned trains. The context was the discussion of the safety of trains in terms of Covid-19 infection. For air conditioned trains, the industry accepted number of air changes per hour is around 8 to 10. For non-air conditioned trains with windows fully open and doors opening regularly at stations, I calculated very approximate values of air changes per hour of around twice this value, but for non-air conditioned trains with windows shut and thus only ventilated by door openings, I calculated approximate values of a of 2.0. On the basis of these calculations, I speculated that the non-air conditioned trains with windows shut probably represented the critical case for Covid-19 transmission. In that post however I was unable to be precise about the level of risk of actually becoming infected and how this related to ventilation rate.

**The work of Jimenez**

I have recently come across the spreadsheet tool produced by Prof. Jose Jimenez and his group at the University of Colorado-Boulder that attempts to model airborne infection rates of Covid-19 for a whole range of different physical geometries, using the best available information on pathogen transport modelling, virus production rates, critical doses etc. They base their analysis on the assumption that aerosol dispersion is the major mode of virus transport, which now seems to be widely accepted (and as anyone who has been following my blogs and tweets will know that I have been going on about for many months). I have thus modified the downloadable spreadsheet to make it applicable to the case of a standard GB railway passenger car compartment. A screen shot of the input / output to the spreadsheet is shown in figure 1 below.

| | A | B | C | D | E | F | G | H |
|---|---|---|---|---|---|---|---|---|
| 1 | **Environmental Parameters** | | | | | **Result for for one journey** | | |
| 2 | Length of vehicle | 20.00 | m | | | | | |
| 3 | Width of vehicle | 3.00 | m | | | **One passenger** | | |
| 4 | Height of vehicle | 3.00 | m | | | Probability of infection | 0.0960% | |
| 5 | Duration of event | 30.00 | min | | | Prob. of hospitalization | 0.0192% | |
| 6 | Number of repetitions of journey | 10.00 | | | | Prob. of death | 0.0000% | |
| 7 | Ventilation w/ outside air | 8.00 | ach | | | | | |
| 8 | Decay rate of the virus | 0.62 | h-1 | | | **All passengers** | | |
| 9 | Deposition to surfaces | 0.30 | h-1 | | | Number of COVID cases arising | 0.0383 | |
| 10 | Additional control measures | 3.60 | h-1 | | | N of hospitalizations arising | 0.0077 | |
| 11 | | | | | | N of deaths arising | 0.0000 | |
| 12 | **Parameters related to people and activity in vehicle** | | | | | | | |
| 13 | Total N people in vehicle | 80.00 | | | | **Result for multiple journeys** | | |
| 14 | Fraction of population inmune | 50.00% | | | | | | |
| 15 | Fraction of people w/ masks | 0.00% | | | | **One passenger** | | |
| 16 | Breathing rate (susceptibles) | 0.42 | m3 / h | | | Probability of infection | 0.9555% | |
| 17 | Quanta exhalation rate (infected) | 25.00 | infectious doses (quanta) h-1 | | | Prob. of hospitalization | 0.1911% | |
| 18 | Exhalation mask efficiency | 50.00% | | | | Prob. of death | 0.0000% | |
| 19 | Inhalation mask efficiency | 30.00% | | | | | | |
| 20 | Q. enhancement due to variants | 1.00 | | | | **All passengers** | | |
| 21 | | | | | | Number of COVID cases arising | 0.3814 | |
| 22 | **Parameters related to the COVID-19 disease** | | | | | N of hospitalizations arising | 0.0763 | |
| 23 | Probability of being infective | 0.20% | | | | N of deaths arising | 0.0000 | |
| 24 | Hospitalization rate | 20.00% | | | | | | |
| 25 | Death rate | 0.00% | | | | | | |
| 26 | | | | | | | | |

**Figure 1 Screen shot of spreadsheet input / output parameters**

The inputs are the geometry of the passenger compartment; the duration and number of occurrences of the journey, the air conditioning ventilation rate; the number of passengers carried; the proportion of the population who may be considered to be immune; the fraction of passengers wearing masks; and the overall population probability of an individual being infected. In addition, there are a number of specified input parameters that describe the transmission of the virus, which the authors admit are best guess values based on the available evidence, but about which there is much uncertainty. The outputs are either the probabilities of infection, hospitalization and death for an individual on a specific journey or for multiple journeys; or the number of passengers who will be infected, hospitalized or die for a specific journey or for multiple journeys.

The spreadsheet is a potentially powerful tool in two ways – firstly to investigate the effect of different input parameters on Covid-19 infection risk, and secondly to develop a rational risk abatement process. We will consider these in turn below.

**Parametric investigation**

In this section we define a base case scenario for a set of input variables and then change the input variables one by one to investigate their significance. The base case is that shown in the screen shot of figure 1 – for a journey of 30 minutes repeated 10 times (i.e. commuting for a week); 80 unmasked passengers in the carriage; a ventilation rate of 8 air changes per hour; a population immunity of 50%; and a population infection rate of 0.2% (one in 500). The latter two figures broadly match the UK situation at the time of writing. For this case we have a probability of one passenger being infected on one journey of 0.096% or 1 in 1042. The arbitrariness of this figure should again be emphasized – it depends upon assumed values of a

number of uncertain parameters. We base the following parametric investigation on this value. Nonetheless it seems a reasonable value in the light of current experience. The results of the investigation are given in Table 1 below.

| | Risk of infection | Risk relative to base case |
|---|---|---|
| 15mins journey | 1/2336 | 0.45 |
| 60mins journey | 1/497 | 2.10 |
| 16ach | 1/2730 | 0.38 |
| 2ach | 1/305 | 3.42 |
| 40 passengers | 1/3767 | 0.28 |
| 20 passengers | 1/17275 | 0.06 |
| 50% masks | 1/1631 | 0.64 |
| 100% masks | 1/2965 | 0.35 |
| 1.0% infected | 1/209 | 4.99 |
| 0.1% infected | 1/2084 | 0.50 |
| 25% immune | 1/695 | 1.50 |
| 75% immune | 1/2084 | 0.50 |

**Table 1 Parametric Investigation**

The table shows the risk of infection for each parametric change around the base case and this risk relative to the base case. There is of course significant arbitrariness in the specification of parameter ranges. Red shading indicates those changes for which the infection risk is more than twice the value for the base case and green shading for those changes for which the infection risk is less than half the value for the base case. The following points are apparent.

- The risk of infection varies linearly with changes in journey time, population infection rate and population immunity. This seems quite sensible, but is effectively built into the algorithm that is used.
- Changes in ventilation rate cause significant changes in infection risk. In particular the low value of 2ach, which is typical on non-airconditioned vehicles with closed windows, increases the infection risk by a value of 3.5.
- The effect of decreasing passenger number (and thus increasing social distancing) is very significant and seems to be the most effective way of reducing infection risk, with a 50% loading resulting in an infection risk of 28% of the base case, and a 20% loading a risk of 6% of the base case.
- The effect of 100% mask wearing reduces the infection risk to 35% of the base case.
- 100% mask wearing and a 50% loading (not shown in the table) results in a reduction of infection risk to 10% of the base case.

From the above, regardless of the absolute value of risk for the base case, the efficacy of reducing passenger numbers and mask wearing to reduce risk is very clear.

**An operational strategy to reduce risk.**

The modelling methodology can also be used to develop a risk mitigation strategy. Let us suppose, again arbitrarily, that the maximum allowable risk of being infected per passenger on the base case journey is 0.1% (i.e. 1 in a thousand). Figure 2 shows the calculated infection risk for a wide range of national infection rate of between 0.01% (1 in 10,000) to 2% (1 in 50). Values are shown for no mask and full capacity; 100% mask wearing and full capacity; and 100% mask wearing and 50 % capacity. It can be seen that the no mask / full capacity curve crosses the 0.1% line at a national infection rate of 0.2% and the 100% mask / full capacity line crosses this boundary at 0.6%.

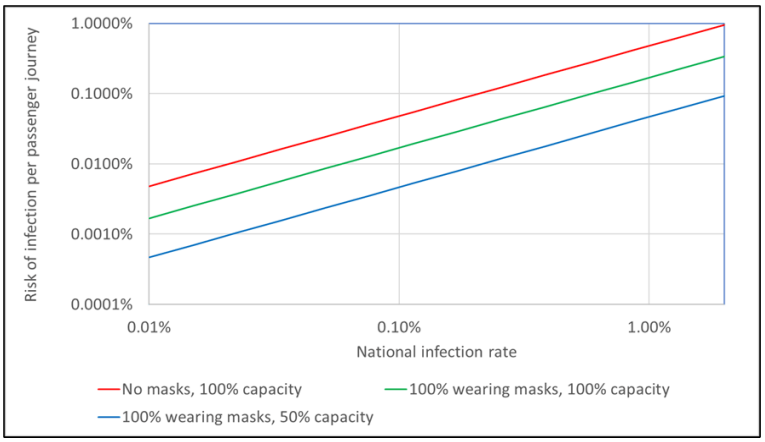


**Figure 2 Effect of national infection rate on infection risk, with and without mask wearing and reduction in loading**

Consideration of the results of figure 2 suggest a possible operational strategy of taking no mitigation risks below an infection rate of 0.2%, imposing a mask mandate between 0.2% and 0.6% and adding a significant capacity reduction above that. This is illustrated in figure 3 below.

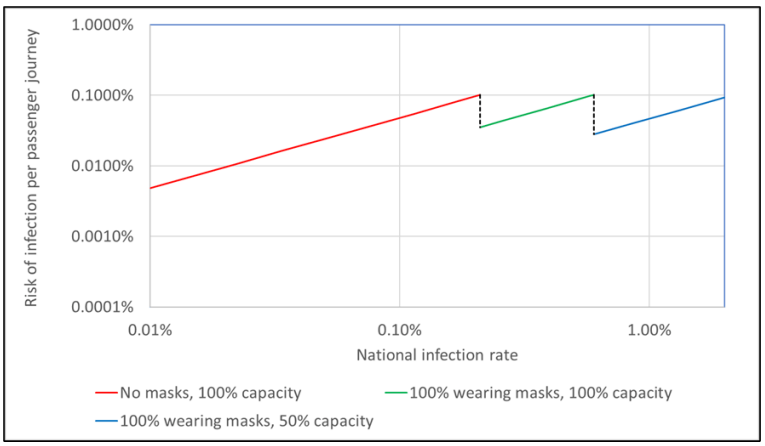


**Figure 3. Mitigation of risk to acceptable level through mask wearing and reduced capacity.**

As has been noted above the absolute risk values are uncertain, but such a methodology could be derived for a variety of journey and train types, based to some extent on what is perceived to be safe by the travelling public. Regional infection rates could be used for shorter journeys. Essentially it gives a reasonably easily applied set of restrictions that could be rationally imposed and eased as infection rate varies, maximizing passenger capacity as far as is possible. If explained properly to the public, it could go some way to improving passenger confidence in travel.

# The calculation of Covid-19 infection rates in churches

**July 12, 2021**

**Preamble**

In a recent post, I looked at the risk of Covid infection on GB trains, based on the spreadsheet calculation methodology of Professor Jimenez and his team at the University of Colorado – Boulder. This method is based solely on aerosol transmission, which is now regarded as being of much more significance than transmission by surface contamination, and the risk of the latter can be easily reduced by normal hygiene precautions. In this post, I apply the same methodology specifically to the case of churches and include a downloadable EXCEL spreadsheet that might be of use to others. There is a level of self-interest of course, as I am a minister at an Anglican church which will shortly be faced with decisions concerning the nature of worship as the Covid restrictions are removed. Essentially the spreadsheet gives a numerical value for the risk of Covid infection with specified amelioration methods in place (social distancing, masks, no singing etc.) and allows a rational assessment of safety to be made.

At the outset, it needs to be made clear that there are very many assumptions in the methodology of Jimenez, with some of the parameters not well specified, and the base values of risk that the model gives must be regarded as indicative only and it is best used in a comparative sense. In what follows, I first describe the input and output parameters of the spreadsheet, and then look at how it might be used to compare risk levels for different situations.

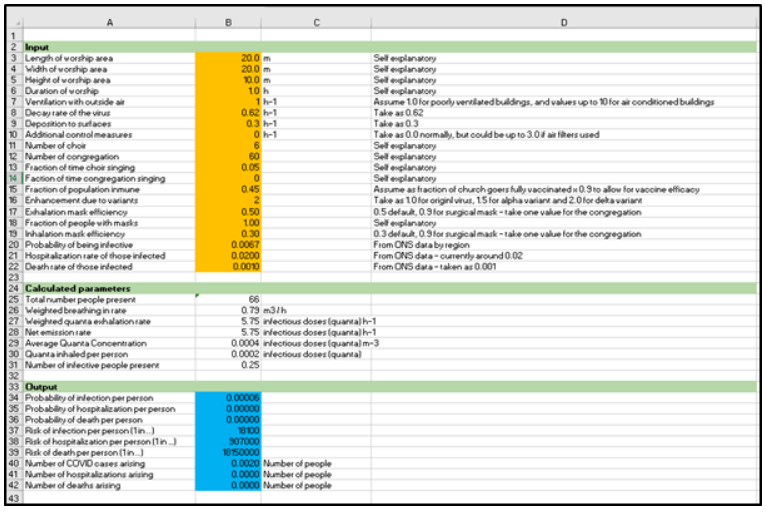

| | A | B | C | D |
|---|---|---|---|---|
| 1 | | | | |
| 2 | **Input** | | | |
| 3 | Length of worship area | 20.0 | m | Self explanatory |
| 4 | Width of worship area | 20.0 | m | Self explanatory |
| 5 | Height of worship area | 10.0 | m | Self explanatory |
| 6 | Duration of worship | 1.0 | h | Self explanatory |
| 7 | Ventilation with outside air | 1 | h-1 | Assume 1.0 for poorly ventilated buildings, and values up to 10 for air conditioned buildings |
| 8 | Decay rate of the virus | 0.62 | h-1 | Take as 0.62 |
| 9 | Deposition to surfaces | 0.3 | h-1 | Take as 0.3 |
| 10 | Additional control measures | 0 | h-1 | Take as 0.0 normally, but could be up to 3.0 if air filters used |
| 11 | Number of choir | 6 | | Self explanatory |
| 12 | Number of congregation | 60 | | Self explanatory |
| 13 | Fraction of time choir singing | 0.05 | | Self explanatory |
| 14 | Faction of time congregation singing | 0 | | Self explanatory |
| 15 | Fraction of population immune | 0.45 | | Assume as fraction of church goers fully vaccinated x 0.9 to allow for vaccine efficacy |
| 16 | Enhancement due to variants | 2 | | Take as 1.0 for original virus, 1.5 for alpha variant and 2.0 for delta variant |
| 17 | Exhalation mask efficiency | 0.50 | | 0.5 default, 0.9 for surgical mask - take one value for the congregation |
| 18 | Fraction of people with masks | 1.00 | | Self explanatory |
| 19 | Inhalation mask efficiency | 0.30 | | 0.3 default, 0.9 for surgical mask - take one value for the congregation |
| 20 | Probability of being infective | 0.0067 | | From ONS data by region |
| 21 | Hospitalization rate of those infected | 0.0200 | | From ONS data - currently around 0.02 |
| 22 | Death rate of those infected | 0.0010 | | From ONS data - taken as 0.001 |
| 23 | | | | |
| 24 | **Calculated parameters** | | | |
| 25 | Total number people present | 66 | | |
| 26 | Weighted breathing in rate | 0.79 | m3/h | |
| 27 | Weighted quanta exhalation rate | 5.75 | infectious doses (quanta) h-1 | |
| 28 | Net emission rate | 5.75 | infectious doses (quanta) h-1 | |
| 29 | Average Quanta Concentration | 0.0004 | infectious doses (quanta) m-3 | |
| 30 | Quanta inhaled per person | 0.0002 | infectious doses (quanta) | |
| 31 | Number of infective people present | 0.25 | | |
| 32 | | | | |
| 33 | **Output** | | | |
| 34 | Probability of infection per person | 0.00006 | | |
| 35 | Probability of hospitalization per person | 0.00000 | | |
| 36 | Probability of death per person | 0.00000 | | |
| 37 | Risk of infection per person (1in...) | 18100 | | |
| 38 | Risk of hospitalization per person (1in...) | 307000 | | |
| 39 | Risk of death per person (1in...) | 18150000 | | |
| 40 | Number of COVID cases arising | 0.0020 | Number of people | |
| 41 | Number of hospitalizations arising | 0.0000 | Number of people | |
| 42 | Number of deaths arising | 0.0000 | Number of people | |
| 43 | | | | |

**Screenshot of spreadsheet**

**The spreadsheet**

The spreadsheet is quite simple and straightforward, and requires no specific expertise to use. A screenshot is given above. The brown cells are input parameters, and the blue cells the output parameters The former are as follows.

- Length, width and height of worship area. The model effectively assumes that the worship area is a three-dimensional box. This is clearly not usually the case, and some degree of judgement will be required in assigning the length, width and height. All dimensions are in metres.
- Duration of worship is specified in hours.
- The ventilation with outside air is specified in air changes per hour. For most old churches that have been well maintained, this will be small and a value of 1.0 can be assumed. For particularly drafty churches, this could be rather higher (at say 3.0). For air-conditioned worship areas a value of 10.0 is appropriate.
- For the decay rate of the virus and the deposition to surfaces standard parameters are assumed. Normally the value for additional control measures will be zero unless there is filtering of recirculated air.
- The number in the choir and congregation are self-explanatory. Ministers should be included in the latter. Because of lack of reliable data on breathing rates and virus emission rates in children, no breakdown by age is required. This is probably a conservative assumption.
- The fractions of time that the choir sings and the fraction of time that the congregation sings are both values between 0 and 1.0. The choir fraction is when they are singing alone – it is assumed they will join with the congregation when the latter sing.
- The fraction of population that is immune is taken to be the proportion of the population that have received a full course of vaccinations, multiplied by 0.9 to allow for virus escape. At the time of writing in the UK, this parameter has a value of around 0.5.
- The parameter that allows for virus transmission enhancement due to variants has a base value of 1.0, a value of 1.5 for the alpha variant, and a value of 2.0 for the delta variant.
- A choice of values for masks efficiency for both breathing in and out are given.
- The fraction of the congregation with masks is a number between 0 and 1.0.
- The probability of being infective is taken from regional ONS data. For example, if the ONS figure of those infected is 1 in 500, then the probability will be 1/500 = 0.002.

- The hospitalization and death rates of those infected can also be taken from ONS data and have small values just above 0.0. At the time of writing the hospitalization rate is around 0.02 (2%) and the death rate is almost negligible and is taken as 0.001 (0.1%).

The next set of parameters in the spreadsheet are those that emerge from the calculation process and are not of direct interest to users. These lead on to the output parameters, which are as follows.

- The probabilities of covid infection, hospitalisation and death of a person attending the service of worship.
- These probabilities expressed as risk – for example a risk of 1 in 1000 of infection.
- The number of covid cases, hospitalisations and deaths arising from attending the service.

**Comparing risk**

The absolute values of probability and risk must only be regarded as approximate. Indeed, Jimenez emphasises that there is a great deal of uncertainty around many of the assumed parameter and urges caution in the interpretation of the results. At best, the results will be accurate to within an order of magnitude. The main utility of the model would seem to be to assess changes in risk – for example, any particular congregation may be comfortable with a certain set of Covid amelioration methods (no singing, masks etc.) and the method can be used to see how this risk might change as these measures are relaxed.

As an example of this, let us consider a church (which is not dissimilar to the one where I am a minister), where the congregation is currently capped at 60, there is 100% marks wearing, and only the choir of 6 sings. For the current infection rate of 1 in 150, this gives a risk of infection of 1 in 18100 for a one-hour service. This level of risk would seem to be acceptable to the congregation. Indeed, for one person attending similar services each week for one year, the risk of covid infection is close to the UK risk of injury in a vehicle accident in a year.

Firstly, suppose that a capacity of 100 is allowed (i.e. social distancing regulations are abolished). This increases the risk of infection to 1 in 11800. Now suppose that in addition masks are no longer required. This leads to a risk of infection of 1 in 4100. Allowing congregational singing raises the risk further to 1 in 1600. As all these figures are dependent upon regional infection rate, they also allow for the congregation to decide at what infection level restrictions can be removed. Should the infection level fall to 1 in 1000, then the overall risk with no amelioration measures decreases from 1 in 1600 to 1 in 11300. Whilst these figures are themselves only approximate, they nonetheless give any congregation the information to make a rational choice of how to proceed as restrictions are eased.

# Pollutants, pathogens and public transport – ventilation, dispersion and dose

November 16, 2021

**Preamble**

The ventilation of buses and trains has come to be of some significance to the travelling public in recent years for a number of reasons. On the one hand, such vehicles can travel through highly polluted environments, such as urban highways or railway tunnels, with high levels of the oxides of nitrogen, carbon monoxide, hydrocarbons and particulate matter that can be drawn into the passenger compartments with potentially both short- and long-term health effects on passengers. On the other, the covid-19 pandemic has raised very significant concerns about the aerosol spread of pathogens within the enclosed spaces of trains and buses. There is a basic dichotomy here – to minimise the intake of external pollutants into vehicles, the intake of external air needs to be kept low, whilst to keep pathogen risk low, then high levels of air exchange between the outside environment and the internal space are desirable. This post addresses this issue by developing a common analytical framework for pollutant and pathogen dispersion in public transport vehicles, and then utilises this framework to investigate specific scenarios, with a range of different ventilation strategies.

The full methodology is given in Appendix 3. This contains all the technical details and a full bibliography. Here we give an outline of the methodology and the results that have been obtained.

**Analysis**

The basic method of analysis is to use the principle conservation of mass of pollutant or pathogen into and out of the cabin space. In words this can be written as follows.

*Rate of change of mass of species inside the vehicle = inlet mass flow rate of species + mass generation rate of species within the vehicle – outlet mass flow rate of species– mass flow rate of species removed through cleaning, deposition on surfaces or decay.*

This results in the equation shown in Box 1 below, which relates the concentration in the cabin to the external concentrations, the characteristics of the ventilation system and the characteristics of the pollutant or pathogen. The basic assumption that is made is of full mixing of the pollutant or pathogen in the cabin. The pdf gives full details of the derivation of this equation, and of analytical solutions for certain simple cases. It is sufficient to note here however that this is a very simple first order differential equation that can be easily solved for any time variation of external concentrations of pollutant generation by simple time stepping methods. For gaseous pollutants, the rate of deposition and the decay rate are both zero which leads to a degree of simplification.

$$\frac{dC}{dt} = \alpha C_e + \frac{g}{\rho V} - (\alpha + \beta + \gamma + \delta)C$$

| | |
|---|---|
| $C$ | Internal pollutant or pathogen concentration |
| $t$ | Time |
| $\alpha$ | Air changes per hour |
| $C_e$ | Weighted average of pollutant concentration at ventilation inlets |
| $g$ | Pollutant or pathogen produced internally |
| $\rho$ | Density of air |
| $V$ | Volume of cabin |
| $\beta$ | Rate of clean air circulation per hour |
| $\gamma$ | Rate of pollution or pathogen deposition to surface per hour |
| $\delta$ | Decay rate of pollutant or pathogen per hour |

**Box 1. The concentration equation**

The pdf also goes on to consider the pollutant or pathogen dose that passengers would be subjected to – essentially the integration of concentration of time history – and then uses this in a simple model of pathogen infection. This results in the infection equation shown in Box 2. Essentially it can be seen that the infection risk is proportional to the average concentration in the cabin and to journey length.

$$P = q_i T \bar{C}\, p(N-1)K\,(1-f_I)(1-f_m\epsilon_i)(1-f_m\epsilon_o)$$

| | |
|---|---|
| $P$ | Probability of infection |
| $q_i$ | Rate of breathing in ($m^3/h$) |
| $T$ | Journey time (h) |
| $\bar{C}$ | Average concentration in cabin (quanta / $m^3$) |
| $p$ | Probability of infection in population |
| $N$ | Number of passengers |
| $K$ | Variant factor |
| $f_I$ | Fraction of population immune |
| $f_m$ | Fraction of passengers wearing masks |
| $\epsilon_i$ | Efficiency of masks whilst breathing in |
| $\epsilon_o$ | Efficiency of masks whilst breathing out |

**Box 2. Infection equation**

The main issue with this infection model is that it assumes complete mixing of the pathogen throughout the cabin space and does not take account of the elevated concentrations around an infected individual. A possible way to deal with this is set out in the pdf. Further work is required in this area.

**Ventilation types**

The concentration and infection equations in Boxes 1 and 2 do not differentiate between the nature of the ventilation system on public transport vehicles. Essentially there are five types of ventilation.

- Mechanical ventilation by HVAC systems
- Ventilation through open windows
- Ventilation through open doors
- Ventilation by a through flow from leakage at the front and back of the vehicle (for buses only)
- Ventilation due to internal and external pressure difference across the envelope.

Simple formulae for the air exchange rates per hour have been derived and are shown in Box 3 below. By substituting typical parameter values the air exchange rates are of the order of 5 to 10 air changes per hour for the first four ventilation types, but only 0.1 for the last. Thus ventilation due to envelope leakage will not be considered further here, although it is of importance when considering pressure transients experienced by passengers in trains.

| | |
|---|---|
| HVAC ventilation | $\alpha_{HVAC} = \frac{\sum \dot{m}_{i,HVAC}}{\rho V}$ |
| Window ventilation | $\alpha_w = \frac{3600\, kv \sum A_{i,w}}{V}$ |
| Door ventilation | $\alpha_d = \frac{3600 ku \sum A_{i,d}}{V}$ |
| Front to rear leakage | $\alpha_l = \frac{3600 A_l v C_d \left(\Delta C_p\right)^{0.5}}{V}$ |
| Envelope leakage | $\alpha_l = \frac{3600}{\tau} \frac{\Delta p}{r p_e}$ |

| | |
|---|---|
| $\sum \dot{m}_{i,HVAC}$ | Total mechanical ventilation mass flow (kg/h) |
| $k$ | Empirical constant |
| $v$ | Vehicle velocity (m/s) |
| $u$ | Nominal wind speed (1.0 m/s) |
| $\sum A_{i,w}$ | Total window area ($m^2$) |
| $\sum A_{i,d}$ | Total door area ($m^2$) |
| $A_l$ | Front to back leakage area ($m^2$) |
| $C_d$ | Discharge coefficient |
| $\Delta C_p$ | Front to back pressure coefficient difference |
| $\Delta p$ | Difference between internal and external pressure (Pa) |
| $\tau$ | Leakage time constant (s) |
| $r$ | Ratio of specific heats |
| $p_e$ | External pressure (Pa) |

**Box 3. Ventilation types**

**Scenario modelling**

In what follows, we present the results of a simple scenario analysis that investigates the application of the above analysis for different types of vehicle with a range different ventilation systems, running through different transport environments. We consider the following vehicle and ventilation types.

- An air-conditioned diesel train, with controllable HVAC systems.
- A window and door ventilated diesel train.
- A bus ventilated by windows, doors, and externally pressure generated leakage.

Two journey environments are considered.

- For the trains, a one-hour commuter journey as shown in figure 1, beginning in an inner-city enclosed station, running through an urban area with two stations and two tunnels, and then through a rural area with three stations (figure 1).
- For buses, a one-hour commuter journey, with regular stops, through city centre, suburban and rural environments (figure 2).

Results are presented for the following scenarios.

- Scenario 1. Air-conditioned train on the rail route, with HVACs operating at full capacity throughout.
- Scenario 2. As scenario 1, but with the HVACs turned to low flow rates in tunnels and enclosed stations, where there are high levels of pollutants.
- Scenario 3. Window ventilated train on rail route with windows open throughout and doors opened at stations.
- Scenario 4. As scenario 3, but with windows closed.
- Scenario 5. Window, door and leakage ventilated bus on bus route with windows open throughout and doors opened at bus stops.
- Scenario 6. As scenario 5, but with windows closed.

Details of the different environments and scenarios are given in tables 1 and 2. Realistic, if somewhat arbitrary levels of environmental and exhaust pollutants are specified for the different environments – high concentrations in cities and enclosed railway and bus stations and lower concentrations in rural areas. The air exchange rates from different mechanisms are also specified, with the values calculated from the equations in Box 3. Note that, in any development of this methodology, more detailed models of the exhaust emissions could be used that relate concentrations at the HVAC systems and window openings to concentrations at the stack, which would allow more complex speed profiles to be investigated, with acceleration and deceleration phases.

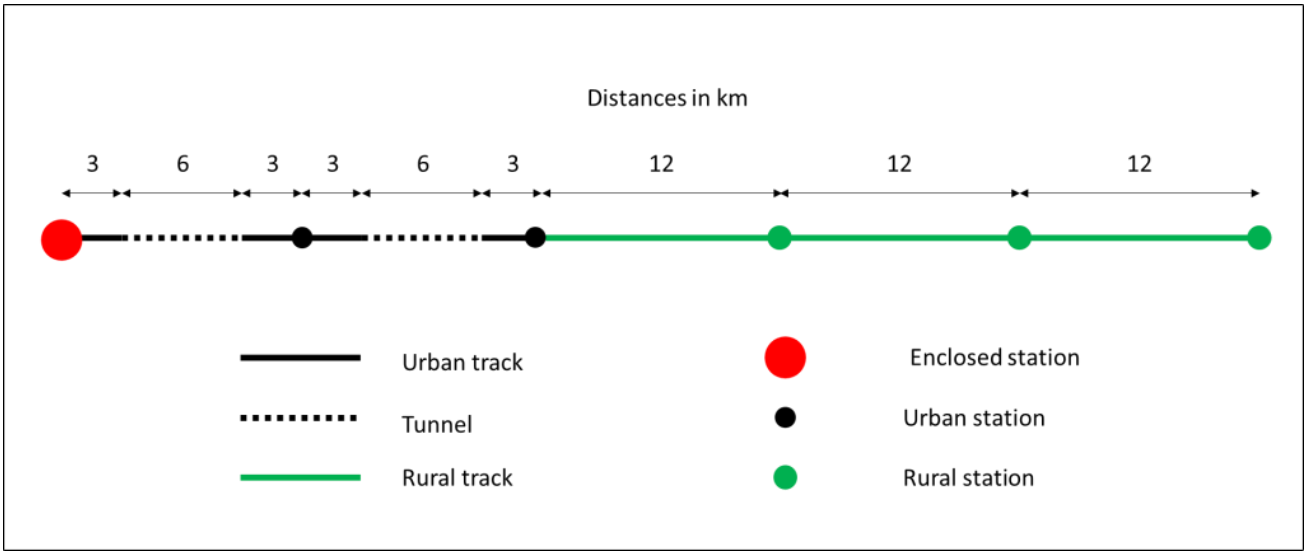


**Figure 1. The rail route**

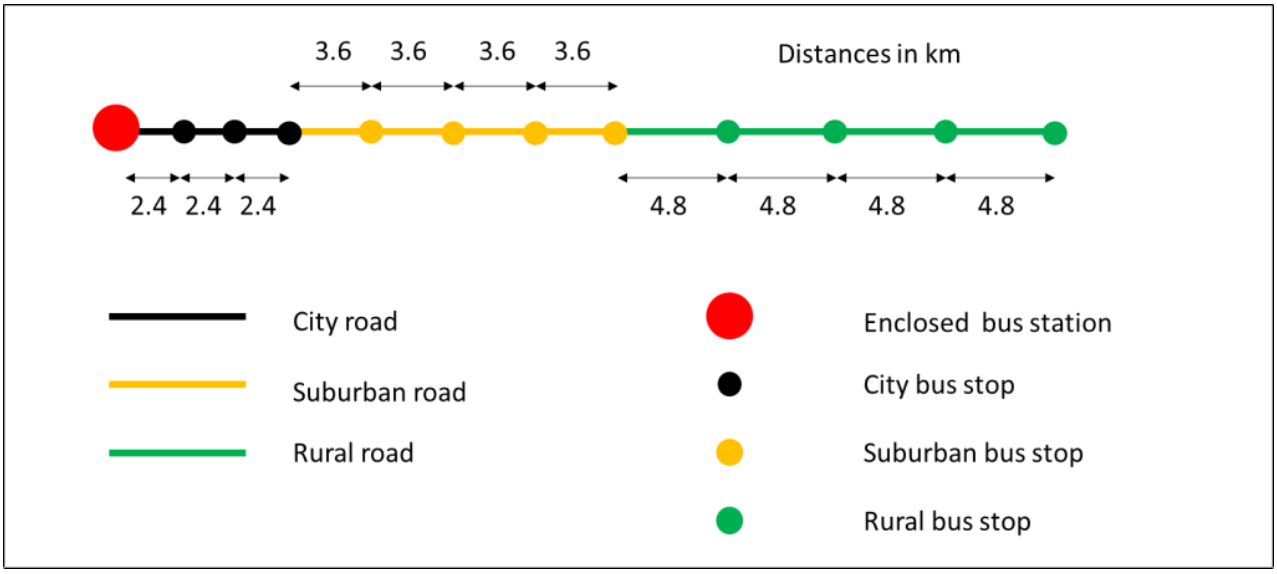


**Figure 2. The bus route**

| | Time (min) | Concentrations | | | | | | Air exchange rates / h | | | | | |
|---|---|---|---|---|---|---|---|---|---|---|---|---|---|
| | | $NO_2$ (μg/m³) | | PM10 (μg/m³) | | $CO_2$ (ppm) | | Scenario 1 | Scenario 2 | Scenario 3 | | Scenario 4 | |
| | | Environment | Exhaust | Environment | Exhaust | Environment | Exhaust | Full HVAC | Controlled HVAC | Window | Door | Window | Door |
| Enclosed station | 0-10 | 300 | 0 | 50 | 0 | 600 | 0 | 10 | 1 | 0 | 10.8 | 0 | 10.8 |
| Urban track | 10-12 | 100 | 200 | 30 | 100 | 300 | 500 | 10 | 10 | 9 | 0 | 0 | 0 |
| Tunnel | 12-16 | 100 | 200 | 100 | 100 | 300 | 500 | 10 | 1 | 9 | 0 | 0 | 0 |
| Urban track | 16-18 | 100 | 200 | 30 | 100 | 300 | 500 | 10 | 10 | 9 | 0 | 0 | 0 |
| Urban station | 18-20 | 100 | 0 | 30 | 0 | 300 | 0 | 10 | 10 | 0 | 10.8 | 0 | 10.8 |
| Urban track | 20-22 | 100 | 200 | 30 | 100 | 300 | 500 | 10 | 10 | 9 | 0 | 0 | 0 |
| Tunnel | 22-26 | 100 | 200 | 100 | 100 | 300 | 500 | 10 | 1 | 9 | 0 | 0 | 0 |
| Urban track | 26-28 | 100 | 200 | 30 | 100 | 300 | 500 | 10 | 10 | 9 | 0 | 0 | 0 |
| Urban station | 28-30 | 100 | 0 | 30 | 0 | 300 | 0 | 10 | 10 | 0 | 10.8 | 0 | 10.8 |
| Rural track | 30-38 | 50 | 200 | 20 | 100 | 300 | 500 | 10 | 10 | 9 | 0 | 0 | 0 |
| Rural station | 38-40 | 50 | 0 | 20 | 0 | 300 | 0 | 10 | 10 | 0 | 10.8 | 0 | 10.8 |
| Rural track | 40-48 | 50 | 200 | 20 | 100 | 300 | 500 | 10 | 10 | 9 | 0 | 0 | 0 |
| Rural station | 48-50 | 50 | 0 | 20 | 0 | 300 | 0 | 10 | 10 | 0 | 10.8 | 0 | 10.8 |
| Rural track | 50-58 | 50 | 200 | 20 | 100 | 300 | 500 | 10 | 10 | 9 | 0 | 0 | 0 |
| Rural station | 58-60 | 50 | 0 | 20 | 0 | 300 | 0 | 10 | 10 | 0 | 10.8 | 0 | 10.8 |

Operating speed on open track and in tunnel 25m/s; Cabin volume 200; Number of passengers 60; Number of infected passengers 1; Carbon Dioxide emitted per passenger 0.0216m³/h; Pathogen quanta emitted per infected passenger 10; Recirculation air exchange rate (Scenarios 1 and 2) 3/h; window opening area (Scenario 3) 0.2m²; door opening area (Scenario 4) 6m²; particulate and pathogen deposition rate 3.3/h; pathogen decay rate 1.6/h.

**Table 1. The rail scenarios**

| | Time (min) | Concentrations | | | Air exchange rates / h | | | | | |
|---|---|---|---|---|---|---|---|---|---|---|
| | | | | | Scenario 5 | | | Scenario 6 | | |
| | | $NO_2$ | PM10 | $CO_2$ | | | | | | |
| | | Environment | Environment | Environment | Window | Door | Leakage | Window | Door | Leakage |
| Bus station | 0-5 | 300 | 50 | 600 | 0 | 10.8 | 0 | 0 | 10.8 | 0 |
| City road | 5-9 | 200 | 40 | 500 | 7.2 | 0 | 2.16 | 0 | 0 | 2.16 |
| City bus stop | 9-10 | 200 | 40 | 500 | 0 | 10.8 | 0 | 0 | 10.8 | 0 |
| City road | 10-14 | 200 | 40 | 500 | 7.2 | 0 | 2.16 | 0 | 0 | 2.16 |
| City bus stop | 14-15 | 200 | 40 | 500 | 0 | 10.8 | 0 | 0 | 10.8 | 0 |
| City road | 15-19 | 200 | 40 | 500 | 7.2 | 0 | 2.16 | 0 | 0 | 2.16 |
| City bus stop | 19-20 | 200 | 40 | 500 | 0 | 10.8 | 0 | 0 | 10.8 | 0 |
| Suburban road | 20-24 | 100 | 30 | 300 | 10.8 | 0 | 3.24 | 0 | 0 | 3.24 |
| Suburban bus stop | 24-25 | 100 | 30 | 300 | 0 | 10.8 | 0 | 0 | 10.8 | 0 |
| Suburban road | 25-29 | 100 | 30 | 300 | 10.8 | 0 | 3.24 | 0 | 0 | 3.24 |
| Suburban bus stop | 29-30 | 100 | 30 | 300 | 0 | 10.8 | 0 | 0 | 10.8 | 0 |
| Suburban road | 30-34 | 100 | 30 | 300 | 10.8 | 0 | 3.24 | 0 | 0 | 3.24 |
| Suburban bus stop | 34-35 | 100 | 30 | 300 | 0 | 10.8 | 0 | 0 | 10.8 | 0 |
| Suburban road | 35-39 | 100 | 30 | 300 | 10.8 | 0 | 3.24 | 0 | 0 | 3.24 |
| Suburban bus stop | 39-40 | 100 | 30 | 300 | 0 | 10.8 | 0 | 0 | 10.8 | 0 |
| Rural road | 40-44 | 50 | 20 | 300 | 14.4 | 0 | 4.32 | 0 | 0 | 4.32 |
| Rural bus stop | 44-45 | 50 | 20 | 300 | 0 | 10.8 | 0 | 0 | 10.8 | 0 |
| Rural road | 45-49 | 50 | 20 | 300 | 14.4 | 0 | 4.32 | 0 | 0 | 4.32 |
| Rural bus stop | 49-50 | 50 | 20 | 300 | 0 | 10.8 | 0 | 0 | 10.8 | 0 |
| Rural road | 50-54 | 50 | 20 | 300 | 14.4 | 0 | 4.32 | 0 | 0 | 4.32 |
| Rural bus stop | 54-55 | 50 | 20 | 300 | 0 | 10.8 | 0 | 0 | 10.8 | 0 |
| Rural road | 55-59 | 50 | 20 | 300 | 14.4 | 0 | 4.32 | 0 | 0 | 4.32 |
| Rural bus stop | 59-60 | 50 | 20 | 300 | 0 | 10.8 | 0 | 0 | 10.8 | 0 |

Operating speed on rural roads, suburban roads and city roads 20m/s, 15m/s and 10m/s respectively; Cabin volume 100 $m^3$; Number of passengers 30; Number of infected passengers 1; Carbon Dioxide emitted per passenger 0.0216$m^3$/h; Pathogen quanta emitted per infected passenger 10; Recirculation air exchange rate (Scenarios 1 and 2) 3/h; window opening area (Scenario 5) 0.2$m^2$; door opening area (Scenario 4) 3$m^2$; leakage area 0.1$m^2$; particulate and pathogen deposition rate 3.3/h; pathogen decay rate 1.6/h.

**Table 2. The bus scenarios**

The results of the analysis are shown in figures 3 and 4 below for the train and bus scenarios respectively. Both figures show time histories of concentrations for NO2, PM2.5, CO2 and Covid-19, together with the external concentrations of the pollutants.

For Scenario 1, with constant air conditioning, all species tend to an equilibrium value that is the external value in the case of NO2 and PM2.5, slightly higher than the external value for CO2 due to the internal generation and a value fixed by the emission rate for Covid 19.

For Scenario 2, with low levels of ventilation in the enclosed station and in the tunnels, NO2 and PM2.5 values are lower than scenario 1 at the start of the journey where the lower ventilation rates are used, but CO2 and Covd-19 concentrations are considerably elevated. When the ventilation rates are increased in the second half of the journey all concentrations approach those of Scenario 1.

The concentration values for scenario 3, with open windows, match those of Scenario 1 quite closely as the specified ventilation rates are similar. However, for Scenario 4, with windows shut and only door ventilation at stations, such as might be the case in inclement weather, the situation is very different, with steadily falling levels of NO2 and PM2.5, but significantly higher values of CO2 and Covid-19. The latter clearly show the effect of door openings at stations.

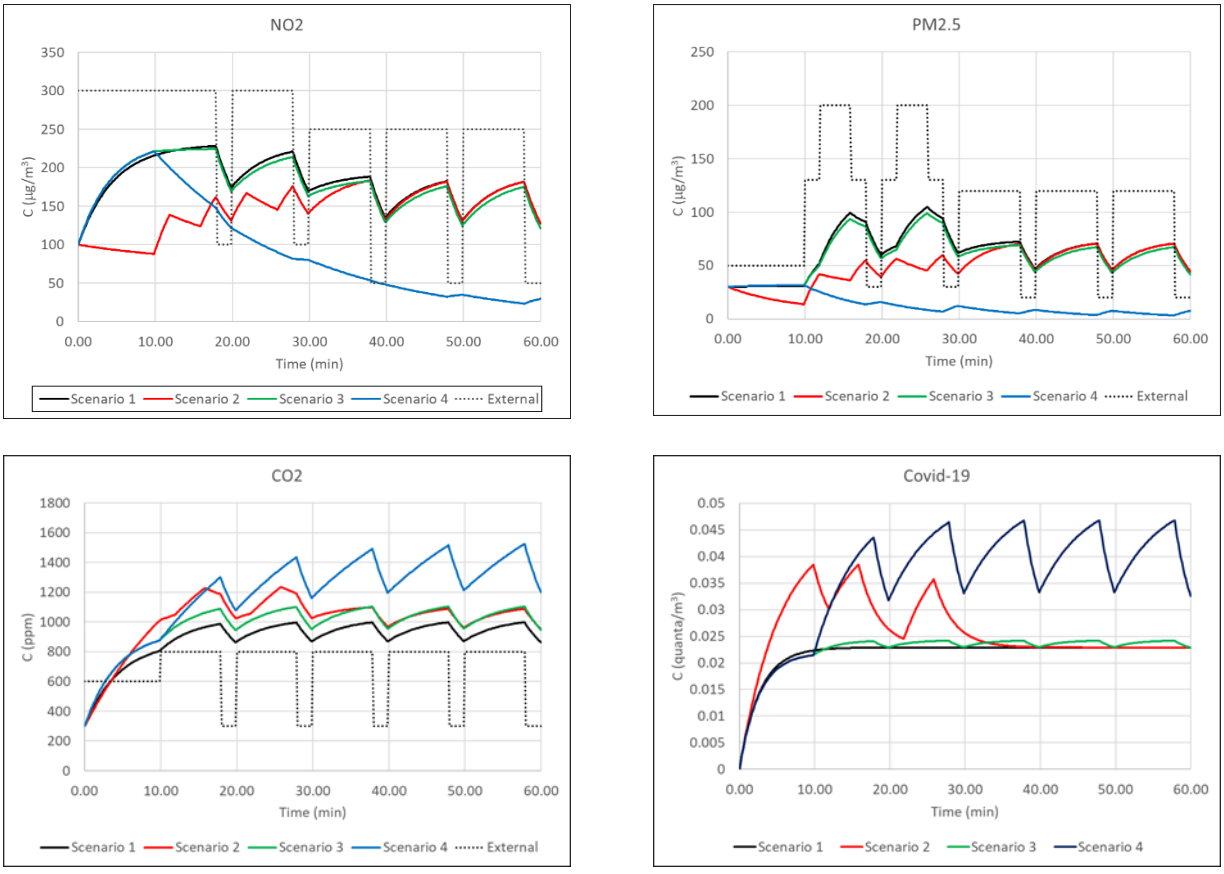


**Figure 3. The train scenario results**

Now consider the bus scenarios in figure 4. For both Scenario 5 with open windows and doors, and Scenario 6 with closed windows and open doors, the NO2 and PM2.5 values tend towards the ambient concentrations and thus fall throughout the journey as the air becomes cleaner in rural areas. The internally generated CO2 and Covid-19 concentrations for CO2 and Covid-19 are however very much higher for Scenario 6 than for Scenario 5.

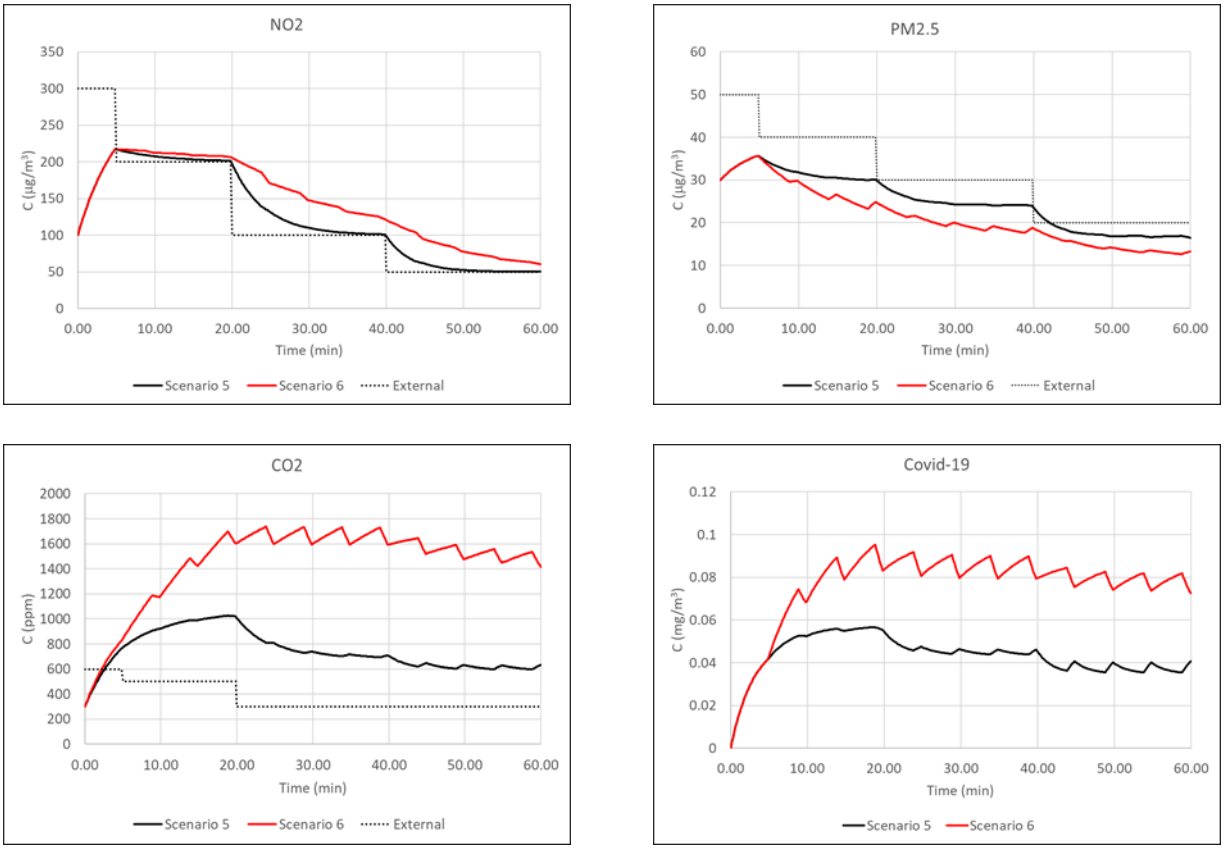


**Figure 5. The bus scenarios**

The average values of concentration for all the scenarios is given in Table 3. The dose and, for Covid-19, the infection probability, are proportional to these concentrations. For NO2 and PM10 the average concentrations reflect the average external concentrations, and, with the exception of Scenario 4, where there is low air exchange with the external environment for part of the journey. The average concentrations for CO2 and Covid-19 for the less ventilated Scenarios 4 and 6 are significantly higher than the other. For Covid-19, the effect of closing windows on window ventilated trains and buses raises the concentrations, and thus the infection probabilities, by 60% and 76% respectively.

| | NO2 (µg/m³) | PM2.5 (µg/m³) | CO2 (ppm) | Covid-19 (quanta/m³) |
|---|---|---|---|---|
| Scenario 1 | 183 | 63 | 890 | 0.022 |
| Scenario 2 | 145 | 49 | 1015 | 0.026 |
| Scenario 3 | 179 | 60 | 978 | 0.022 |
| Scenario 4 | 96 | 13 | 1193 | 0.036 |
| Scenario 5 | 125 | 25 | 745 | 0.043 |
| Scenario 6 | 146 | 21 | 1452 | 0.076 |

**Table 3. Average concentrations**

**Closing comments**

The major strength of the methodology described above is its ability, in a simple and straightforward way, to model pollutant and pathogen concentrations for complete journeys, and to investigate the efficacy of various operational and design changes on these concentrations. It could thus be used, for example, to develop HVAC operational strategies for a range of different journey types. That being said, there is much more that needs to be done – for example linking the methodology with calculations of exhaust dispersion around vehicles, with models of particulate resuspension or with models of wind speed and direction variability. It has also been pointed out above that the main limitation of the infection model is the assumption of complete mixing. The full paper sets out a possible way forward that might overcome this. Nonetheless the model has the potential to be of some utility to public transport operators in their consideration of pollutant and pathogen concentrations and dispersion within their vehicles.

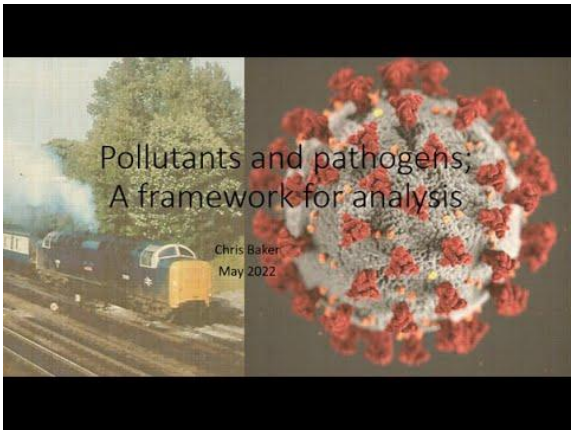


**Pollutants and Pathways – A framework for analysis**
**June 1 2022**

# Measurements of Carbon Dioxide concentrations in a church

May 24, 2022

*The measurements reported in this post were made by colleagues of the School of Engineering at the University of Birmingham – Dr David Soper and Dr Mike Jesson – whose help is gratefully acknowledged.*

**Introduction**

Over the course of the Covid-19 pandemic, there has understandably been increased concern over ventilation within buildings and on buses and trains etc. This has been reflected in church circles where church ventilation has also been much discussed. Whilst more modern churches will have been specifically designed with ventilation in mind, with proper ventilation paths between windows and doors, the same cannot be said about older churches. For many such churches the only ventilation is offered by the opening of doors, and by leakage through windows and roofs. Because of the large vertical size of such buildings, this lack of ventilation is ameliorated by the ability of any pollutants of pathogens to diffuse throughout the large church space.

One such church is St. Michael on Greenhill in Lichfield (figure 1 below), which is essentially two large, connected boxes – a nave, and a chancel, with a main door in the north wall of the nave and a smaller door into the choir vestry on the south side, and internal doors between the vestry area, the nave and the chancel (figure 2). A though ventilation path is rarely established however as the external and internal doors are seldom open at the same time. There are plans to build new parish rooms to the south of the church, on the grassed area of the figure below.

**Figure 1 St. Michael's, Lichfield**

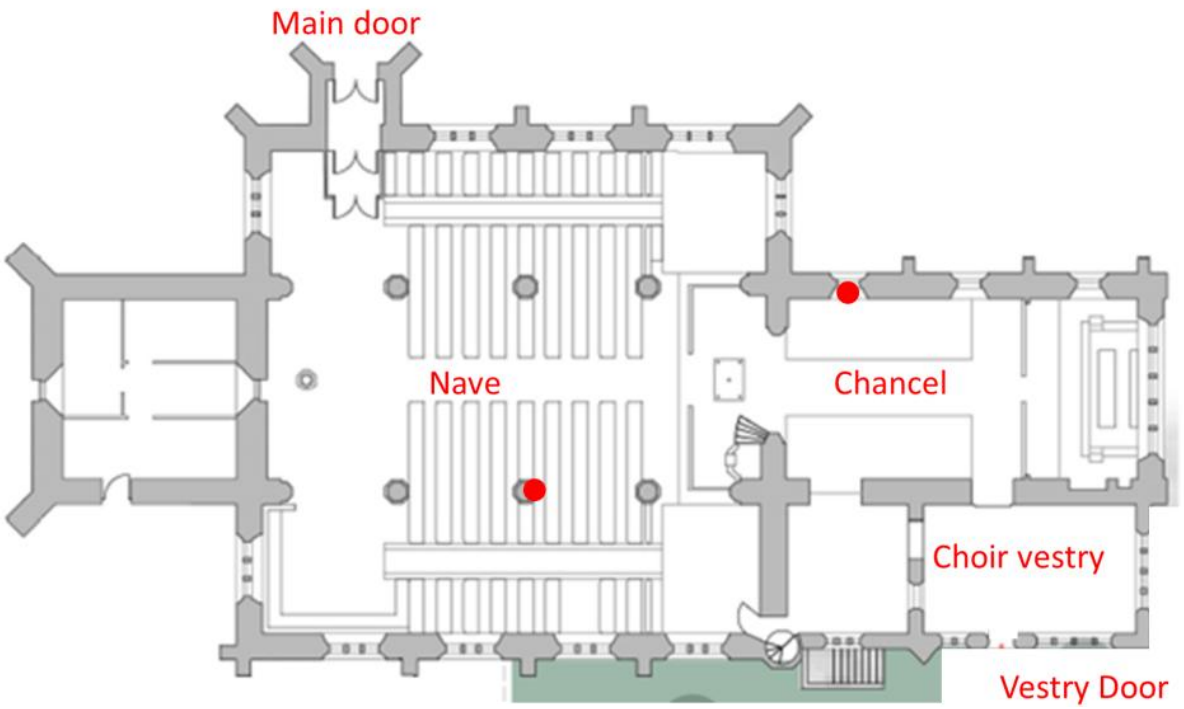


**Figure 2. Plan of church (the measurement positions are indicated by red circles)**

This brief post outlines a short series of measurements to measure carbon dioxide ($CO_2$) levels in St. Michael's. $CO_2$ is produced naturally by people during breathing and $CO_2$ concentration levels are often taken to be an indication of pathogen levels when the population is infected. These measurements were made on Sunday May 15th 2022, when the service pattern was somewhat different from normal, with the normal 8.00 and 10.00 Holy Communion services supplemented by the Annual Parochial Church Meeting (APCM) at 11.15 and a 4.00 service at which a new Rector was Instituted by the Bishop and Archdeacon. As such it gave the opportunity to look at the effects of different congregation numbers (10 in the chancel for the 8.00 service, 50 for the 10.00 service and the APCM, and 150 for the Institution). A screen shot of a video of the Induction service is shown in figure 3 to give some idea of the density of the congregation.


**Figure 3. The congregation during the 4.00 service**

**The measurements**

Carbon Dioxide measurements were made with small transducers and data loggers at different points around the church. These were attached to pillars of left on suitable window ledges. These sampled automatically every minute and the results were transmitted wirelessly to a Raspberry Pi computer and from there to a University of Birmingham web site from where the data could be accessed in real time. These measurements were supplemented by measurements of temperature and pressure using further transducers with built in data loggers.

For the sake of simplicity only the results from two of the $CO_2$ sensors will be shown, as the results from them all were very similar. The location of these are shown on the plan of Figure 2 – one on a pillar in the nave, and one on a window ledge in the chancel. The photographs of the instruments shown in figure 4 indicate that they are quite small and discrete and indeed were barely noticed by the congregation. The results will be presented from midnight on Saturday May 14th to midnight on Sunday May 15th.

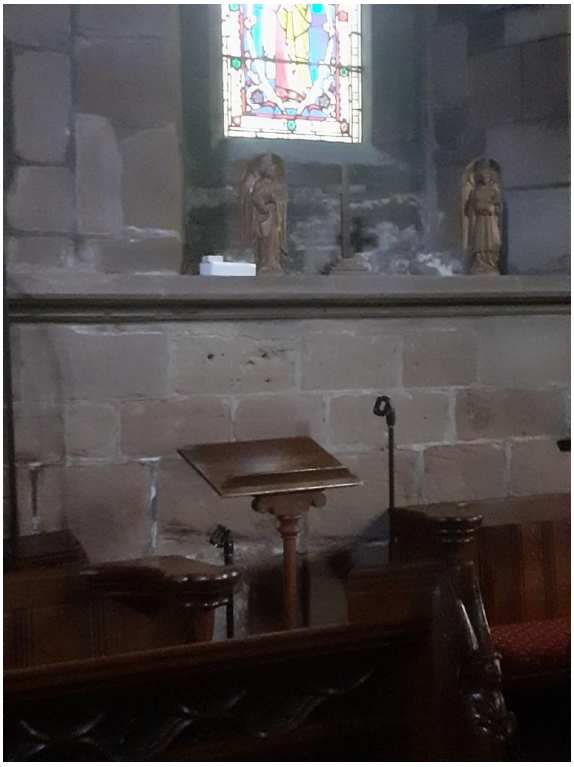

Chancel

Nave

**Figure 4 Sensors (white boxes) in the chancel and nave**

**The results of the trials**

The weather on May 15th was quite pleasant with early morning temperatures of 10°C rising to around 20°C in the late afternoon and evening. The external humidity varied from 20% to 100% throughout the day. Inside the church however there was far less variation with temperatures between 16 and 21°C and humidity between 55 and 70%. The was a light southerly wind in the morning, with a somewhat stronger easterly wind from mid-afternoon onwards.

The results of the $CO_2$ measurements are shown on the graph of figure 5. These are shown in terms of parts per million (ppm) of carbon dioxide in the atmosphere by volume and are relative to a general background level of around 400 ppm.

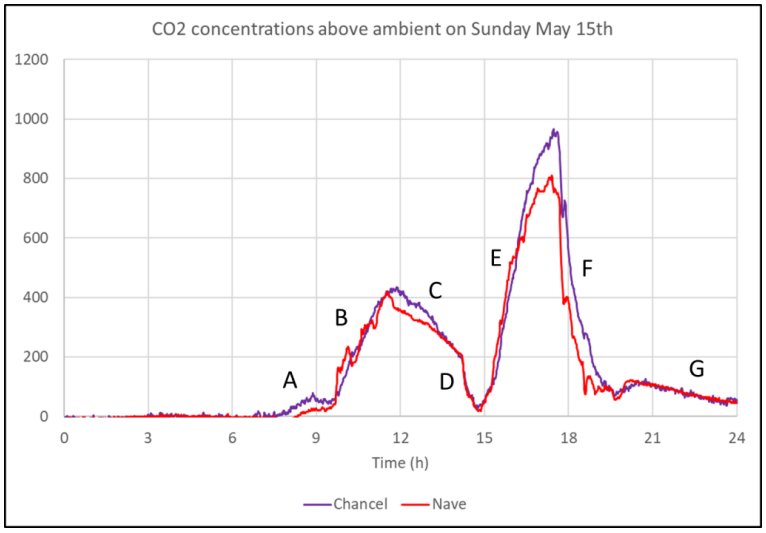


**Figure 5. The carbon dioxide concentration measurements**

The church was opened at around 7.30 am for the 8.00 Holy Communion service held in the chancel, which went on until till around 8.45. Around 10 people attended. There can be seen to be a small increase in $CO_2$ levels in the chancel over the course of the service (A). Later in the morning there was a 10.00 Holy communion service in the nave with around 50 in the congregation, with a small choir of 4 or 5 in the chancel. This was followed immediately by the APCM from 11.15 to 11.45 in the nave with about the same number attending. During this period there can be seen to be a steady increase in $CO_2$ levels both in the nave and the chancel (B). At 12.00 the church emptied and the doors were closed. This led to a steady decrease in concentrations (C) till about 2.00 when people started to arrive at the church to set up for the major service of the day – the Institution of the new Rector by the Bishop of Lichfield. At this point both the main door and the choir vestry door were opened (as Gazebos were being set up to the south of the church for refreshments after the service), and a ventilation path was opened through the church, with major $CO_2$ concentration reductions (D). Around 3.00 the congregation for the 4.00 Induction service began to arrive and the church rapidly filled with around 150 attending, including a choir of around 20 in the chancel. There were significant increases in $CO_2$ concentrations during the course off the service through till around 5.30 (E). When the service was over, both the main door and the choir vestry door were again opened, and there was a rapid drop in concentration levels till around 7.00 when the choir vestry door was closed (F). After some clearing up, the church emptied by around 8.00 and there was a gradual fall off in concentration levels (G).

Two main points emerge from these measurements. Firstly, and quite obviously, the levels of $CO_2$ increase with the number of people in church and with the time they spend there – B and E on the above figure. Secondly it is clear that there are two different types of ventilation – the slow diffusion of $CO_2$ throughout the building and leakage through the building envelope – roof, doors, windows etc. (C and G); and the rapid lowering of concentration levels when there is a direct ventilation path through the building between the two doors (D and F).

Now from the slope of the graph for the times when concentrations are falling, it is possible to get estimates of the time it takes for the concentrations to fall by 50%. For C and G these times are around 2.5 hours, whilst for D and F these times are between 10 and 30 minutes. Thus the through ventilation reduces the carbon dioxide levels much more quickly than simple diffusion and leakage.

**Implications**

The results show firstly that the method that was used is a simple and viable way of assessing the main ventilation parameters in a church. Colleagues from the University of Birmingham recognise that there is still work to on improving the frequency response of the sensors but overall the method has much promise. Secondly there are some implications for St. Michael's itself – that large congregations in the church for lengthy periods of time can result in significant $CO_2$ concentrations (and thus pathogens in times of infection), and that through ventilation is much more effective in reducing these concentrations than simply relying on diffusion and leakage. In the Parish Rooms developments that are under consideration for the area adjoining the choir vestry, it may be worth investigating if it is possible to design through ventilation paths through the church and the new development.

# The simulation of local tornado wind conditions

August 15, 2024

**Preamble**

At the recent Bluff Body Aerodynamics Conference in Brimingham at the end of July / start of August 2024, there was considerable discussion concerning the simulation of tornado and downburst flow for the purposes of measuring structural loads. The current experimental methodology uses large scale tornado / downburst generators that have to be physically very large to have reasonable model scales, with either the whole downflow mechanism being moved across a model, or a model being moved beneath the generator. Such tests are complex and time consuming, the more so because to obtain reliable load statistics multiple tuns are required for each case considered with various tornado or downburst characteristics, building position and orientation relative to the core flow etc.

In the discussions of the various presentations, there was some talk of modelling local flow characteristics around building models, rather than modelling the complete flow field. After mulling over some possibilities for this, in this blog post I set out my preliminary thoughts on how such local simulations might be achieved. I have no access to labs or funding, so these ideas will be for someone else to take forward if they are thought to have merit.

**The proposal**

The basic idea is as follows.

- The local wind field around a building should be simulated in a duct, where rapid changes in wind speed such as those found beneath tornadoes and downbursts can be simulated using active control of fans / screens etc. This has been attempted in the past and the technique is clearly possible. The near ground local shear and turbulence could be generated using spires and roughness in the usual way.
- The rapid horizontal direction changes seen by a building as the flow structures pass over it should be simulated by rotating the model at the required speed.
- Vertical direction changes (which it will be seen below are usually small) could be simulated in one of two ways – either by tilting the building model vertically (which would result in some ground plane distortion) or perhaps by rapid changes in duct roof profile to produce the appropriate upward or downward vertical velocity component.

In principle there seems to be no reason why it should not be possible to simulate the necessary velocity and direction changes, but there are two issues that need to be investigated. Firstly, what exactly are the local wind velocity and direction changes at a particular point when a tornado or downburst passes over them, and secondly how rapid are these changes – are they possible to achieve at reasonable model scales. We address these issues in what follows.

**Specification of wind conditions**

There are a number of ways in which wind conditions experienced by buildings as tornados or downbursts pass over them can be specified.

- Through the use of full-scale data, although this is somewhat sparse, particularly close to the ground.
- Through large scale LES simulations, a number of which are available, but are usually for certain specific situations and not easily generalized.
- Through the use of simple analytical models which capture the main features of the flow, and by their nature can be generalized quite easily.

Here we use the latter method (which will come as no surprise to those who know me!). Specifically we use the methods of Baker and Sterling (2017) and Sterling et al (2023). These give the equations for the three components of velocity, relative to the tornado / downburst centre, shown in Box 1. It is then assumed that the building is stationary as the storm passes over it and the overall horizontal velocity and horizontal and vertical flow directions calculated from assuming a vector sum of a steady wind velocity in the storm direction of travel and the velocity induced by the tornado / downburst (figure 1).

From Baker and Sterling (2017) for the velocity components in tornadoes

$$\bar{u} = -\frac{1}{S}\frac{2\bar{r}}{(1+\bar{r}^2)}\frac{2\bar{z}}{(1+\bar{z}^2)} \qquad \bar{v} = 2.88\frac{\bar{r}}{[1+\bar{r}^2]}\ln(1+z^2) \qquad \bar{w} = \frac{\delta}{S}\frac{4}{(1+\bar{r}^2)^2}\ln(1+z^2)$$

$$\bar{u} = u/v_m \qquad \bar{v} = v/v_m \qquad \bar{w} = w/v_m$$

$$\bar{r} = r/r_m \qquad \bar{x} = x/r_m \qquad \bar{y} = y/r_m \qquad \bar{z} = z/z_m$$

$$\bar{U} = U/v_m \qquad \delta = z_m/r_m$$

$u$, $v$ and $w$ are the velocity components in the radial, circumferential and vertical directions; $r$ is the radial distance from the tornado centre, $x$ is the direction of tornado translation, $y$ is the perpendicular of the building from the track of the tornado centre and $z$ is the height above the ground; $r_m$ and $z_m$ are the values of $r$ and $z$ at which $v$ has a maximum value $v_m$; $S$ is the ratio of the maximum value of the circumferential to the radial velocity; $U$ is the tornado translational velocity in the $x$ direction; and $\delta$ is the ratio of $z_m$ to $r_m$.

For $\bar{z} = 1.0$ these reduce to

$$\bar{u} = -\frac{2}{S}\frac{\bar{r}}{(1+\bar{r}^2)} \qquad \bar{v} = 2\frac{\bar{r}}{[1+\bar{r}^2]} \qquad \bar{w} = \frac{\delta}{S}\frac{2.77}{(1+\bar{r}^2)^2}$$

For downbursts, from Sterling, Huo and Baker (2023), at $\bar{z} = 1.0$

$$\bar{u} = \frac{2\bar{r}}{(1+\bar{r}^2)} \qquad \bar{w} = -\frac{2.77\delta}{(1+\bar{r}^2)^2}$$

**Box 1 Tornado and downburst equations**

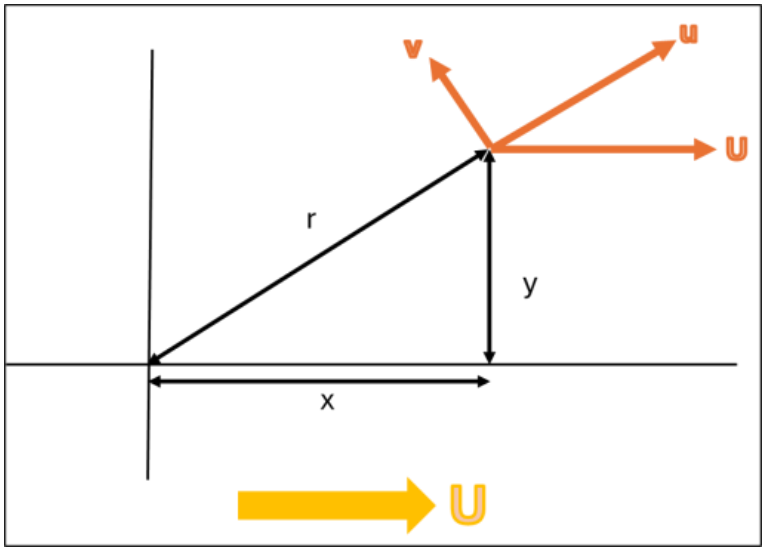


**Figure 1. Co-ordinate system**

Clearly the model requires a number of parameters to be specified. These have been taken from the data collation of Baker and Sterling (2019) (which was compiled to assess the adequacy of tornado vortex generators) and four conditions specified – for small, medium and large tornados and for a downburst of similar size to a medium tornado. The parameters for these cases are shown in Table 1. I make no claim as to the overall adequacy or otherwise of this method – as it stands it is simply a convenient tool with which to investigate the broad parameters of the problem, and other methodologies could be used to determine the wind conditions relative to a building.

| | $r_m$ (m) | $v_m$ $(m/s)$ | $\delta$ | $U$ (m/s) | $S$ |
|---|---|---|---|---|---|
| Small tornado | 50 | 40 | 0.1 | 4 | 5 |
| Medium tornado | 200 | 50 | 0.24 | 10 | 10 |
| Large tornado | 500 | 60 | 0.33 | 12 | 12 |
| Downburst | 200 | 50 | 0.24 | 10 | - |

**Table 1. Tornado and downburst parameters used in calculation**

**Wind speed and direction relative to a stationary building**

Clearly the wind speed and wind direction changes experienced by a stationary building as a storm passes over them will depend upon the position of the building relative to the storm track. If the building is directly on the track, then some very rapid changes in speed and direction can be expected. This is shown in figures 2a to 2c for the large tornado case. The x axis is the time at full scale equivalent values as the storm passes over the building. The origin is at the point when the centre of the storm is directly over the building. As might be expected there is a very rapid change in the speed and horizontal direction as the vortex core passes over, and a very large change in vertical direction. Two points can be made, Firstly, in this region the model is at its least realistic as the sharp changes will be smoothed in reality by vortex wandering and viscous effects. However secondly, there will undoubtedly be large vertical flow direction changes as the core passes over, although perhaps not as high or as rapid as shown

in figure 2, and the type of model simulation proposed here would be unable to simulate such changes and such simulations are probably not adequate close to the core. In what follows we thus confine our attention to two model positions, at one core radius either side of the vortex direction of travel where one would expect the simulation to be adequate..

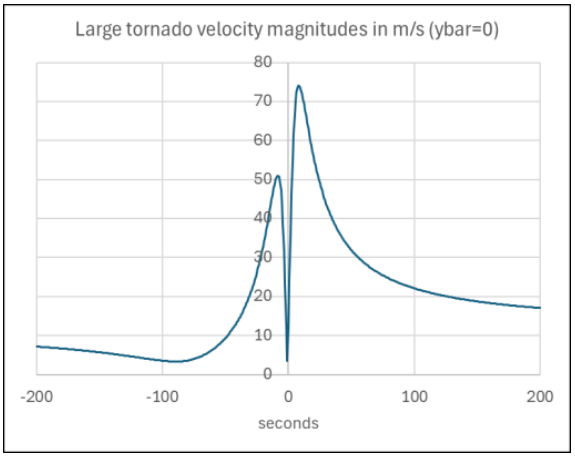


a

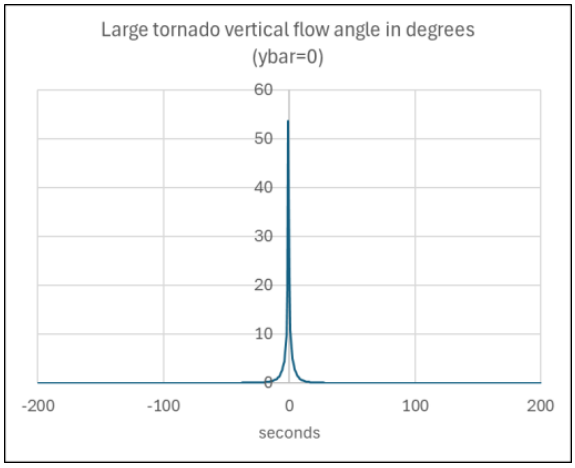


B

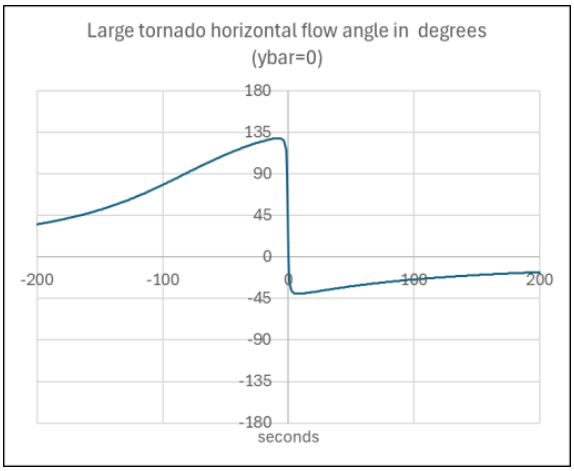


c

**Figure 2. Wind conditions experienced by building directly on the storm track as large tornado passes over**

The results of this analysis are shown in figures 3a to 3d for the small, medium and large tornados and figures 4a to 4c for the downburst. The following points can be made.

- The velocity magnitude variations are the same for both building positions, and all show a rapid rise then a fall as would be expected.
- The vertical direction change is characterized by a sharp peak. For the tornado cases, this variation is always less than 1 degree, but for the downburst case it is considerably greater.

- For the downburst, the horizontal direction variation differs in sign between the two positions but are otherwise identical. However, for the tornado cases the horizontal direction variation is different for the two building positions due to the asymmetry introduced by the rotation of the storm. For the case with the building to the top of the storm track in figure 1, there is a steady, if rapid, change of direction around the building and back to the starting point. For the bottom case, the flow directions move through 130 degrees and then back to the original position.

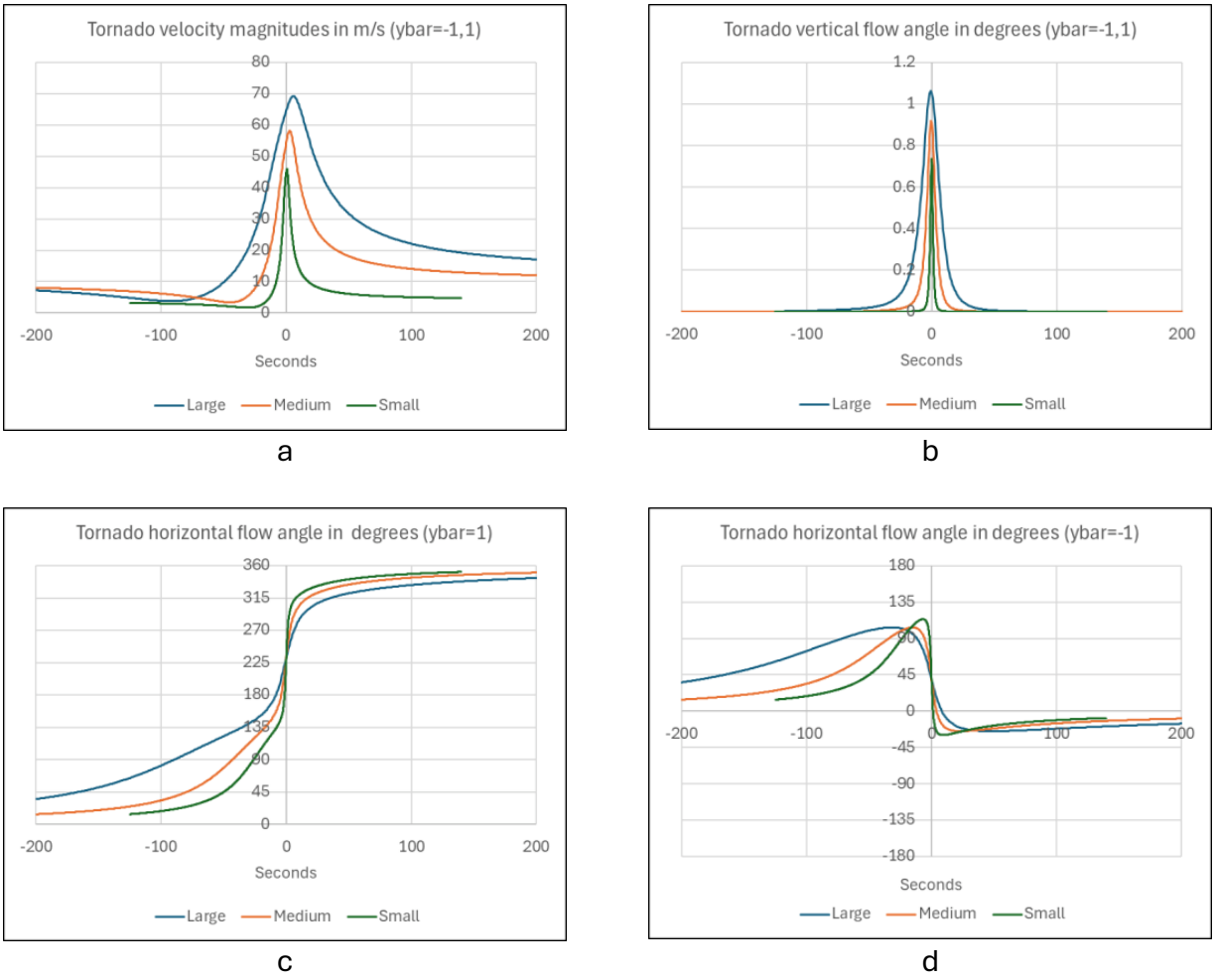


**Figure 3. Wind conditions experienced by building one core radius away from the storm track as large, medium and small tornados passes over**

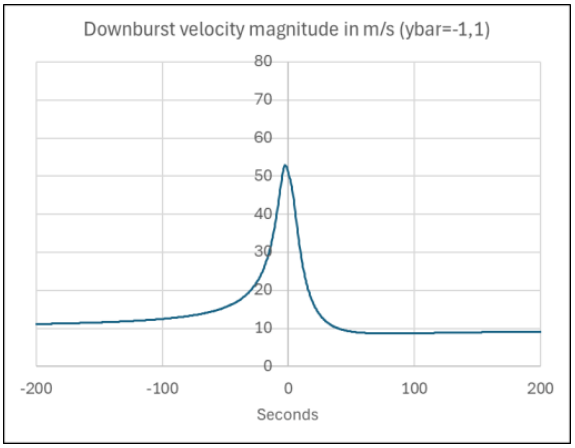


a

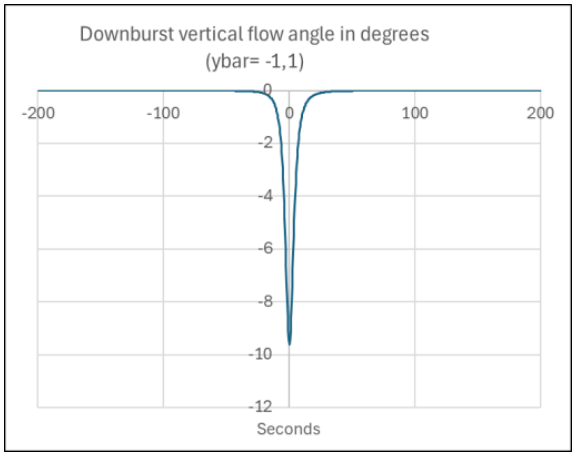


B

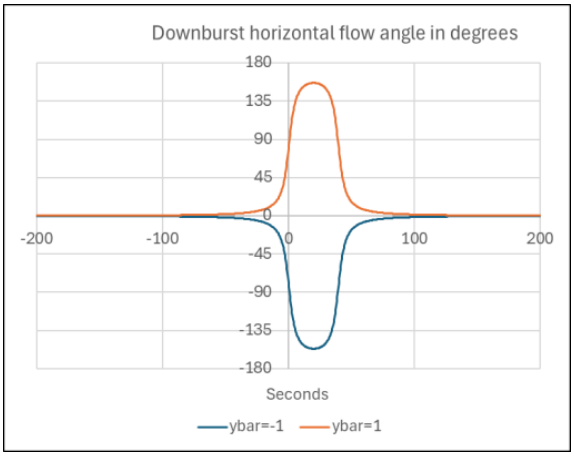


c

**Figure 4. Wind conditions experienced by building one core radius away from the storm track as downburst passes over**

### Can the velocity and direction variations be modelled?

The question then arises as to whether these predicted velocity and direction variations can be achieved in practice. As noted above the *x* axis on figures 3 and 4 is the full-scale time in seconds. If, say, a building model scale of 1:25 is adopted, which is broadly in line with current practice, and a velocity scale of 2:1 is used (ie the simulation velocities are half full-scale velocities, which seems practical), then the model time scale is 1:12.5 i.e. the model changes have to take place 12.5 times faster than the full-scale cases. If we take the modelling above as broadly correct in regard to the time scales of velocity and direction variations, then the horizontal direction and velocity variations for the large, medium and small tornados and the downburst takes place over periods of around 50, 30 and 10 seconds respectively, resulting in model times of 4, 2.5 and 0.8 seconds. For the direction changes, these time scales seem reasonable and should be achievable by a suitable mechanical system. However, for the velocity changes, that rely on moving air masses with significant inertia, the time scale

required for the small tornado would represent a challenge. The vertical direction variations are over much smaller time scales in each case but could probably be achieved with a mechanical system to tilt the model, but probably not with a system that tries to deflect the moving air downwards or upwards.

**Concluding remarks**

Based on what has been set out above, it would appear that the type of local simulation described in this post has some potential. The use of such a simulation would be restricted however to medium and large storms, as the velocity changes for small storms would be difficult to achieve at model scale. Similarly, the conditions very close to the storm track, in particular the vertical velocity changes, are unlikely to be able to be adequately modelled.

However, I am now retired, with no access to either lab facilities or funding, so if such a simulation is to be further investigated, someone else will need to do it!

# Professor Julian Hunt FRS, Baron Hunt of Chesterton (1941-2026)

June 11, 2026

**Author's note**

This post contains the text of a tribute to Julian Hunt that I delivered (through a recording) to the Wind Engineering community gathered at London Ontario for the Conference Dinner of the Computational Wind Engineering Conference in June 2026. I cannot claim to have known Julian well – he would have regarded me as a simple acquaintance – and much of the material below is derived from other public sources. However it does contain some personal memories, that are of particular relevance to those in the wind engineering discipline and I hope it will be of some interest to readers in that community. Note that the tribute as delivered was somewhat shorter than that contained below because of the restrictions of time.

**Other obituaries**

Other obituaries can be found via the following links.

- Trinity College, Cambridge
- University of Cambridge
- Royal Meteorological Society
- Royal Society
- Cambridge Environmental Research Consultants
- The Times
- The Guardian
- The Telegraph

**The tribute**

Julian Charles Ronald Hunt was born in Madras in British India in 1941, where his father was a civil servant and diplomat, but spent most of his childhood in England with relatives. He attended Westminster School and Trinity College Cambridge, where he read Mechanical Sciences and graduated with a 1st Class BA in 1963, before carrying out postgraduate research in the field of magnetohydrodynamics, for which he was awarded a PhD in 1967. He had been elected a Fellow of Trinity College in 1966 and in 1967 he undertook post-doctoral research as a Fulbright Scholar at Cornell. From 1968 to 1970, he was a research officer with the Central Electricity Generating Board where, amongst other things, he studied the collapse of the Ferrybridge Cooling Towers. On his return to Cambridge in 1970 he was made a university lecturer in applied mathematics and engineering, and was later appointed Reader and Professor of Fluid Dynamics in 1990. He held numerous visiting professorships, and was also a visiting scholar at the United States EPA in 1977 and the National Center for Atmospheric Research in 1983. He was a founding director of Cambridge Environmental Research Consultants in 1985, which developed his academic work into practical applications, and remained as Chairman of the company until 2022.In 1989 he was elected as a Fellow of the Royal Society and in 1992, became Director General of the Meteorological Office. In 1997 he became Professor of Climate Modelling at University College London, from where he retired in 2008.

Julian Hunt married Marylla Shephard in 1965 and they had three children: novelist Jemima; medical doctor Matilda; and historian and former Member of Parliament, Tristram. He was politically active and joined the British Labour Party in the 1960s, and was served as a Councillor on Cambridge City Council from 1971 to 1974, being leader of the Labour Group in 1972. He was created a life peer as Baron Hunt of Chesterton (a suburb to the north of Cambridge) in 2000. He died on April 20th 2026.

I first came across Julian as a final year undergraduate at Cambridge in the early 1970s when he lectured to me – a short course on vorticity and a longer course on pollutant dispersal based on Gaussian plume modelling, which emphasised the importance of the Richardson number, named after the noted mathematician and meteorologist Lweis Fry Richardson. It was some years later that I realised that he was Julian's great uncle. Julian's lectures were always entertaining, but more than a little chaotic and taking any sort of coherent notes was far from easy. Nonetheless much of the material he covered was to inform my research and scholarship for many years afterwards. I undertook my Bachelor's project in the Hydraulic Laboratory of the Department of Engineering, where there was a prominently displayed photograph of Julian Hunt as a research student from a few years previously, with a suitably 1960s flowing hair style, collecting signatures for an anti-Vietnam war petition.

I saw rather more of him as a PhD student, where his work on flow topology helped me in the interpretation of oil flow visualization of horseshoe vortices. He gave a seminar on this topic in the Department of Applied Mathematics on this work, and it was there that I observed one of

the few occasions when he appeared unsure of himself, wondering what the audience of very able mathematicians would make of his essentially observational topological work.

On another memorable occasion, as I was walking through Cambridge to do some shopping, he cycled towards me, braked heavily on seeing me, took out a notebook and paper and, whilst still astride his bicycle, sketched out how my smoke flow visualization of horseshoe vortices could be used to check his theory of flow between two buildings. This brief encounter was to result in a short paper in one of the early editions of the Journal of Wind Engineering and Industrial Aerodynamics.

Throughout the following decades, Julian was an ever present in the Fluid Mechanics and Wind Engineering Community, at conferences and seminars, and was very supportive in the early days of the UK Wind Engineering Society. His talks were always stimulating even if the style remained a little chaotic and always delivered with confidence. On one occasion I remember him walking into a meeting of the Hazards forum a little late and finding his name down to give a presentation, that he had clearly forgotten about. For the next 20 minutes he sat at the back of the room and wrote one out (it was the days of OHP acetates, not PowerPoint) and then proceeded to give a coherent presentation that gave no clue as to its recent genesis.

Whilst perhaps best known to the wider world for his work on meteorology, climatology and hazard prediction Julian Hunt's contribution to the development of wind engineering has of course been significant, laying the basis for the study of wind effects on pedestrians, wind flow over hills, wind forces on and flows around buildings and the dispersion of pollutants, all based on his fundamental work on the nature of atmospheric turbulence. Much of his work on pollutant dispersion has been incorporated in the ADMS modelling suite which is used worldwide as a powerful design tool.

But, as well as these very real achievements, I would suggest Julian's greatest gift was his ability to analyse a problem, identify the most significant parameters, and develop simple theoretical approaches that could be both practically useful and offer considerable and generisable insights. With our current abilities to generate very large experimental and computational datasets that can so easily cloud our basic understanding of the phenomena we study, cultivating such an approach is perhaps more important than ever, to underpin the huge advances in technology that we are experiencing.

Ladies and Gentlemen, as I am recording this well before you all sat down to eat this evening, I have no idea what will be the state of the meal you are enjoying, but if you still have something left in the glass before you, I would ask you to raise it in a toast, to the memory of Professor Lord Julian Hunt FRS, Baron Hunt of Chesterton.

# Appendix 1. International Wind Engineering Seminars 2020/2021

**Abstracts, speaker biographies, questions and answers**

# International Wind Engineering seminar 1 - Tornadoes – research and design

**Thursday October 8th 14.00 UK time**

**Main speaker**

Identifying and classifying tornadoes in sparsely-populated regions: observations and research needs. Prof Greg Kopp, ImpactWX Chair in Severe Storms Engineering University of Western Ontario

**Short contributions**

Full-Scale Inquiry into Tornado Wind and Loading Characteristics, Dr Franklin T. Lombardo, University of Illinois

Compact debris flow in tornadic flow fields. Prof. Mark Sterling, Beale Professor of Civil Engineering, University of Birmingham

WHAM Research: What Flow Structure of Tornado Should We Design Against? Grace Yan, Associate Professor, Missouri University of Science and Technology

Consideration of tornado modeling based on the experimental and numerical results, Shuyang Cao, Professor, Tongji University, China; Jinxin Cao, Associate Professor, Tongji University, China

The lodging of cereal crops by tornadoes, Chris Baker, Emeritus Professor of Environmental Fluid Mechanics, University of Birmingham

Translation Speed Effects on the Static Pressure Distribution of a Tornado Vortex, Fred Haan, Jr., Professor, Calvin University, Grand Rapids, Michigan, USA

**Abstracts**

***Identifying and classifying tornadoes in sparsely-populated regions: observations and research needs*** Prof Greg Kopp, ImpactWX Chair in Severe Storms Engineering University of Western Ontario. The Northern Tornadoes Project (NTP) is a new effort to identify and classify every tornado in Canada. While Canada has the second most tornadoes of any country in the world, recent studies correlating known tornado occurrences with lightning strike and population data lead to estimates that only 1/4 to 1/3 of the tornadoes are identified on average. Over 2+ years of study, NTP has increased the tornado counts across the country by 78%. However, the project has identified many continued issues with both identifying and classifying tornado occurrence in sparsely populated regions, particularly related to a lack of damage indicators. The presentation will discuss these issues and raise the research needs for obtaining accurate tornado climatologies in such regions.

***Full-Scale Inquiry into Tornado Wind and Loading Characteristics*** Dr Franklin T. Lombardo, University of Illinois Tornadoes cause a significant amount losses in the United States and worldwide. Recent events in the U.S., such as the Joplin, MO and Moore, OK have caused

engineers to rethink philosophies on designing structures to withstand tornadoes. Currently, tornadoes are not included in design although provisions will likely be included in the next version of the U.S. wind load standard (ASCE 7-22). As tornado events are rare and transient in nature, full-scale measurements especially near the ground have been limited. Therefore, the first edition of tornado specific design will have a significant number of assumptions on properties relevant to wind loading (e.g., wind profiles, turbulence, aerodynamics). The limited full-scale wind speed data that have been collected show tornadoes possess different physical properties (e.g., rapid wind speed and direction changes, different vertical profiles, non-zero vertical wind speed) than ABL flow. Full-scale wind loading data, however, is practically non existent. This presentation will discuss ongoing research at the University of Illinois aimed at significantly increasing the quantity and quality of full-scale measurements of tornadoes that are relevant to wind engineering through a comprehensive scientific inquiry. Research to be discussed includes: 1) estimating wind speeds and wind field characteristics through patterns of damage observed in trees, corn and soybeans; 2) capturing wind characteristics (including turbulence) using novel and low-cost, rapidly deployable sensors; 3) exploration of tornado-like aerodynamics with a small bluff body in dustdevils and 4) various other complementary projects such as linking observations with LES and citizen science efforts. Progress on tornado loading design through the ASCE 7-22 tornado task committee over the last 2.5 years and leading the development a design profile (Kz) for tornadoes will be briefly highlighted.

***Compact debris flow in tornadic flow fields.*** Prof Mark Sterling, Beale Professor of Civil Engineering, University of Birmingham. The wind loading arising from tornadoes can be of significance in many parts of the world. Such loading has received considerable interest in the past and forms the basis of a large number of current research projects. A common feature of most tornadoes is a cloud of debris which is generated and transported as a result of the flow field associated with the tornado. However, the flight of windborne debris within such flow fields has received relatively little attention despite the implications that such phenomena can have on structural loading. This presentation will combine physical and numerical simulations in order to examine the trajectory of compact debris in a tornado-like flow field.

***WHAM Research: What Flow Structure of Tornado Should We Design Against?*** Grace Yan, Associate Professor, Missouri University of Science and Technology. Tornadoes have induced substantial structural damage, injuries and deaths in the USA. They occur in Mainland America, mainly “Tornado Alley” and Southeast of the USA, and contribute $10B annually to the nation’s loss portfolio. The devastation from recent tornadoes (e.g., Joplin, MO, in 2011;

Tuscaloosa, AL, in 2011 and Moore, OK, in 2013) left no doubt as to the vulnerability of the central and southeastern USA to tornadoes, and prompted an urgent need in developing and enforcing a tornado-resistant design for normal buildings. This requires in-depth understanding of tornadic wind effects. To find tornadic wind effects, what type of tornadoes should we look at? Tornadoes have different flow structures, single-celled single-vortex, double-celled single vortex and multiple vortices; Even for a single tornado incident, the flow structure varies with time and location. Based on which type of tornado should the wind effects be used to modify the coefficients in the pressure calculation equation in ASCE7-16? In other words, which type of tornado induces more unfavorable wind loading?

***Consideration of tornado modeling based on the experimental and numerical results,*** Shuyang Cao, Professor, Tongji University, China; Jinxin Cao, Associate Professor, Tongji University, China. Physical and numerical simulations of tornado-induced effects on low-rise buildings, bridges and other structures have been carried out in our lab. This short presentation

will discuss following issues related to appropriate modeling of tornado effects: 1) The relationship of flow-based swirl ratio and geometry-based swirl ratio; 2) Should the vortex wander be considered as a representative of the instantaneous vortex structure? 3) Is it possible to find scale ratios from various ones that play dominant roles in determining the wind effects on structures from benchmark test results?

***The lodging of cereal crops by tornadoes, Chris Baker***, Emeritus Professor of Environmental Fluid Mechanics, University of Birmingham. Tornado tracks have often been observed in fields of crops and efforts have been made in the past to infer tornado strength from the width of these tracks. This presentation will briefly present work by the author in this area, and will describe a generalized model of crop lodging that has been used in the past for a variety of crops, together with a new tornado model that captures the apparent near ground velocity field. Lodging patterns similar to those seen in the field can be predicted and the model offers the possibility that it can be used in a more quantitative way if robust crop agronomic data is available.

***Translation Speed Effects on the Static Pressure Distribution of a Tornado Vortex***, Fred Haan, Jr., Professor, Calvin University, Grand Rapids, Michigan, USA. Tornado vortices generate regions of reduced static pressure near their cores. In tornado simulator tests or in design estimates, it is typically assumed that this static pressure acts a bit like a reference pressure that can be subtracted from the windfield-induced pressure on a building to analyze the "aerodynamic" pressure apart from the "static" pressure. The static pressure to be subtracted is often measured or modeled with a stationary vortex. This framework may be too simplistic. If one considers the unsteady effect of the translation speed of a vortex, it is clear that a translation speed dependent pressure is generated in addition to the static pressure drop associated with a stationary vortex. Potential flow simulations with a single vortex show that this speed dependent pressure can add 20% to the static pressure of a stationary vortex

when the translation speed is 10% of the maximum tangential velocity. It can add 40% to the static pressure when the translation speed is 20% of maximum tangential velocity.

**Speaker biographies**

***Prof Greg Kopp*** is a Professor of Civil & Environmental Engineering at the University of Western Ontario, where he has been since 1997. He currently holds the ImpactWX Chair in Severe Storms Engineering, where he leads the Northern Tornadoes Project, which is related to the topic of his talk today. He also joined the University of Birmingham in 2019 as Professor of Wind Engineering. Greg has been active in service to the community and is currently Chair of the ASCE 49 Standards Committee on Wind Tunnel Testing for Buildings and Other Structures, amongst other roles.

***Dr Frank Lombardo*** received his Ph.D. from Texas Tech University in 2009 studying thunderstorm wind characteristics and subsequent loading on a low-rise building. Dr. Lombardo was a postdoctoral research associate at NIST where he played a significant role in the investigation of the Joplin, Missouri tornado in 2011 and the creation of updated wind maps for ASCE 7-16. Lombardo has been at the University of Illinois at Urbana-Champaign (UIUC) since 2015. In his time at UIUC, he has been awarded competitive research projects through NOAA, NSF and NIST studying wide-ranging aspects of wind science and engineering and was the recipient of the 2019 International Association of Wind Engineering Junior Award. He also

serves as vice-chair of the tornado task committee, which has proposed tornado loading provisions for ASCE 7-22.

***Prof Mark Sterling*** is Beale Professor of Civil Engineering and Deputy Pro Vice-Chancellor (Staffing) at the UoB with over 20 years research experience in wind engineering. His research focuses on transient winds, particularly the effects of extreme winds on infrastructure, vehicles and biological systems. A member of the BSI wind loading committee responsible for updating EN1991-1-4 and a member of an ASCE committee re-writing the wind tunnel standards code of practice, both of which ensures his research effectively translates into practice.

***Dr Grace Yan*** is Associate Professor of Missouri University of Science and Technology, Director of the Wind Hazard Mitigation (WHAM) Laboratory. She is passionate about the mitigation of hazards induced by extreme winds, such as tornadoes and hurricanes, and the achievement of community resilience. Her research includes the simulation of different wind fields numerically and experimentally, dynamic responses on civil structures induced by extreme winds, and reproduction of damage scenarios induced by extreme winds using numerical simulations. She published 47 journal papers and 57 conference papers. She is the recipient of 25 research grants with a total fund of $9.94 M.

***Dr. Shuyang Cao*** is a professor at the Civil Engineering college of Tongji University and a professor at the State Key Laboratory for Disaster Reduction in Civil Engineering, China. Before he joined Tongji University, he was an associate professor at the wind engineering center of Tokyo Polytechnic University and an assistant professor of Tokyo Institute of Technology, Japan. Dr. Shuyang Cao works in both structural and environmental wind engineering fields. His research interest includes the development of numerical and physical modeling techniques for wind engineering problems, structure aerodynamics and wind-resistant design of structures.

***Prof Chris Baker*** read Engineering at St Catharine's College in Cambridge, graduating with a BA in 1975, and an MA and a PhD in 1978. Following a Research Fellowship at St Catharine's College and the Department of Engineering, in the early 1980s he began work in the Aerodynamics Unit of British Rail Research in Derby, before moving to an academic position in the Department of Civil Engineering at the University of Nottingham. He remained there till 1998 as a lecturer, reader and professor with research interests in vehicle aerodynamics, wind engineering, environmental fluid mechanics and agricultural aerodynamics. In 1998 he moved to the University of Birmingham as Professor of Environmental Fluid Mechanics in the School of Civil Engineering. From 2003 to 2008 he was Head of Civil Engineering and was the Director of the Birmingham Centre for Railway Research and Education from 2005 to 2014. He retired at the end of 2017 and took up an Emeritus position. He continues to be involved in research in train aerodynamics, wind engineering and transport issues. In July 2020 he was awarded the Davenport Medal, the senior award of the International Association of Wind Engineering.

***Prof Fred Haan*** is a Professor of Engineering at Calvin University in the United States. He has conducted research in wind engineering for more than 20 years primarily in experimental aerodynamics and extreme wind simulation techniques. Fred received his PhD from the University of Notre Dame in 2000, and has worked on wind-induced vibration of long-span bridges, vortex-induced vibrations, atmospheric boundary layer simulation and laboratory tornado simulations. While on the faculty at Iowa State University, he worked with Partha Sarkar to develop and build the world's first large tornado simulator intended to test tornado-induced loading on buildings and structures.

# International Wind Engineering Seminar 2: Indoor and Outdoor Ventilation and Dispersion

**Thursday November 5th 12.00 noon UK time**

**Main Speaker**

Outdoor and indoor ventilation and dispersion associated with COVID-19 transmission.
Prof Bert Blocken, Eindhoven University, The Netherlands; KU Leuven, Belgium

**Panel Members**

Prof Ted Stathopoulos, Concordia University, Montreal, Canada

Prof Kenny Kwok, University of Sydney, Australia

Prof Yoshihide Tominaga, Niigata Institute of Technology, Japan

Dr. Eoghan Clifford NUI Galway, Republic of Ireland

**Abstract**

Within a time span of only a few months, the SARS-CoV-2 virus has managed to spread across the world. This virus can spread by close contact, which includes large droplet spray and inhalation of microscopic droplets, and by indirect contact via contaminated objects. This presentation addresses large droplet and aerosol dispersion in outdoor and indoor environments, associated with different types of sports activities or scenes. First, droplet and aerosol spreading in cycling pelotons is analyzed, and the wide range of often contradictory views from scientists from different fields are summarized. Second, a strategy is proposed to safely re-open and keep open indoor sports centers during the COVID-19 pandemic. Third, some recently realized and ongoing practical research projects are briefly outlined, including the measurement and reduction of aerosol concentrations in a fitness center, the measurement and reduction of aerosol concentrations in the team bus of a professional cycling team for the past Tour de France and a project on aerosol assessment in football stadia.

**Speaker and panel member biographies**

***Professor Bert Blocken*** ( born in1974 in Hasselt, Belgium) is a Civil Engineer holding a PhD in Civil Engineering / Building Physics. He is Full Professor at Eindhoven University of Technology (TU/e) in the Netherlands and part-time Full Professor at KU Leuven in Belgium. His main areas of expertise are urban physics, wind engineering and sports aerodynamics. He has led the design and construction of the Eindhoven Atmospheric Boundary Layer Wind Tunnel and currently acts as its Scientific Director. He has published 194 papers in international peer reviewed journals. He is supervising a team of 6 senior researchers and 24 PhD students.

***Professor Theodore (Ted) Stathopoulos*** is currently Professor at Concordia University, Montreal, Canada. His research in the area of wind effects on buildings and their codification has been influential in the development of codes and standards around the world. He has an extensive publication record with more than 500 articles in refereed journals and conference proceedings. He is a member of the ASCE 7 Committee on Minimum Wind Loads and the respective committee of the Canadian Code. He is a Fellow of the Canadian Academy of Engineering, the Institution of Civil Engineers and the American Society of Civil Engineers and its Structural Engineering Institute. He is the Editor of the Journal of Wind Engineering and Industrial Aerodynamics. He has been appointed Distinguished Professor in Building Physics, Urban Physics and Wind Engineering by the Technical University of Eindhoven, The Netherlands He has received an Honorary Doctorate from the Aristotle University of Thessaloniki, Greece; and another one from the Technical University of Eindhoven, The Netherlands.

***Dr. Eoghan Clifford*** is a chartered engineering and currently works as a Senior Lecturer in Civil Engineering, NUI Galway. He is the Programme Director of the BSc Project & Construction Management at NUI Galway and the Academic Director of the CEIM Programme within the School of Engineering. He is also a visiting research fellow at the Athlone Institute of Technology. His key research and educational interests lie in the areas of fluid dynamics, cycling aerodynamics, wastewater and water engineering and the development of tools and sustainable technology that can improve outcomes in these sectors. He is also collaborating with the technical University of Eindhoven on modelling the aerodynamics of paralympic cyclists on tandem and handcycles.

***Professor Kenny Kwok*** is a Professor of Engineering at The University of Sydney. His research interests include wind engineering, structural dynamics, vibration control, human perception of motion, and environmental fluid mechanics. His research focuses on fundamental aspects of building aerodynamics and wind-structure-occupant-damper interactions, and their practical applications in real life situations. He has published over 500 articles in journals, book chapters, invited and keynote papers, and conference papers. He is the recipient of 2019 ASCE Jack E. Cermak Medal, 2019 IAWE Senior Award and Davenport Medal, and a Life Member of Australasian Wind Engineering Society.

***Prof. Yoshihide Tominaga*** is a Professor of Architecture and Urban Environment Division and Director of Wind and Fluid Engineering Research Center at the Niigata Institute of Technology, Japan. His area of expertise is numerical and experimental modelling of micro-scale wind flow

and the related processes in the urban environment, including cross-ventilated room airflow, pedestrian wind comfort, air pollutant dispersion, snowdrift etc. He has served as chair of the wind environment committee of the Architectural Institute of Japan (AIJ), which initiated 'AIJ guidelines for practical applications of CFD to pedestrian wind environment around buildings' .

# International Wind Engineering Seminar 3: Modeling the Dynamics of Tall Buildings Under Winds: From Historical Perspective to Recent Advances and Beyond

**Thursday December 3rd 12.00 UK time**

**Main Speaker**

Prof Ahsan Kareem, NatHaz Modelling Laboratory, University of Notre Dame, USA

**Panel Discussion**

Professor Yukio Tamura, School of Civil Engineering, Chongqing University, China Dr. Melissa Burton, Arup, Toronto, Canada

Dr. Tracy Kijewski-Correa, Keough School of Global Affairs and College of Engineering, University of Notre Dame, USA

Dr. John Kilpatrick, RWDI, Guelph, Canada

**Abstract**

The seminar will briefly summarize the history of wind engineering of tall buildings from the design of the World Trade Center Towers to the present-day skyscrapers and beyond. First of all, the equations of fluid motion are mathematically intractable, which has led to reliance on the physical modeling in wind tunnels. From earlier studies at the National Physical Laboratory in the UK involving the World Trade Center Towers, it was realized that it was essential to model the inflow that was reflective of the atmospheric boundary layer rather than a uniform flow in an aeronautical tunnel. At that juncture, the dynamic response was evaluated using base-pivoted aeroelastic models while a search for a more expeditious means of assessing wind loads was in progress, which led to the development of various force balances. In this context, a general overview of the basic techniques for the quantification of wind loads and their dynamic effects using analytical, experimental, computational fluid dynamics (CFD) and model-based and data driven simulation schemes, database-enabled platforms, code and standards-based procedures and lessons from full-scale monitoring will be presented in a historical perspective. This will be followed by a synopsis of the emerging frontiers in computational approaches for shape and topological optimization, the vulnerability of glass cladding in extreme winds, the role of organic damping and damping devices for the mitigation of building motion. In closing, the concept of morphing tall buildings using sensing, computational intelligence and actuation of the dynamic façade for futuristic buildings will be presented.

**Speaker and panel member biographies**

**Ahsan Kareem** is the Robert M. Moran Professor of Engineering and the Director of the NatHaz Modeling Laboratory at the University of Notre Dame. His work focuses on

probabilistic characterization and formulation of dynamic load effects due to wind, waves and earthquakes

on tall buildings, long span bridges, offshore structures and other structures, via analytical and computational methods, fundamental experimental laboratory and full-scale measurements utilizing cyber and cyber-physical infrastructures, for their safety assessment and mitigation measure. He is elected President of the International Association for Wind Engineering (IAWE). He has been awarded numerous honors, including the Presidential Young Investigator Award from the White House Office of Science and Technology. A recipient of ASCE's: Theodore von Karman Medal, Masanobu Shinozuka Medal, James Croes Medal, Earnest Howard Medal, Robert H. Scanlan Medal and Jack E. Cermak Medal and State-of-the-Art Award, inducted to the Offshore Technology Conference Hall of Fame and Distinguished Member of ASCE; Alan G. Davenport Medal of IAWE; Distinguished Research Award of IASSAR (Int'l Assoc. for Structural. Safety and Reliability); the University of Notre Dame. He has served as a High-End Foreign Expert at Tongji University and delivered 2013 Scruton Lecturer at the Institute of Civil Engineers, London, UK. He has been appointed Honorary Professor at several universities overseas, serves on the Editorial Board of several international journals incuidng Guest Editor of Engineering, CAE Journal, and has recently co-authored two books. He is an elected Member of the US National Academy of Engineering and a foreign member of the Indian Academy of Engineering, Engineering Academy of Japan and Chinese Academy of Engineering.

**Melissa Burton** is a Principal at Arup. Her work focuses on the intersection of the built and natural environments. She started her career looking at how the wind climate affects the buildings we design, and how the consequential reaction of the buildings affects the people that occupy them. Her technical expertise extends to beyond code approaches using advanced analytical tools to quantify and reduce design risk from wind loading. She has most recently collaborated with the Charles Pankow Foundation to publish criteria and methodologies for designing tall buildings to be more resilient in wind events.

**Tracy Kijewski-Correa** is the Leo E. and Patti Ruth Linbeck Collegiate Chair and Associate Professor, Department of Civil and Environmental Engineering & Earth Sciences, and Associate Professor of Global Affairs at the University of Notre Dame Her research focuses on disaster risk reduction (DRR) and civil infrastructure challenges posed by increased urbanization and vulnerability. Her interdisciplinary scholarship links science and technology to vulnerable communities, delivering scalable paradigms to enhance the resilience and sustainability of civil infrastructure and inform the decisions of stakeholders such as homeowners, designers, planners, emergency managers and policymakers. She currently serves as the inaugural director of the Structural Extreme Event Reconnaissance (StEER) network, which organizes networks of engineers to assess damage after disasters globally and use this knowledge to drive recovery and future DRR practices.

**John Kilpatrick,** Ph.D., P.Eng., C.Eng., F.ICE, is the Wind Engineering Practice Leader at RWDI and a Principal of the firm. John is a former Chair of the UK Wind Engineering Society, and is a contributing author to the ASCE/SEI Prestandard for Performance-Based Wind Design and ASCE 49 Standard for Wind Tunnel Testing for Buildings and Other Structures.

**Yukio Tamura** is a Professor of the School of Civil Engineering, Chongqing University, China, and the Honorary Director of the Wind Engineering Research Center, Tokyo Polytechnic University, Japan. He served as the President of the International Association for Wind Engineering for eight years from 2007 to 2015. He is currently serving as an Adjunct/Guest/Honorary Professor of 19 universities in China, Korea, Malaysia, Poland, and USA. Professor Yukio Tamura is a member of the Engineering Academy of Japan, a Foreign Fellow of the Indian National Academy of Engineering, and a Foreign Member of Chinese Academy of Engineering.

**Questions to the panel**

Questions from Albert Hansel to Prof. Kareem:

1. Does the philosophy of earthquake design such as the formation of plastic hinge in the beams also applied to wind loading?

2. In light of design processes especially for tall buildings, should the earthquake loading separated with wind loading, or we can combined them together at the same time?

3. How much approximate damping ratio that we usually use in wind loading for design? for example in earthquake we usually use 5% of damping ratio

AK: (1) It could but at this time it is being explored under the performance-based design approach. (2) There are some combination rules in special cases, but as such concurrent occurrence of earthquakes and a severe wind events are not considered. There a a few studies that are exploring based on risk the combination of the two loads. However, there is a very limited data to build upon. (3) Each standard or a building code has its own specification, for wind typically it is 1% though several of the tall towers even of concrete exhibit values lower than this number for low wind speeds, i.e., for serviceability/human comfort. ASCE & addresses this in detail.

Question from Karim Mostafa to Dr. Kareem, Thank you Dr. Kareem for your presentation, my question is Could it be possible to depend mainly on CFD models instead of wind tunnels models in the near future or wind tunnels are always and will remain a necessary tool for verification of CFD models?

AK: I am hopeful that computational resources large enough become available so that CFD can be conducted reliably and accurately. This may happen soon but will be limited to select groups. I think in the near future we will have to rely on the wind tunnel and slowly we may start to see CFD competing on a limited basis. Also one needs to explore a combination

of machine learning to enhance the CFD based schemes, which may help to usher CFD on the table sooner.

Question from Simon Leefe to Dr. Kareem: where can I obtain further details of the synthetic influx boundary condition of CFD?

AK: You may find it on the web site of NHERI SimCenter web site at

https://simcenter.designsafe-ci.org/research-tools/tinf/. The tool name is TinF.

From Chris Geurts to Everyone: Dear all, thanks Ahsan, and Tracey for your comments on the importance of full scale measurements. I hope that we are able to get this done in practice. My experience so far with full scale measurements is that it needs a driving question for a party to

invest in such activities. Usually a client is happy to have the building built, sometimes then sells it to another party and no one has, or feels, the interest to start (and pay for) monitoring. Currently we are starting a monitoring programme in the Netherlands. Maybe not so high, but we typically have very soft soils, so the effect of deep foundations are of our particular interest. Any tips and tricks for us on how to 'sell' these activities to customers are very welcome!

YT: At the dawn of tall buildings, e.g. the late 1960s to the early 1970s in Japan, some owners could understand the meaning and significance of the full-scale monitoring for the following two purposes: confirmation of the assumptions at the design stage; and purely scientific fact findings. Recently, the full-scale monitoring is commonly made for buildings which install some special damping devices to confirm their performance. Some big real-estate companies are

interested in monitoring behaviors of a group of own buildings to immediately capture the situations of their buildings in case of disasters. They also understand the merit of the full-scale monitoring with "Invest Today, Save Tomorrow" policy.

TKC: The sell is always more challenging after a building is commissioned, so I do believe it is going to be better going forward that we build this into the contract when the building is designed and constructed. This was how the door was opened for Burj Khalifa (via Samsung as part of their contract to build the tower). For post-construction instrumentation, the no-cost sell for us was easier, in that we argued much like personal health, it is helpful to verify from time to time that the vitals are as expected and affirm the structure is operating as intended. This also ensures that their structure can have a well-calibrated Digital Twin to engage in evaluating future modifications to the building (or assessments after some shock as Yukio also suggested). So these were cases where a grant paid for the hardware and we just needed the permission to get into the building. Cases of at-cost post-construction instrumentation have been isolated for us but in all cases stemmed from the owner having a concern (so it was for either "sick" buildings or buildings undergoing some design revision or

retrofit where they needed to calibrate a reliable FEM for an older building), so as you suggest, they really need to have a pressing need or question to be willing to make that investment, since benefits for day-to-day operations are too little to justify the cost.

AK: I concur with YT and TKC. Sometimes even if it is at no cost to the owner and the owner realizing some value to monitoring, their legal office advises them against permitting because if we find anything it may be detrimental to the rental space market for the building. In one case I asked what could we find that could impact, the answer was if we find asbestos. So this was the technical level with which the legal office was placing their opinion!

From Giuseppe Piccardo to Everyone: Question from Giuseppe Piccardo to Prof. Kareem and Dr. Burton: thank you very much for the presentation and for the heartfelt memory of our dear Giovanni, thank you! The higher oscillation modes can be of actual technical interest even for tall buildings or just for special cases of super tall buildings ? (but I remember a seminar where

they didn't seem particularly important even for NY 432 Park Avenue). Then Dr Melissa Burton added that she often found results highly influenced by higher modes in terms of building serviceability. Is there an influence of VIV on the higher modes? Thanks again.

YT: I presume Melissa will answer, but the following is just for your reference. As the human perception threshold suggests that people are more sensitive to vibration in the frequency region 1Hz – 2Hz, even if the higher-mode acceleration amplitude is lower than the fundamental mode, people can be more sensitive to the higher mode vibration with a higher frequency in the case of tall and super-tall buildings as shown here. In this case, the effect of VIV is not significant for the higher modes.

TKC: My experiences in monitoring have affirmed that higher modes are not an issue for the vast majority of tall buildings UNLESS the fundamental mode is very low-frequency, e.g., 0.1 Hz or lower. The most flexible building I have worked on, Burj Khalifa, did have notable higher frequency mode participation in its responses. This produced a "tail wagging the dog effect" where the spire could actually excite the main tower via a second sway mode that kicked out at lower elevations (akin to what Melissa noted). Most buildings at best have only the fundamental mode in the "sweet spot" where the wind field's energy is highest, but in the case of Burj Khalifa it had up to 6 modes that could be easily excited by wind. The emphasizes the importance of considering these higher mode effects, particularly for occupant comfort, as the affected floors

will not be the top floors for these modes, but lower floors of the building. (See Dr. Tamura's comment above)

AK: I concur with observations made by YT and TKC. When in my lecture I mentioned the higher modes I was referring to super tall buildings where higher modes could be closer to the VIV type wake excitation. The other point I was making was about the spatial geometry of the

mode shape and the distribution of the fluctuations in loading. After all the net effect is the weighted loading concerning the mode shape. If they negate each other it would not matter even if the frequency alone is in the range of excitation. When one talks about VIV what comes to mind is a resonant type behavior with more of a sinusoidal type excitation. Most of the acrosswind loading on buildings shows spiky spectra but not like those of a sinusoidal loading. So when you heard about 432 PA they may have preferred to call it to wake excited rather than a VIV type. However, if we have motion-induced loads or negative damping come into play it can further complicate the situation. We may have VIV with lock-in features if we keep building needle-like structures which would require fortifying them with damping devices. That is where your models may come into play. Actually, there are energy-harvesting structures that exhibit VIV and that energy is captured.

Question from Yufen Zhou to all panelists: Regarding occupational comfort, for buildings that are in the design stage without the full scale monitoring data available, how can we ensure that the acceleration response from the analysis predicts the full scale performance in a conservative way? In other words, can the common approach from HFFB wind tunnel tests or CFD capture effectively the possible discomfort level of tall buildings in the future under wind?

YK: In general, HFFB can be useful, but considering the higher-mode problems, the pressure integration technique using the simultaneous multi-channel pressure measuring system (SMPMS) might be better.

TKC: Echoing Prof. Tamura's point, the first issue is understanding the dynamics sufficiently to appreciate if HFFB is sufficient (with higher modes, you need to use other approaches to determine the wind load). Even with a well executed FEM, you still will need to guess a damping value. This is our biggest uncertainty in the process. We have continued to work to document the effect of high efficiency tall buildings with strong cantilever overturning behaviors and the fact that they have very little energy dissipation (far less than systems dissipating through frame racking). So the biggest threat to occupant comfort prediction mistakes is picking damping too high. It is very common for us to see damping below 1% critical in service conditions for tall buildings with high efficiency systems, even if they are made of concrete. Our model helps to predict damping values for such systems but the key takeaway is only through monitoring will we be able to continue to update/refine that model and our FEM and wind tunnel methodologies so they can be helpful in predicting the responses of future designs — its a critical feedback loop!

AK: Both YT and TKC have made good points. We cannot overemphasize the importance of damping. I have been involved in several buildings in which a minor increase in damping would qualify the building to be OK from human comfort consideration. Therefore, as we have done in ASCE 7 damping in wind is chosen to be on the lower side to give you the conservative results you were referring to.

# International Wind Engineering Seminar 4: Developments in Bridge Aerodynamics

**Thursday January 7th 2021,12.00 UK time**

**Main Speaker**

Dr John Owen, School of Engineering, University of Nottingham, United Kingdom, The Response of Bridges to Wind – Some Lessons from Monitoring Large Bridges

**Short presentations**

Prof Steve Cai, Louisiana State University, Time domain simulation of turbulence effects on the aerodynamic flutter of long span bridges.

Prof Claudio Mannini, University of Florence, Nonlinear modelling of self-excited forces for a long-span bridge under turbulent wind

Prof Ole Andre Øiseth, Norwegian University of Science and Technology. Lessons learned from long-term wind and acceleration monitoring of the Hardanger Bridge.

Prof Luca Caracoglia, North Eastern University, Boston, Relevance of Uncertainty Quantification to Study Wind Load Variability and its Effects on Long-Span Bridge Aeroelasticity

**Abstracts**

***The Response of Bridges to Wind – Some Lessons from Monitoring Large Bridges.*** This presentation will consider the lessons that can be learnt from monitoring the wind induced response of long span bridges by reviewing monitoring exercises on three different bridges. Developments in instrumentation and data analysis will briefly be reviewed before looking at specific wind response phenomena. The presentation will consider observations of vortex induced vibration and buffeting response and consider how these can be used to improve design predictions and modelling methods. With regard to buffeting, the influence of uncertainty in wind field parameters on the response of the bridge will be examined and the consequences for design identified. An example of non-stationary response due to thunderstorm activity will be presented, which demonstrates that non-stationary wind features can lead to significant structural response. The presentation will conclude by looking forward to how best to exploit the data from monitoring systems installed as "standard" on new bridges.

***Time-Domain Simulations of Turbulence Effects on the Aerodynamic Flutter of Long-Span Bridges.*** Though turbulence effects on bridge flutter have been studied in the last few decades, its true effects remain a debate due to the limitation of previous wind tunnel facilities. In order to investigate and explain the effect of wind turbulence on the flutter

instability, a time-domain simulation is carried out, which avoids the complicated random parametric excitation analysis

used in previous studies. The simulations show the turbulence can change the vibration patterns and weaken the spatial vibration correlation to some extent. Due to this stabilizing effect, the critical flutter velocity is increased by 5% to 10% over that under smooth flow.

***Nonlinear modelling of self-excited forces for a long-span bridge under turbulent wind.*** The prediction of the dynamic response of a long-span bridge under turbulent wind is a complicated task due to the important role played by nonlinearities and fluid memory. It is well known that a key issue is the nonlinear dependence of self-excited forces on the unsteady angle of attack induced by large-scale turbulence. The advantages of a relatively simple time-variant model over the classical linear time-invariant approaches are discussed and quantified based on a specific wind tunnel test campaign. In particular, the experiments for two different bridge sections revealed the viability for practical engineering applications of the basic assumption of slowly-varying angle of attack.

***Lessons learned from long-term wind and acceleration monitoring of the Hardanger Bridge.*** The Hardanger Bridge is spanning the Hardanger fjord which is located at the west coast of Norway. A comprehensive monitoring campaign started in 2013 shortly after the bridge was opened to traffic and it is still ongoing. The monitoring data has revealed that uncertain turbulence parameters have a significant impact on the observed dynamic response and that the current design practice underestimates the dynamic response of the bridge severely. The monitoring data also underlines that nonstationary events can be severe and govern the bride design. This presentation outlines the lessons learned and gives an introduction to the methods developed for improved response predictions.

***Relevance of Uncertainty Quantification to Study Wind Load Variability and its Effects on Long-Span Bridge Aeroelasticity.*** This short presentation will examine past and recent research activities in the field of bridge aeroelasticity under the influence of uncertain, experimentally measured loads and modeling simplifications. Description will include: (1) probability-based, stochastic algorithms for evaluating buffeting response influenced by various error sources, (2) Monte-Carlo sampling used to analyze bridge performance over time through life-cycle cost estimation, and (3) flutter reliability contaminated by random Scanlan (flutter) derivatives. In this context, the presentation will briefly introduce how Artificial Intelligence may be employed to investigate flutter occurrence without requiring solution of the multimode equations. Application examples will be derived from models of either existing or simulated long-span bridges.

**Speaker biographies**

***Dr John S Owen*** is an Associate Professor in the Department of Civil Engineering at the University of Nottingham, where he has been for 27 years, serving two terms as Head

of Department. He is a past chair of the UK Wind Engineering Society and was co-chair of the 6th European and African Conference on Wind Engineering. John's principal research interests are in the dynamic response of structures to the wind and the use of dynamic data in structural health monitoring. He has been involved in monitoring the response of long span bridges to wind for many years, initially leading the monitoring programme on the Kessock Bridge (Scotland) and more recently working on the Forth Road Bridge (Scotland) and Phu My Bridge (Vietnam). John has also worked closely with colleagues in computational wind engineering to simulate the aero-elastic behaviour of bridge sections and has led a number of wind tunnel studies on section and full aero-elastic bridge models. He was responsible for the design and commissioning of the atmospheric boundary layer wind tunnel at Nottingham. Most recently, John has been working on the resilience of infrastructure in Typhoons developing a risk based methodology for networks in Vietnam.

***Steve Cai*** is the coordinator of Structures Group at Louisiana State University and the holder of the Edwin B. and Norma S. McNeil Distinguished Professorship since 2010. He had his BS, MS and PhD from Zhejiang University, Tsinghua University, and Univ. of Maryland, respectively. His research interests include bridge performance evaluation, hazard mitigation of costal infrastructures (and vehicles) under wave/wind actions, and long-span bridge aerodynamics. He has served on many editorial boards and technical committees. Other major professional services include served as Secretary and Treasurer of American Association for Wind Engineering for more than 10 years.

***Claudio Mannini*** is an assistant professor of the Department of Civil and Environmental Engineering, University of Florence, Italy. He got his Ph.D. in 2006. He received the ANIV Award in 2008, the IAWE Junior Award in 2011, and the EASD Junior Research Prize in 2014. His main research interests are bluff-body aerodynamics and wind-induced vibrations, addressed from theoretical, computational and experimental points of view. Since his Ph.D. thesis, he has always been enthralled by the aerodynamics of long-span bridges.

***Ole Øiseth*** is a full professor in structural dynamics at the Department of Structural Engineering at the Norwegian University of Science and Technology. He is the head of the structural mechanics research group and the educational coordinator of the study program in civil and environmental engineering. The dynamics of structures subjected to environmental loading is his main research field. His research interests are stochastic dynamics, wind engineering, marine engineering, structural reliability and structural health monitoring. He has supervised 20 PhD candidates and 80 master students within these research fields since 2012.

***Luca Caracoglia*** is currently an Associate Professor in the Department of Civil and Environmental Engineering of Northeastern University, Boston, Massachusetts, USA. His research interests are in structural dynamics, random vibration, wind engineering, fluid structure interaction of civil engineering structures, linear and nonlinear cable network dynamics, wind-based energy harvesting systems and wind energy. Luca Caracoglia

received the NSF CAREER Award in 2009. He was elected Fellow of the American Society of Civil Engineers in 2020.

# International Wind Engineering Seminar 5. Wind loading code developments

**Thursday February 11th 2021,12.00 UK time**

**Main Speaker**

Svend Ole Hansen, Svend Ole Hansen ApS, Eurocode on Wind Actions

**Short presentations**

Francesco Ricciardelli, Professor of Structural Engineering, University of Campania "Luigi Vanvitelli", Italy, Calibration of Code factors for Climatic Actions

Professor John Dora, infrastructure resilience, asset management and standards expert, Developments in addressing climate change in design codes

Donald Scott Latest updates to the ASCE 7 Wind Provisions and Development of Performance Based Wind Design Prestandard.

**Abstracts**

***Eurocode on Wind Actions.*** The second generation of Structural Eurocodes are currently being prepared, and this includes a revision of the Eurocode on wind actions EN 1991-1-4. The talk will focus on the expected content of the revised EN 1991-1-4. The scope of EN 1991-1-4 has been extended to structures with heights of up to 300 m, and a new wind model providing accurate mean wind velocities and turbulence intensities for heights of up to 300 m has been included. The revised EN 1991-1-4 extends the number of pressure and force coefficients considerably enabling a much larger variety of structures to be covered. The two procedures used to calculate along-wind dynamic response in the current EN 1991-1-4 have been harmonized into a single procedure, which also covers structures with simple mode shapes having changing signs. A single procedure for calculating vortex-induced vibrations has replaced the two procedures of the current Eurocode. The revised EN 1991-1-4 includes completely new Annexes on across-wind and torsional actions on susceptible buildings, guidance on derivation of design parameters from wind tunnel tests and numerical simulations, guidance on probabilistic models for wind actions, and response of steel lattice towers and guyed masts.

***Calibration of Code factors for Climatic Actions.*** Calibration of Partial and Combination factors for climatic actions for Code implementation requires the probabilistic modelling of the action itself and of the structural behaviour, and the choice of a required reliability level. In the case of wind, probabilistic modelling of the action is based on the combined probabilistic modelling of reference mean wind velocity, of the characteristics of the Atmospheric Boundary Layer, of pressure or force coefficients and of the dynamic factor. Sources of uncertainty shall also be accounted for. For Combination factors, possible cross-

correlation between two actions shall also be checked. The presentation is aimed at pointing out difficulties arising in the calibration process.

***Developments in addressing climate change in design codes.*** Climate change has implications for any code that involves designing for weather effects; important design codes such as the Structural Eurocodes including EN 1991 Part 1-4 has guidelines based upon historic weather observations. This talk will outline how standards' developers are intending to address future climate patterns, with reference to developments in Europe through CEN/Cenelec, the European standards' organisation, and ISO, the international organisation for standardisation.

***Latest updates to the ASCE 7 Wind Provisions and Development of Performance-Based Wind Design Prestandard.*** As an integral part of the building codes in the United States, the currently adopted ASCE/SEI 7-16: Minimum Design Loads and Associated Criteria for Buildings and Other Structures describes the means for determining natural hazard loading, including wind loads, on buildings and other structures. Current efforts are nearing completion of the first ever tornado loading for buildings for incorporation into the 2022 edition of the ASCE 7 standard, along with the use of Performance-Based Wind Design principals being added to the standard. This presentation will look at the current major provisions being incorporated into ASCE/SEI 7-22.

**Speaker biographies**

***Dr. Svend Ole Hansen*** is director and founder of Svend Ole Hansen ApS and SOH Wind Engineering LLC, and he has been a lecturer in wind engineering at the Technical University of Denmark and Syddansk University. His text books on wind engineering are widely read and well regarded, and he has in more than 40 years authored a large number of papers on wind actions and wind-induced vibrations of structures. He was member of the Project Team preparing the current Eurocode on wind actions EN 1991-1-4, and he has been the Leader of the Project Team revising the current EN 1991-1-4.

***Francesco Ricciardelli*** is Professor of Structural Engineering at the University of Campania "L. Vanvitelli", Editor-in-Chief of Wind and Structures, Vice-President of the Italian Association for Wind Engineering, Member of several Committees within CEN, among which TC250/SC1, TC250/SC1.WG1, TC250/SC1.T3, TC250/SC1.T6 (Team Leader), TC250/SC1.WG1/T2 (Convenor), and has served in Italian National standardization bodies (CNR, UNI). He is the author of about 170 papers most of which are in the areas of Wind Engineering and Structural Dynamics.

***John Dora*** is a visiting professor at the University of Surrey, a visiting lecturer at the University of Birmingham and the international organisation for standardisation's global lead on adaptation to climate change. With nearly 40 years' experience in infrastructure resilience and asset management, he is adviser to CEN/ Cenelec, and works closely with BSI. He chaired the committee that drafted the first ISO on adaptation to climate change, ISO 14090, and is

the chair of the UK's Infrastructure Operators' Adaptation Forum. He initiated and led the first adaptation studies for the entire GB rail network (2009-2016). Recent clients include: the UK rail regulator, the UK Met Office, UIC – the worldwide railway organisation and the UN Economic and Social Commission for Asia and the Pacific.

***Donald R. Scott, S.E.***, is a Senior Principal with PCS Structural Solutions. Mr. Scott has over 38 years of experience in the design, evaluation, and rehabilitation of building structures. He was the principal investigator for the ASCE/SEI Prestandard for Performance-Based Wind Design. Mr. Scott is Chair of the SEI Codes and Standards Executive Committee, Chair of the ASCE 7 Wind Load Subcommittee, member of the ASCE 7 Main Committee and past Chair of the NCSEA

Wind Engineering Committee. Mr. Scott is a member of the SEI Board of Governors and a past President of the Board of Directors of the Applied Technology Council.

# International Wind Engineering Seminar 6 "Wind-related Disaster Risk Reduction: Current Status and Future Prospects"

**Thursday March 4th 2021,12.00 UK time**

**Main Speaker**

Professor Yukio Tamura, School of Civil Engineering, Chongqing University, China, Wind-related Disaster Risk Reduction: Current Status and Future Prospects

**Short presentations**

Professor Forrest J. Masters, Ph.D., P.E. (FL), Professor and Associate Dean for Research and Facilities, Herbert Wertheim College of Engineering, University of Florida. Revisiting Hurricane Maria's impact to Puerto Rico: Topographic wind speed up in complex terrains.*

Professor Chris Baker, Emeritus Professor of Environmental Fluid Mechanics, School of Engineering, University of Birmingham. The resilience of transport and agricultural networks to strong winds.

* with contributions from Jorge X. Santiago-Hernandez, Graduate Research Assistant, Engineering School for Sustainable Infrastructure & Environment, University of Florida, Luis D. Aponte-Bermúdez, Ph.D., P.E. Professor, Department of Civil Engineering and Surveying, University of Puerto Rico at Mayagüez Edward C. Garcia, Graduate Research Assistant, Department of Civil Engineering and Surveying, University of Puerto Rico at Mayagüez

**Abstracts**

***Wind-related Disaster Risk Reduction: Current Status and Future Prospects***. In the seminar, the current status of wind-related disaster risk reduction activities and future prospects are summarized. Wind engineers have been making great efforts to reduce wind-related disasters in the past few decades, but the number of devastating wind-related disasters and accompanying economic losses are still significantly increasing, and climate change due to global warming is hypothesized to exacerbate this trend in the future. The seminar aims to discuss what we should do now to cope with future unfavorable wind effects on our society. First, the various types of winds that cause serious disasters to our society are overviewed from extremely strong winds to moderate and light winds. Some typical examples of wind-induced damage to buildings and structures are introduced, and the importance of the performance of claddings and components is particularly demonstrated. Then, some problems with the wind-resistant design principles are discussed, such as reassessment of the relation between design-load level and lifetime of individual buildings and elements including temporary buildings. In connection with this, a kind of paradigm shift in building design method focusing on a group of unspecified buildings rather than an individual specified building is recommended. Many other relevant issues are also discussed as follows:

structures such as scaffoldings, cranes, movable roofs designed under the assumption that they will be controlled or maintained for strong wind cases based on a specified wind speed; design and construction principles of disaster prevention bases, evacuation facilities, high-risk facilities, high-priority facilities; engineering modeling of strong wind events; and so on. Some statistics of wind-related disasters are

introduced, and future trends under climate change due to global warming are discussed. To stop the repetition of wind-related disasters, the necessity of accurate estimations of the performances of claddings and components are again emphasized, and it is recommended to devote more research attention to performance estimation. In conjunction with this, the necessity of full-scale storm simulators (FSSS) are finally demonstrated, with a motto of "Invest today, Save tomorrow".

***Revisiting Hurricane Maria's impact to Puerto Rico: Topographic wind speed up in complex terrains.*** Complex topography can double the fluctuating surface velocity relative to flat terrain conditions, thus topography induced accelerations are regularly implicated in windstorm damage. The presentation will describe ongoing research on the use of machine learning, numerical weather prediction, and computational fluid dynamics (CFD) to predict wind 'speedup' in mountainous areas and other regions with steep slopes. It will review testing currently underway at the Terraformer boundary layer wind tunnel (BLWT) at the NSF Natural Hazards Engineering Research Infrastructure (NHERI) Experimental Facility at the University of Florida, which is using precision guided multi-port pitot tubes and particle image velocimetry (PIV) to collect high-resolution velocity field data over geometrically scaled models of sections of the main island of Puerto Rico and the municipal Islands of Vieques and Culebra. Comparison will be made between the lab measurements and predictions from shallow neural networks, RANS/LES CFD, and high-resolution Weather Research and Forecasting Model (ARW Core) modeling. The presentation will conclude with comments about the appropriate use of BLWTs for modeling wind-speed up and the prospects for using digital elevation data and machine learning to automate prediction.

***The resilience of transport and agricultural networks to strong winds.*** The effects of high winds on individual buildings and structures has been given a great deal of attention over recent decades. Rather less attention has been given to the effects of high winds on geographically large-scale networks – such as transportation systems and large scale agricultural and forestry networks. This presentation will briefly discuss the nature of wind effects on such systems and the methods that can be used to both determine risk of different levels of system failure and to minimize the damaging effects of high winds as far as possible. It will be seen that the wind engineering information required to make such assessments is rather different from that required for the analysis of individual buildings and requires different non-standard statistical descriptions of the wind and also information on large scale temporal and spatial wind coherence. Statistical tools that can combine both deterministic aspects (such as transport timetables or specific agronomic interventions) with wind statistical

information are required. The propagation of local failures with such systems will also be discussed.

**Speaker biographies**

***Professor Yukio Tamura*** is a Professor of the School of Civil Engineering, Chongqing University, China, and the Honorary Director of the Wind Engineering Research Center, Tokyo Polytechnic University, Japan. He served as the President of the International Association for Wind Engineering for eight years from 2007 to 2015. He is currently serving as an Adjunct/Guest/Honorary Professor of 19 universities in China, Korea, Malaysia, Poland, and USA. Professor Yukio Tamura is a member of the Engineering Academy of Japan, a Foreign Fellow of the Indian National Academy of Engineering, and a Foreign Member of Chinese Academy of Engineering.

***Dr. Forrest Masters*** is a Professor in the Engineering School of Sustainable Infrastructure & Environment and serves as Associate Dean for Research and Facilities in the Herbert Wertheim College of Engineering. He earned his PhD in civil (structural) engineering from the University of Florida in 2004. Dr. Masters has received support from more than 50 grants from state, federal and private sources, including the NSF CAREER and MRI Programs. He also leads one of seven Natural Hazards Engineering Research Infrastructure (NHERI) experimental facilities for the NSF to study the damaging effects of extreme wind events on civil infrastructure. Dr. Masters has published more than 100 papers in peer-reviewed journals and conference proceedings and given more than 100 invited presentations. He serves on the Board of the Federal Alliance for Safe Homes, and recently served on the NIST National Advisory Committee on Windstorm Impact Reduction. In 2014, Dr. Masters was awarded the junior International Association of Wind Engineering award, which is the highest award in his field that recognizes significant and original contributions to research by an individual under the age of 40. He was also honored with the Outstanding Achievement Award in Mitigation at the National Hurricane Conference.

***Professor Chris Baker*** read Engineering at St Catharine's College in Cambridge, graduating with a BA in 1975, and an MA and a PhD in 1978. Following a Research Fellowship at St Catharine's College and the Department of Engineering, in the early 1980s he began work in the Aerodynamics Unit of British Rail Research in Derby, before moving to an academic position in the Department of Civil Engineering at the University of Nottingham. He remained there till 1998 as a lecturer, reader and professor with research interests in vehicle aerodynamics, wind engineering, environmental fluid mechanics and agricultural aerodynamics. In 1998 he moved to the University of Birmingham as Professor of Environmental Fluid Mechanics in the School of Civil Engineering. From 2003 to 2008 he was Head of Civil Engineering and was the Director of the Birmingham Centre for Railway Research and Education from 2005 to 2014. He retired at the end of 2017 and took up an Emeritus position. He continues to be involved in research in train aerodynamics, wind engineering and

transport issues. In July 2020 he was awarded the Davenport Medal, the senior award of the International Association of Wind Engineering.

**Questions and answers**

Question from Yong Wang to Prof. Tamura. You emphasized the important combined effects of wind and water hazards, which can cause large scale loss. Could you suggest the most promising methodology for the study of wind and water effects? It seems to me that there may exist difficulties to simulate the effects of water even in the full-scale storm simulator.

Answer. Thanks for your good comment. It might also be possible to study water hazards in full scale, but honestly speaking, the necessity for a full-scale facility for water is not clear to me. When we consider the combined effects of water and wind, I didn't intend to test the combined effects of wind and water forces. In the case of water hazards, prediction of floods including storm surge and recommendations for evacuation timing are the most important issues. For those purposes, a full-scale facility is not necessary for water, but it is clearly necessary for wind.

Question from Asih to Prof. Tamura. You mentioned that its important for Wind Engineers to move from focusing from Load and Wind Action to Resistance and Structural Performance. What do you think of the recent Performance based Wind Code in the ASCE, is this the direction you are talking about?

Answer. Thanks for the good question. Performance-based design is actually a possible direction. In the case of wind-resistant design, "performance of cladding and components" is very important. Without knowing the real performance of cladding and component systems, we cannot realize performance-based wind-resistant design. For this, we need full-scale storm simulators. I think database assisted design or AI assisted design might be a possible direction, too.

Question from Ron Aquino to Prof. Tamura. Thank you for your lecture. "O hisashiburi!" While education and enforcement is important when it comes to building codes, do you think there is still any room for improvement in existing wind loading codes, both international/reference codes (ASCE, AIJ, AS/NZS, EN, etc) and national (e.g. codes that adopted ASCE, etc)? In what areas? Is moving to a performance-based approach rather than a code-based approach one of them?

Answer. Thanks, Ron, for your nice question. I think there are many issues to be improved, as I mentioned in my lecture. These include a design method for long-span roof structures, for which the traditional GLF method is not appropriate; a GLF for "ultimate limit state" design, which should be different from GLF for serviceability limit state" design; a design concept and definition of "temporary buildings" including construction work offices and scaffoldings; a current "Minimum LCC" design concept based only on the lifetime of an

individual building. Yes, PBD is a possible direction, but for that, we need to know the real "Performance" of buildings, especially "Performance of Cladding and Components". That's why I emphasized the necessity for a full-scale storm simulator.

Question from Yufen Zhou to Prof. Masters.. Thank you for the interesting presentation. Could you talk about the role of machine learning in the PIV tests? How would machine learning help with the PIV data from wind tunnel test?

Answer. The PIV data are being used to train the machine learning model, with the goal of using the model to predict speedup in all regions that have similar characteristics to the topography in the study region.

Question from Fred Haan to Prof. Masters. Did you have a chance to compare the velocity profiles from your topo tests with any full-scale data? Does any such full-scale data exist?

Answer. That is the long term plan, however it is not in the scope of the project we discussed. Once we train the model, we can apply it to study any weather station that is located in an area similar to Puerto Rico to test how well it works.

# Appendix 2. Some musings on tornado vortex models

# Some musings on tornado vortex models

**Chris Baker**
**Emeritus Professor of Environmental Fluid Mechanics**
**University of Birmingham**
**June 2020**

## 1. Introduction

Tornadoes are very complex flow structures - they are extremely variable in size and strength; they have a range of different morphologies that can vary throughout their lifetime; and their occurrence is very difficult to predict. Very broadly they may be considered to be of two types. The first is a single cell vortex, with a rapidly rotating circumferential flow, with a radial inflow and a central updraft. The second type is a two-cell vortex, with a central region dominated by a downdraft and a radial outflow, surrounded by an outer region with radial inflow and an updraft. There is some evidence that weaker tornadoes are of the one-cell type and stronger tornadoes of the two-cell type.

Over the last few decades, there have been attempts by many different researchers, including the author, to develop analytical models of tornado vortices. Whilst such models can only ever hope to be massive simplifications of actual tornado events, there are nonetheless good reasons for making the attempt. Firstly such models can help develop an understanding of the nature of the flows in tornadoes and the physical principles that underlie them. The importance of this basic understanding should not be underestimated. Secondly analytical models can help with the interpretation of experimental and numerical results, providing a framework for data analysis and presentation. Thirdly, and perhaps most importantly, these models offer a simple framework that can be used in engineering design processes in a number of different ways. The very variability of real tornadoes means that to estimate tornado loadings on structures, many different tornado realisations are required to build up a suitable load probability distribution. Such distributions would be extremely time consuming to obtain through either physical or numerical modelling, whereas simple analytical models, for all their approximations and deficiencies, can provide an efficient way to achieve this.

In this note, we will consider one specific class of tornado models – those that are based on either the Navier-Stokes or the Euler equations, considering a range of models by different authors and also some new models. It is not the intention here to compare these models with full-scale data, but rather to consider in detail the nature of their derivation and the common assumptions that underlie them. In doing this we attempt to cast those models that are considered in a common format, where they can be compared with each other. In this we take forward the work of Kim and Matsui (2017) who compared the results of a range of different models. It will be seen that such an in depth comparison allows considerable insight into the nature of the models and reveals their limitations and possibilities.

In section 2 we briefly present the different types of tornado model. In section 3 we consider in depth those models that are based on the full Navier-Stokes equations, and in section 4 we consider those models based on the Euler equations. Section 5 attempts to synthesise the analysis and suggest ways that the various models could be further developed.

## 2. Types of tornado model

Tornado models can be considered to be of three types. The first are those simple models, many of which have been used for many decades, and simply fit empirical forms to the tangential velocity profiles. These include the models of Rankine (1858) in its original and modified form, Bjerknes (1921) and Wood and White (2013). The second type use different empirical forms for all the velocity components. This type includes the models of Fujita (1978) and Xu and Hangan (2009). The different velocity components of models of this type are therefore not consistent with the equations of motion. The model of Kuo (1971) and Wen (1975) is also in this category, as in its final form it consists of a series of empirical correlations for velocity components, although it is, at least in part, based on a solution of the boundary layer equations beneath a rotating flow.

The third type of model make some assumptions with regard to the spatial form of one velocity component, and then calculate the equivalent forms for the other velocity components and the pressure variation through the continuity and momentum equations, usually with major simplifying assumptions. The models of Burgers (1948), Rott (1958), Sullivan (1959), Vatistas et al (1991), Baker and Sterling (2017) and Baker et al (2020) are of this type. The first four of these are based on the full Navier-Stokes equations, whilst the last two are based on the Euler equations

Whilst acknowledging the utility of the first and second type of model in practical situations, it is with the third, self-consistent class of models that this note is concerned. We consider the solutions to the Navier-Stokes equations in section 3, and solutions to the Euler equations in section 4.

## 3. Navier Stokes solutions

### 3.1 Basic equations

In this section we will consider a number of models that are used to represent tornadoes, which are all solutions of the Navier-Stokes equations. These equations will be expressed using cylindrical co-ordinates, with co-ordinates $r$, $\theta$ and $z$ in the radial, circumferential and vertical directions and $U, V$ and $W$ as the corresponding velocities. These variables will be expressed in a normalised form using t $\bar{r} = r/r_m$, $\bar{z} = z/z_m$, $\bar{U} = U/V_m$, $\bar{V} = V/V_m$ and $\bar{W} = W/V_m$. $V_m$ is a reference velocity; $r_m$ is a reference length in the radial direction and $z_m$ is a reference length in the vertical direction. The ratio of the two reference lengths will be denoted by $\delta = z_m/r_m$. The normalised pressure will be given by $\bar{P} = P/\rho V_m^2$, where $P$ is the pressure $\rho$ is the pressure and $\rho$ is the density of air.

The models that will be described below all contain the following basic assumptions

- The flow is steady, so there are no time derivatives $\frac{\partial}{\partial t} = 0$.
- The flow is incompressible so $\rho$ is constant.
- The flow is axially symmetric, so all circumferential derivatives are zero $\frac{\partial}{\partial \theta} = 0$

The continuity and momentum equations can thus be written as follows.

$$\frac{1}{\bar{r}}\frac{\partial(\bar{U}\bar{r})}{\partial \bar{r}} + \frac{1}{\delta}\frac{\partial \bar{W}}{\partial \bar{z}} = 0 \tag{3.1}$$

$$\bar{U}\frac{\partial \bar{V}}{\partial \bar{r}} + \frac{\bar{U}\bar{V}}{\bar{r}} + \frac{\bar{W}}{\delta}\frac{\partial \bar{V}}{\partial \bar{z}} = \frac{1}{R}\left(\frac{1}{\bar{r}}\frac{\partial}{\partial \bar{r}}\left(\bar{r}\frac{\partial \bar{V}}{\partial \bar{r}}\right) - \frac{\bar{V}}{\bar{r}^2} + \frac{1}{\delta^2}\frac{\partial^2 \bar{V}}{\partial \bar{z}^2}\right) \tag{3.2}$$

$$\bar{U}\frac{\partial \bar{U}}{\partial \bar{r}} - \frac{\bar{V}^2}{\bar{r}} + \frac{\bar{W}}{\delta}\frac{\partial \bar{U}}{\partial \bar{z}} = -\frac{\partial \bar{P}}{\partial \bar{r}} + \frac{1}{R}\left(\frac{1}{\bar{r}}\frac{\partial}{\partial \bar{r}}\left(\bar{r}\frac{\partial \bar{U}}{\partial \bar{r}}\right) - \frac{\bar{U}}{\bar{r}^2} + \frac{1}{\delta^2}\frac{\partial^2 \bar{U}}{\partial \bar{z}^2}\right) \tag{3.3}$$

$$\bar{U}\frac{\partial \bar{W}}{\partial \bar{r}} + \frac{\bar{W}}{\delta}\frac{\partial \bar{W}}{\partial \bar{z}} = -\frac{\partial \bar{P}}{\partial \bar{z}} + \frac{1}{R}\left(\frac{1}{\bar{r}}\frac{\partial}{\partial \bar{r}}\left(\bar{r}\frac{\partial \bar{W}}{\partial \bar{r}}\right) + \frac{1}{\delta^2}\frac{\partial^2 \bar{W}}{\partial \bar{z}^2}\right) \tag{3.4}$$

Here $R$ is a Reynolds number defined as $R = V_m r_m/\upsilon$ where $\upsilon$ is the kinematic viscosity of air.

### 3.2 Analysis

All the models discussed blow are based on two further assumptions. The first is that the flow is quasi-cylindrical with $\frac{\partial}{\partial \bar{z}} \ll \frac{\partial}{\partial \bar{r}}$. The second is that all three velocity components can be considered as products of two functions, one a function of $\bar{r}$ only and the other a function of $\bar{z}$ only i.e.

$$\bar{U} = u_r u_z \tag{3.5}$$

$$\bar{V} = v_r v_z \tag{3.6}$$

$$\bar{W} = w_r w_z \tag{3.7}$$

The continuity equation thus becomes

$$\left(\frac{u_r}{\bar{r}} + \frac{\partial u_r}{\partial \bar{r}}\right)u_z + \frac{w_r}{\delta}\frac{\partial w_z}{\partial \bar{z}} = 0 \tag{3.8}$$

which gives

$$w_r = -\delta\left(\frac{u_r}{\bar{r}} + \frac{\partial u_r}{\partial \bar{r}}\right) \tag{3.9}$$

and

$$u_z = \frac{\partial w_z}{\partial z} \tag{3.10}$$

The circumferential momentum equation becomes

$$u_r u_z \frac{\partial v_r}{\partial r} v_z + \frac{1}{r} u_r u_z v_r v_z + \frac{w_r w_z v_r}{\delta} \frac{\partial v_z}{\partial z} = \frac{1}{R}\left(\frac{\partial^2 v_r}{\partial r^2} v_z + \frac{1}{r}\frac{\partial v_r}{\partial r} v_z - \frac{v_r v_z}{r^2}\right) \tag{3.11}$$

After some manipulation equations (3.9) to (3.11) give

$$\frac{\left(\bar{r}^2 \frac{\partial^2 v_r}{\partial \bar{r}^2} + \bar{r}\frac{\partial v_r}{\partial \bar{r}}(1 - \bar{r}Ru_r u_z) - v_r(1 + \bar{r}Ru_r u_z)\right)}{w_r v_r \bar{r}^2} = \left(\frac{w_z \frac{R\partial v_z}{\delta \partial \bar{z}}}{v_z}\right) \tag{3.12}$$

This is almost in a variable –separated form with functions of $\bar{r}$ on the left hand side and functions of $\bar{z}$ on the right hand side, except for the terms that include $u_z$ on the left hand side. To overcome this, and to make the equations tractable, the models below implicitly assume $u_z = 1$ i.e. there is no vertical variation of the radial velocity. From the equation (3.10)

$$w_z = \bar{z} \tag{3.13}$$

i.e. the variation of vertical velocity is linear with height above the ground. Letting $u_z = 1$ one can write equation (3.12) as

$$\frac{\left(\bar{r}^2 \frac{\partial^2 v_r}{\partial \bar{r}^2} + \bar{r}\frac{\partial v_r}{\partial \bar{r}}(1 - \bar{r}Ru_r) - v_r(1 + \bar{r}Ru_r)\right)}{w_r v_r \bar{r}^2} = \left(\frac{\bar{z}\frac{R\partial v_z}{\delta \partial \bar{z}}}{v_z}\right) = \gamma \tag{3.14}$$

Here $\gamma$ must be a constant, since it cannot be a function of either $\bar{r}$ or $\bar{z}$. Looking first at the term in $\bar{z}$ we obtain

$$\left(\frac{\bar{z}\frac{R\partial v_z}{\delta \partial \bar{z}}}{v_z}\right) = \gamma \tag{3.15}$$

This integrates to give

$$\ln(v_z) = \frac{\gamma\delta}{R}\ln(\bar{z}) \tag{3.16}$$

$$v_z = \bar{z}^{\frac{\gamma\delta}{R}} \tag{3.17}$$

Now at this point, the various models effectively assume that $\gamma = 0$, to avoid the circumferential velocity $v_z$ falling to zero at $\bar{z} = 0$, which would not be appropriate for the geometries that were considered. However it is not (at this point in the analysis) strictly necessary, and indeed an increase of $v_z$ from zero might be thought to be appropriate for tornado like flows. Now considering the term in $\bar{r}$ we obtain

$$\frac{\left(\bar{r}^2 \frac{\partial^2 v_r}{\partial \bar{r}^2} + \bar{r}\frac{\partial v_r}{\partial \bar{r}}(1 - \bar{r}Ru_r) - v_r(1 + \bar{r}Ru_r)\right)}{-\delta\left(\frac{u_r}{\bar{r}} + \frac{\partial u_r}{\partial \bar{r}}\right) v_r \bar{r}^2} = \gamma \tag{3.18}$$

$$\bar{r}^2 \frac{\partial^2 v_r}{\partial \bar{r}^2} + \bar{r}\frac{\partial v_r}{\partial \bar{r}}(1 - \bar{r}Ru_r) - v_r\left(1 + \bar{r}Ru_r - \delta\left(\frac{u_r}{\bar{r}} + \frac{\partial u_r}{\partial \bar{r}}\right)\bar{r}^2\gamma\right) = 0 \tag{3.19}$$

Further analysis of this equation to obtain expressions for $v_r$ clearly requires some assumption to be made concerning the nature of the variation of the radial velocity with radius $u_r$. Each of the three models that we consider in what follows makes different

assumptions in this regard. As noted above, all however assume that $\gamma = 0$ and thus use the simpler equation

$$\bar{r}^2 \frac{\partial^2 v_r}{\partial \bar{r}^2} + \bar{r} \frac{\partial v_r}{\partial \bar{r}} (1 - \bar{r} R u_r) - v_r (1 + \bar{r} R u_r) = 0 \qquad (3.20)$$

Now let us consider the pressure variation through the radial and vertical momentum equations (3.3) and (3.4), again making the assumption that the flow is quasi-cylindrical with $\frac{\partial}{\partial \bar{z}} \ll \frac{\partial}{\partial \bar{r}}$, and putting the velocities in their functional form

$$u_r u_z{}^2 \frac{\partial u_r}{\partial \bar{r}} - \frac{v_r{}^2 v_z{}^2}{\bar{r}} + \frac{w_r w_z u_r}{\delta} \frac{\partial u_z}{\partial \bar{z}} = -\frac{\partial \bar{p}}{\partial \bar{r}} + \frac{1}{R}\left(\frac{u_z}{\bar{r}} \frac{\partial}{\partial \bar{r}}\left(\bar{r} \frac{\partial u_r}{\partial \bar{r}}\right) - \frac{u_r u_z}{\bar{r}^2}\right) \qquad (3.21)$$

$$u_r u_z w_z \frac{\partial w_r}{\partial \bar{r}} + \frac{w_r{}^2 w_z}{\delta} \frac{\partial w_z}{\partial \bar{z}} = -\frac{\partial \bar{p}}{\partial \bar{z}} + \frac{1}{R}\left(\frac{w_z}{\bar{r}} \frac{\partial}{\partial \bar{r}}\left(\bar{r} \frac{\partial w_r}{\partial \bar{r}}\right)\right) \qquad (3.22)$$

Now since $u_z = v_z = 1$ and $w_z = \bar{z}$

Thus the equations become

$$u_r \frac{\partial u_r}{\partial \bar{r}} - \frac{v_r{}^2}{\bar{r}} = -\frac{\partial \bar{p}}{\partial \bar{r}} + \frac{1}{R}\left(\frac{u_z}{\bar{r}} \frac{\partial}{\partial \bar{r}}\left(\bar{r} \frac{\partial u_r}{\partial \bar{r}}\right) - \frac{u_r}{\bar{r}^2}\right) \qquad (3.23)$$

$$u_r \bar{z} \frac{\partial w_r}{\partial \bar{r}} + \frac{w_r{}^2}{\delta} \bar{z} = -\frac{\partial \bar{p}}{\partial \bar{z}} + \frac{1}{R}\left(\frac{\kappa \bar{z}}{\bar{r}} \frac{\partial}{\partial \bar{r}}\left(\bar{r} \frac{\partial w_r}{\partial \bar{r}}\right)\right) \qquad (3.24)$$

Thus the nature of the pressure distribution will depend upon the assumed and calculated forms of the velocity components. That being said, in many of the published discussions of these models, the following very simplified equations are used (usually with little justification)

$$\frac{\partial \bar{p}}{\partial \bar{r}} = \frac{v_r{}^2}{\bar{r}} \qquad (3.25)$$

$$\frac{\partial \bar{p}}{\partial \bar{z}} = 0 \qquad (3.26)$$

### 3.3 Burgers-Rott model

The first model that will be considered is that developed independently by Burgers (1948), and Rott (1958). This model is perhaps the most widely quoted as having relevance to tornadoes and has been used by researchers for many decades across a variety of fields – indeed the author used it to describe the flow in the core of a horseshoe vortex around the base of a cylindrical obstacle (Baker, 1978). The vortex core here was only a centimetre of so across – a very different scale from a typical tornado. The method uses equation (3.20) above and assumes a linear variation of radial velocity with radius from the core

$$u_r = -\kappa_1 \bar{r} \qquad (3.27)$$

Here, and in what follows, the parameters $\kappa_i$ will be used to denote constants of different types. This gives

$$\bar{r}^2 \frac{\partial^2 v_r}{\partial \bar{r}^2} + \frac{\partial v_r}{\partial \bar{r}} (\bar{r} + \bar{r}^3 \kappa_1 R) - v_r (1 - \bar{r}^2 \kappa_1 R) = 0 \qquad (3.28)$$

This equation can be solved by letting

$$\Gamma = 2\pi \bar{r} v_r \qquad (3.29)$$

which results in the equation

$$\bar{r}\frac{\partial^2\Gamma}{\partial\bar{r}^2}+\frac{\partial\Gamma}{\partial\bar{r}}(-1+\kappa_1\bar{r}^2R)=0 \tag{3.30}$$

This has the solution

$$\Gamma=2\pi\bar{r}v_r=\kappa_2\left(1-e^{-\bar{r}^2\kappa_1R/2}\right) \tag{3.31}$$

where $\kappa_2$ is a constant of integration and thus

$$v_r=\frac{\kappa_2}{2\pi\bar{r}}\left(1-e^{-\bar{r}^2\kappa_1R/2}\right) \tag{3.32}$$

If we fix the maximum value of $v_r$ to be 1.0 at $\bar{r}=1$, then we obtain

$$\frac{\kappa_1R}{2}=2.51 \tag{3.33}$$

$$\frac{\kappa_2}{2\pi}=1.4 \tag{3.34}$$

and thus

$$v_r=\frac{1.4}{\bar{r}}\left(1-e^{-1.26\bar{r}^2}\right) \tag{3.35}$$

From equations (3.27) and (3.33), the radial velocity is given by

$$u_r=-\kappa_1\bar{r}=-\frac{5.02}{R}\bar{r} \tag{3.36}$$

From equations (3.9) and (3.36) we obtain

$$w_r=2\delta\kappa_1=\delta\frac{10.04}{R} \tag{3.37}$$

Also equation (3.13) is

$$w_z=\bar{z} \tag{3.38}$$

Because of the initial assumptions, we also have $u_z=v_z=1$. These equations show that the radial velocity, whilst going to zero at the vortex centre in a realistic way, is unbounded at large distances from the vortex centre. Similarly the vertical velocity is zero at the ground as is required, but is unbounded in a vertical direction. The radial velocity functions are shown in table 1 and plotted in figure 1. It can be seen if this formulation is used, where the maximum normalised circumferential velocity is unity at $\bar{r}$=1, then the radial and vertical profiles are functions of Reynolds number whilst the circumferential velocity profile is invariant. For small-scale laminar flows this Reynolds number would be based on the normal viscosity, which is only a function of material properties, but for large-scale flows, it is necessary to assume that the turbulent eddy viscosity is a constant throughout the flow. This must be regarded as something of a doubtful assumption. Nonetheless the form of this equation has been widely used to fit full scale and model scale tornado vortex data in the past.

Finally let us consider the pressure variation within the vortex. For the Burgers-Rott vortex, equations (3.23) and (3.24) become

$$\kappa_1{}^2\bar{r}-\frac{v_r{}^2}{\bar{r}}=-\frac{\partial\bar{P}}{\partial\bar{r}}+\frac{1}{R}\left(-\frac{\kappa_1}{\bar{r}}\right) \tag{3.39}$$

$$4\delta\kappa_1{}^2\bar{z}=-\frac{\partial\bar{P}}{\partial\bar{z}} \tag{3.40}$$

These equations thus give the following solution.

$$\bar{P}=\int\frac{v_r{}^2}{\bar{r}}d\bar{r}-\frac{\kappa_1{}^2\bar{r}^2}{2}+\frac{\kappa_1}{R}\ln(\bar{r})-2\delta\kappa_1{}^2\bar{z}^2 \tag{3.41}$$

Substituting for $\kappa_1$ this becomes

$$\bar{P} = \int \frac{v_r^2}{\bar{r}} d\bar{r} - \frac{1}{R^2}(12.6\bar{r}^2 + 5.02\ln(\bar{r}) - 50.4\,\delta\bar{z}^2) \tag{3.42}$$

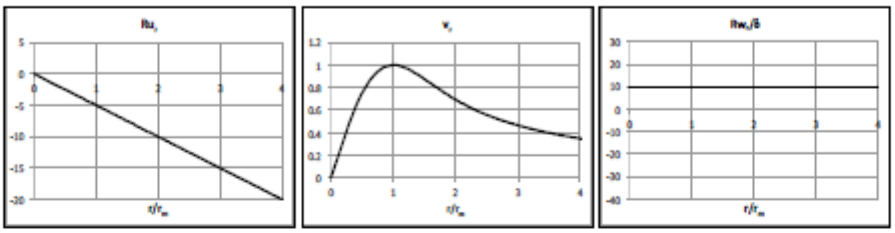

**Figure 1 The Burgers-Rott vortex**

### 3.4 Sullivan model

The model developed by Sullivan (1959) is outlined in a commendably short (two-column) paper, and presents, without a great deal of explanation, an analytical form for a two-cell vortex. However the analysis leading to this solution is actually very interesting and the solution as presented is only one of a more general set of solutions that can be obtained using Sullivan's approach. We take this wider view here. Again, the solution begins with equation (3.20), with $\gamma = 0$, and thus $u_z = v_z = 1$. The radial velocity function $u_r$ is assumed to be

$$u_r = -\kappa_1\bar{r} + \frac{\kappa_2\left(1-e^{-\kappa_3\bar{r}^2}\right)}{\bar{r}} \tag{3.43}$$

It is not immediately apparent how Sullivan arrived at this formulation – possibly by trial and error to see what worked. In an attempt to be consistent with Sullivan's methodology, but expressing it more generally we write this assumption as

$$u_r = -\frac{2\beta\kappa_3}{R}\bar{r}\left(1 - \frac{\alpha\left(1-e^{-\kappa_3\bar{r}^2}\right)}{\beta\kappa_3\bar{r}^2}\right) \tag{3.44}$$

where

$$\left(\frac{\kappa_2 R}{2}\right) = \alpha \tag{3.45}$$

$$\left(\frac{\kappa_1 R}{2\kappa_3}\right) = \beta \tag{3.46}$$

Sullivan only gives a solution for $\alpha = 3$ and $\beta = 1$, but we do not make that assumption at this stage here. When this form for radial velocity is substituted into equation (3.20), there is no direct analytical solution, but rather $v_r$ is specified in terms of integral functions as follows

$$v_r = \frac{\kappa_4}{\bar{r}}\frac{H(x)}{H(\infty)} = \frac{\kappa_4}{\bar{r}}\frac{H(\kappa_3\bar{r}^2)}{H(\infty)} \tag{3.47}$$

where

$$H(x) = \int_0^x e^{\beta f(x)}\,dx \tag{3.48}$$

and

$$f(x) = \left(-t + \alpha \int_0^t \left(\frac{(1-e^{-y})}{y}\right) \partial y\right) \tag{3.49}$$

For any one set of values of $\alpha$ and $\beta$ the constants $\kappa_3$ and $\kappa_4$ can be determined by setting $v_r = 1$ at $\bar{r} = 1$.

The remaining velocity components can calculated from equations (3.9) and (3.13) above which give

$$w_r = \delta\left(\frac{4\beta\kappa_3}{R}\right)\left(1 - \frac{\alpha}{\beta}e^{-\kappa_3 r^2}\right) \tag{3.50}$$

and

$$w_z = \bar{z} \tag{3.51}$$

Again the velocity components are given in table 1 and plotted in figure 2 for a range of values of $\alpha$ and $\beta$. It can be seen that this model allows a range of different solutions to be obtained for both one cell and two cell vortices. The limit between the two-cell and the one-cell formulations is given by

$$\frac{\alpha}{\beta} = 1 \tag{3.52}$$

As far as can be ascertained there is no simple formulation for the pressure variation for this model, and a numerical solution of equations (3.23) and (3.24) is required

This model is useful in providing a framework for the consideration of two cell tornadoes and the transition between one and two cell types – indeed it is probably more useful than usually realized because of this property. Like the Burgers-Rott model, it is based on the equations of motion that include viscosity and thus the Reynolds number again appears in the formulation used here in the radial and vertical component. If it is to be used at practical scales, a constant eddy viscosity has to be assumed. Again the radial and vertical velocities are not bounded. Again the radial and vertical velocities are not bounded.

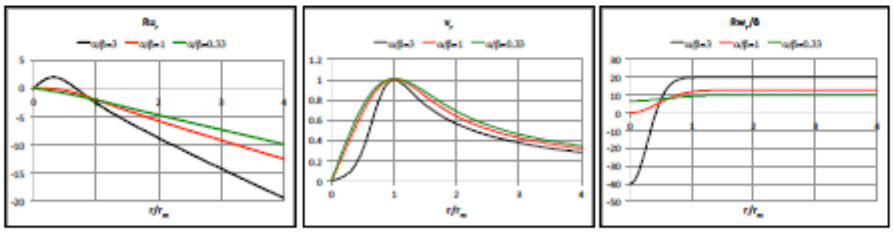

**Figure 2 The Sullivan vortex**

### 3.5 The model of Vasistas et al

The broad outline of the Vatistas et al (1991) model is the same as for Burgers-Rott and Sullivan. Again it implicitly assumes that $\gamma = 0$, and thus $u_z = v_z = 1$. However, instead of assuming a form for $u_r$, an assumption is made for $v_r$ as follows

$$v_r = \frac{2^{1/n}\bar{r}}{(1+\bar{r}^{2n})^{1/n}} \tag{3.53}$$

The parameter $n$ can be used to vary the shape of the velocity profile. It can be seen that $v_r = 1$ when $\bar{r} = 1$ regardless of the value of $n$. Substituting into equation (3.18) gives a straightforward solution for $u_r$

$$u_r = -\frac{2^{1+1/n}(n+1)}{R}\frac{(\bar{r}^{2n-1})}{1+\bar{r}^{2n}} \tag{3.54}$$

The continuity equation then gives

$$w_r = \delta\frac{2^{2+1/n}n(n+1)}{R}\frac{\bar{r}^{2n-2}}{(1+\bar{r}^{2n})^2} \tag{3.55}$$

and, as before

$$w_z = \bar{z} \tag{3.56}$$

The velocity functions are shown in table 1 and plotted in figure 3. It can be seen that variations in $n$ result in significant changes in the radial and vertical profiles in particular. Unlike the Burgers-Rott and the Sullivan vortices, this radial and vertical velocities are bound at large values of radius and height respectively.

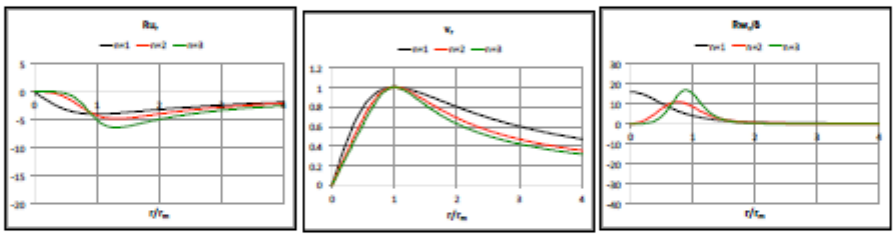

**Figure 3. The vortex of Vasistas et al**

## 4. Euler equation solutions

### 4.1 Basic equations

The second approach to modelling tornadoes is to use the Euler rather than the Navier-Stokes equations, which involves setting all the viscosity terms to zero. This implies that an inviscid flow is being modeled and removes the need for assuming a constant eddy viscosity. It will be seen it also allows more flexibility in terms of the specification of the axial velocity profiles. Removing the viscous terms in equations (3.1) to (3.4) we obtain

$$\frac{1}{\bar{r}}\frac{\partial(\bar{U}\bar{r})}{\partial\bar{r}}+\frac{1}{\delta}\frac{\partial\bar{W}}{\partial\bar{z}}=0 \tag{4.1}$$

$$\bar{U}\frac{\partial\bar{V}}{\partial\bar{r}}+\frac{\bar{U}\bar{V}}{\bar{r}}+\frac{\bar{W}}{\delta}\frac{\partial\bar{V}}{\partial\bar{z}}=0 \tag{4.2}$$

$$\bar{U}\frac{\partial\bar{U}}{\partial\bar{r}}-\frac{\bar{V}^2}{\bar{r}}+\bar{W}\frac{\partial\bar{U}}{\partial\bar{z}}=-\frac{\partial\bar{P}}{\partial\bar{r}} \tag{4.3}$$

$$\bar{U}\frac{\partial\bar{W}}{\partial\bar{r}}+\frac{\bar{W}}{\delta}\frac{\partial\bar{W}}{\partial\bar{z}}=-\frac{\partial\bar{P}}{\partial\bar{z}} \tag{4.4}$$

In the next section we present an analysis that is common to all the model descriptions that follow in section 4.4 to 4.6. Of these models, two have been published and two are new models derived here for the first time.

### 4.2 Analysis

As in section 3 we assume that the three components of velocity are product of functions of $\bar{r}$ and $\bar{z}$

$$\bar{U}=u_r u_z \tag{4.5}$$

$$\bar{V}=v_r v_z \tag{4.6}$$

$$\bar{W}=w_r w_z \tag{4.7}$$

From the continuity equation (4.1) we obtain

$$\left(\frac{u_r}{\bar{r}}+\frac{\partial u_r}{\partial\bar{r}}\right)u_z+\frac{1}{\delta}w_r\frac{\partial w_z}{\partial\bar{z}}=0 \tag{4.8}$$

which leads to

$$\frac{\partial\bar{W}}{\partial\bar{z}}=w_r w_z'=-\delta\left(\frac{u_r}{\bar{r}}+u_r'\right)u_z \tag{4.9}$$

and

$$w_r=-\delta\left(\frac{u_r}{\bar{r}}+\frac{\partial u_r}{\partial\bar{r}}\right) \tag{4.10}$$

$$u_z=\frac{\partial w_z}{\partial\bar{z}} \tag{4.11}$$

From the circumferential momentum equation we obtain

$$u_r u_z\frac{\partial v_r}{\partial\bar{r}}v_z+\frac{1}{\bar{r}}u_r u_z v_r v_z+\frac{1}{\delta}w_r w_z v_r\frac{\partial v_z}{\partial\bar{z}}=0 \tag{4.12}$$

Separating the variables we obtain

$$\left(\frac{1}{v_r}\frac{\partial v_r}{\partial\bar{r}}+\frac{1}{\bar{r}}\right)\left(\frac{u_r}{\frac{u_r}{\bar{r}}+\frac{\partial u_r}{\partial\bar{r}}}\right)=\frac{w_z}{u_z}\frac{1}{v_z}\frac{\partial v_z}{\partial\bar{z}}=\gamma \tag{4.13}$$

where $\gamma$ is a constant. Writing this as separate equations in $\bar{r}$ and $\bar{z}$ we obtain.

$$\left(\frac{1}{v_r}\frac{\partial v_r}{\partial \bar{r}}+\frac{1}{\bar{r}}\right)=\gamma\frac{\left(\frac{u_r}{\bar{r}}+\frac{\partial u_r}{\partial \bar{r}}\right)}{u_r} \tag{4.14}$$

$$\frac{1}{v_z}\frac{\partial v_z}{\partial \bar{z}}=\gamma\frac{u_z}{w_z} \tag{4.15}$$

Integrating equation (4.14) for $v_r$

$$\ln(v_r)=\int\left(\gamma\frac{\left(\frac{u_r}{\bar{r}}+\frac{\partial u_r}{\partial \bar{r}}\right)}{u_r}-\frac{1}{\bar{r}}\right)d\bar{r}=\int\left(\gamma\frac{\frac{\partial u_r}{\partial \bar{r}}}{u_r}+\frac{(\gamma-1)}{\bar{r}}\right)d\bar{r} \tag{4.16}$$

$$\ln(v_r)=\ln({u_r}^{\gamma})+\ln(\bar{r}^{\gamma-1})+\ln(\kappa_1) \tag{4.17}$$

where $\kappa_1$ is a constant of integration.

$$v_r=\kappa_1\bar{r}^{\gamma-1}{u_r}^{\gamma} \tag{4.18}$$

Integrating equation (4.15) for $v_z$

$$\ln(v_z)=\gamma\int\frac{\frac{\partial w_z}{\partial \bar{z}}}{w_z}d\bar{z}=\gamma\ln(w_z)+\ln(\kappa_2) \tag{4.19}$$

where $\kappa_2$ is also a constant of integration

$$v_z=\kappa_2(w_z)^{\gamma} \tag{4.20}$$

Now consider the parameter $\gamma$. From equation (4.18) it can be seen that $\gamma$ has a minimum value of 1.0, if the velocity at the vortex centre is to remain finite. Since both radial and vertical velocities can be negative, equations (4.18) and (4.19) imply that $\gamma$ must be an integer. In the solutions that follow, we will in general assume, for the sake of simplicity, that $\gamma=1$.

Now let us consider the pressure distribution within this type of vortex. From equation (4.3) we have

$$\frac{\partial \bar{P}}{\partial \bar{r}}=-u_r\frac{\partial u_r}{\partial \bar{r}}{u_z}^2+K\bar{r}^{2\gamma-3}{u_r}^{2\gamma}(w_z)^{2\gamma}+\delta\left(\frac{u_r}{\bar{r}}+\frac{\partial u_r}{\partial \bar{r}}\right)u_r w_z\frac{\partial u_z}{\partial \bar{z}} \tag{4.21}$$

Thus the pressure will depend in quite a complicated way on the velocity functions for each of the models that follow. Note however that at $\bar{z}=0$ then, in all models $w_z=0$, and thus the second and third terms on the right hand side of the equation fall to zero. The equation thus becomes

$$\frac{\partial \bar{P}}{\partial \bar{r}}=-\frac{\partial({u_r}^2)}{\partial \bar{r}}{u_z}^2 \tag{4.22}$$

and integrating gives

$$\bar{P}=\kappa_3-{u_r}^2{u_z}^2 \tag{4.22}$$

Since $u_r$ must be zero at $\bar{r}=0$, this implies that there is no local pressure minimum on the ground beneath vortices based on the solution of the Euler equation, which is not realistic. Thus further calculations of pressure variation will not be presented in what follows, although this point will be discussed further in section 5.

### 4.3 Baker and Sterling (2017)

The model of Baker and Sterling (2017) begins with the following assumptions for $u_r$ and $u_z$.

$$u_r = -\frac{2}{\kappa_1}\frac{\bar{r}}{1+\bar{r}^2} \tag{4.23}$$

$$u_z = \frac{2.88}{\kappa_2}\frac{\bar{z}}{1+\bar{z}^2} \tag{4.24}$$

$u_r$ is zero at the centre, falls to a negative (inward) peak and then approaches zero for large radii. Similarly $u_z$ is zero at the peaks, peaks at a specific height and then falls to zero at large heights. This model, in which the radial velocity is bounded both radially and vertically, thus attempts to model near ground boundary layer in the region between the ground and the peak value. Note that these equations are somewhat different from those given in Baker and Sterling (2017) as the normalization of velocities in that paper were with the maximum radial velocity, whereas here we will use the circumferential velocity at $\bar{r} = \bar{z} = 1$ (see below). The vertical velocity then follows equations (4.10) and (4.11)

$$w_r = \frac{4\delta}{\kappa_1}\frac{1}{(1+\bar{r}^2)^2} \tag{4.25}$$

$$w_z = \frac{1.44}{\kappa_2}\ln(1+z^2) \tag{4.26}$$

This shows a peak at the vortex centre and falls to zero at large radii, although it is unbounded vertically where there is a slow (logarithmic) increase in velocity with height. The circumferential velocity is then calculated from the circumferential momentum equation, using equations (4.18) and (4.20). For $\gamma = 1$ we obtain

$$v_r = \frac{2\bar{r}}{1+\bar{r}^2} \tag{4.27}$$

$$v_z = 1.44\ \ln(1+\bar{z}^2) \tag{4.28}$$

The circumferential velocity has a maximum value of 1.0 at $\bar{r} = \bar{z} = 1$.The velocity functions are tabulated in Table 1 and, together with the profiles from the other methods outlined below, are also shown in figure 4. The unbounded functions of height for circumferential and vertical velocities for this method are very clear.

The radial velocity is maximum at $\bar{r} = 1$ and $\bar{z} = 1$, with a value of $1.44/\kappa_1\kappa_2$, and thus $S$, the ratio of the maximum circumferential velocity to maximum radial velocity is $0.69\kappa_1\kappa_2$.

This model was originally used to analyse debris flight in tornadoes, but has since been used in Baker and Sterling (2018a) to develop a wind loading calculation methodology, and in Baker and Sterling (2018b) to investigate tornado loads on trains. Both use the velocity components at $\bar{z} = 1$, and effectively only consider low-rise structures. The methodology is not appropriate for medium to high-rise structures, as the circumferential and vertical velocity profiles are unbounded with height.

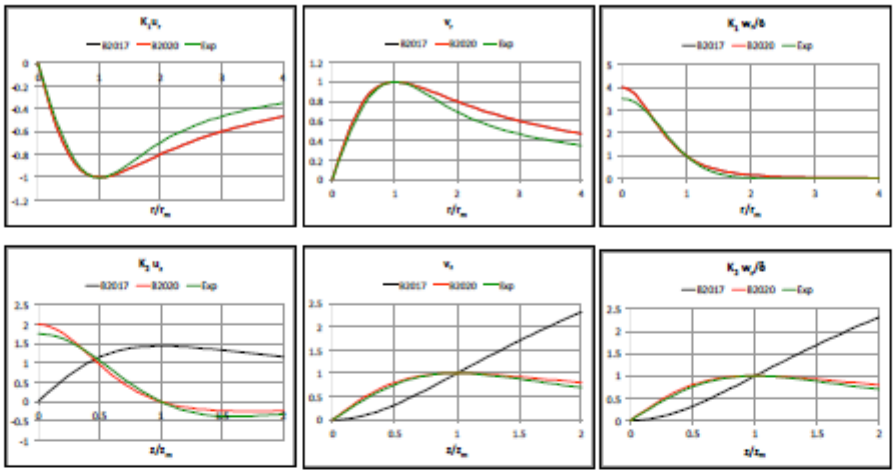

**Figure 4 The Euler methods of Baker and Sterling (2017) and Baker et al (2020) and the new Model A**

(Model A is denoted by Exp)

### 4.4 Baker and Sterling (2020)

This method begins by assuming forms for the circumferential rather than the radial velocity components

$$v_r = \frac{2\bar{r}}{1+\bar{r}^2} \tag{4.29}$$

$$v_z = \frac{2\bar{z}}{1+\bar{z}^2} \tag{4.30}$$

Note that this function has a maximum at $\bar{r} = \bar{z} = 1$. Equations (4.10), (4.11), (4.18) and (4.20) then give the following forms for $\gamma = 1$.

$$u_r = -\frac{2}{\kappa_1}\frac{\bar{r}}{1+\bar{r}^2} \tag{4.31}$$

$$u_z = \frac{2}{\kappa_2}\frac{(1-\bar{z}^2)}{(1+\bar{z}^2)^2} \tag{4.32}$$

$$w_r = \frac{4\delta}{\kappa_1}\frac{1}{(1+\bar{r}^2)^2} \tag{4.33}$$

$$w_z = \frac{2}{\kappa_2}\frac{\bar{z}}{1+\bar{z}^2} \tag{4.34}$$

The radial velocity is maximum at $\bar{r} = 1$ and $\bar{z} = 0$, with a value of $2/\kappa_1\kappa_2$, and thus $S$, the ratio of the maximum circumferential velocity to maximum radial velocity is $0.5\kappa_1\kappa_2$.

The velocity functions are tabulated in table 1 and shown in figure 4. The radial velocity variation with radius is very different from that of Baker and Sterling (2017), which was the assumption, which led to the other profiles, rather than a calculated value from assumed circumferential velocity profiles. The Baker et al (2020) profile shows a non-

zero value at $\bar{z} = 0$, falling to zero at $\bar{z} = 1$ and then taking on a slightly negative value for greater values of $\bar{z}$.

### 5.5 Model A

Model A, the first of the two new models presented here, again begins with equations that have an exponential form for the circumferential velocity components that have the correct asymptotic behavior at large values of $\bar{r}$ and $\bar{z}$.

$$v_r = \frac{1.398}{\bar{r}}\left(1 - e^{-1.256\bar{r}^2}\right) \tag{4.35}$$

$$v_z = \frac{1.398}{\bar{z}}\left(1 - e^{-1.256\bar{z}^2}\right) \tag{4.36}$$

This function has a maximum at $\bar{r} = \bar{z} = 1$. As above these result in the following expressions for the other velocity components

$$u_r = -\frac{1.398}{\kappa_1 \bar{r}}\left(1 - e^{-1.256\bar{r}^2}\right) \tag{4.37}$$

$$u_z = \frac{1.4}{\kappa_2 \bar{z}^2}\left(e^{-1.256\bar{z}^2}(1 + 2.512\bar{z}^2) - 1\right) \tag{4.38}$$

$$w_r = -\frac{3.511\delta}{\kappa_1} e^{-1.256\bar{z}^2} \tag{4.39}$$

$$w_z = \frac{1.398}{\kappa_2 \bar{z}}\left(1 - e^{-1.256\bar{z}^2}\right) \tag{4.40}$$

$\overline{U} = u_r u_z$ is maximum at $\bar{r} = 1$ and $\bar{z} = 0.48$, with a value of $0.53/\kappa_1\kappa_2$ , and thus $S$, the ratio of the maximum circumferential velocity to maximum radial velocity is $1.89\kappa_1\kappa_2$.

The velocity functions are tabulated in table 1 and shown in figure 4. These can be seen to be very similar to those of Baker et al (2020).

### 5.6 Model B

The final model presented here (new Model B) has a slightly more complex algebraic form than those just discussed. It will be seen that it allows both one cell and two cell vortices to be modeled. This form again starts with expressions for the circumferential velocity.

$$v_r = 2g\frac{f\bar{r}(f^2\bar{r}^2+\alpha)}{(1+f^2\bar{r}^2)^2} \tag{4.41}$$

$$v_z = \frac{2\bar{z}}{(1+\bar{z}^2)} \tag{4.42}$$

Clearly $v_z$ has a maximum at $\bar{z} = 1$. However the maximum of $v_r$ is a function of the parameter $\alpha$, which will be seen in what follows to be a useful means of changing the shape of the velocity profile to give both one cell and two cell forms. The parameters $f$ and $g$ are thus functions of $\alpha$ that are used to ensure the maximum of $v_r = 1$ at $\bar{r} = 1$. These functions are given by the somewhat complicated algebraic expressions

$$f = \left(\frac{3}{2}\left(1 - \alpha + \left(1 + \alpha^2 - \frac{14}{9}\alpha\right)^{1/2}\right)\right)^{1/2} \tag{4.43}$$

$$g = \frac{(1+f^2)^2}{2f(f^2+\alpha)} \tag{4.44}$$

The other velocity components then follow as before.

$$u_r = -\frac{2g}{\kappa_1}\frac{fr(f^2r^2+\alpha)}{(1+f^2r^2)^2} \tag{4.45}$$

$$u_z = \frac{2}{\kappa_2}\frac{(1-z^2)}{(1+z^2)^2} \tag{4.46}$$

$$w_r = -\frac{\delta}{\kappa_1}\left(\frac{4(f^2r^2(2-\alpha)+\alpha)}{(1+f^2r^2)^3}\right) \tag{4.47}$$

$$w_z = \frac{1}{\kappa_2}\frac{2z}{1+z^2} \tag{4.48}$$

$\overline{U} = u_r u_z$ is maximum at $\bar{r} = 1$ and $\bar{z} = 0$, with a value of $2/\kappa_1\kappa_2$, for all values of $\alpha$ and thus $S$, the ratio of the maximum circumferential velocity to maximum radial velocity is $0.5\kappa_1\kappa_2$.

The velocity functions are set out in table 1, and shown in figure 5. It can be seen that for negative values of $\alpha$ there are reversals in all three components of velocity at small radii, indicating a two-cell vortex type. The reversal in the circumferential velocity however does not seem terribly realistic. Nonetheless the model shows the transition between one cell and two cell vortex types.

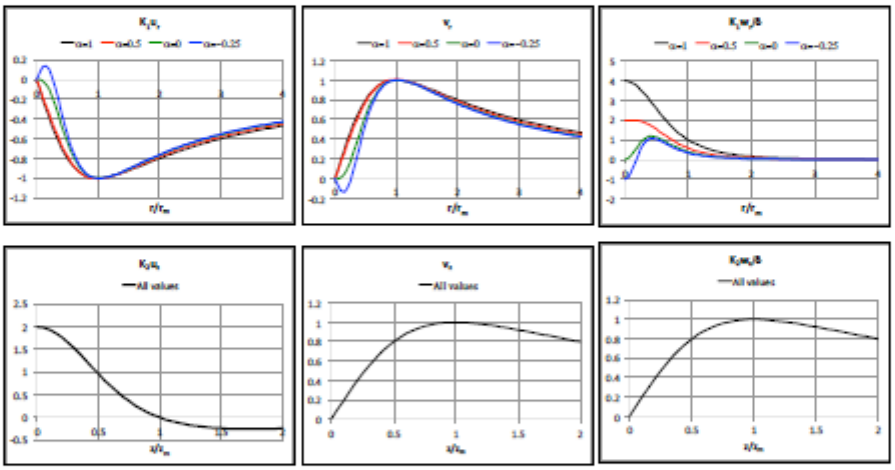

**Figure 5. The new Model B**

16

## 5. Discussion and concluding remarks

### 5.1 A common framework

In this note we have looked in particular at tornado models which are solutions of either the full Navier-Stokes or Euler equations. These models all of course begin from the same equations and the same basic assumptions - steady, incompressible and axisymmetric flow. It has been shown that all the models described rely on the fundamental assumption the specification of the velocity components as products of two functions - one of radial position, and one of vertical position. In addition the method of solution is similar for all the models, and is based on the technique of separating the variables. Thus all the models that are discussed here have an underlying commonality that is not always appreciated.

### 5.2 Solutions to the Navier Stokes equations

The Navier-Stokes models make the further assumption of quasi-cylindricality, and thus ignore the second derivative terms in the vertical direction. Also, to make analytical solutions possible, the radial velocity is assumed to be invariant in the vertical direction. In the method of separating the variables a constant $\gamma$ is introduced and all the models implicitly assume that this parameter has a value of zero. This is however not wholly necessary - a point will be discussed further below. A general solution of the equations can then be derived that relates the different velocity functions to each other, without making any particular assumptions concerning the form of these functions. This again shows the underlying commonality of the models.

The solutions then proceed by making assumptions concerning the nature of one of the velocity components – either the radial or circumferential velocity – and solving the general form for the other components. If the solutions of the various models are normalised such that the circumferential velocity is a maximum with a value of one at a normalised radius of one, then the circumferential velocities themselves are invariant with Reynolds number, whereas the magnitudes of the radial and vertical velocities are inversely proportional to Reynolds number. For all the models, the vertical velocities are not bounded and increase linearly with height. For two of the three models considered the radial velocities are also unbounded and increase with distance from the vortex centre.

### 5.3 Solutions to the Euler equations

For the models that solve the Euler equations the assumption of quasi-cylindricality is not required as this assumption only affected the viscous terms. Again the method of separation of variables is used in the solution for all models, and a constant, again referred to as $\gamma$, appears in the solution. This is not the same as the constant in the solution to the Navier-Stokes equation although it fulfills the same function. In this case this constant needs to be a positive integer for the solution to proceed, and a value of one is assumed for simplicity. A general solution can thus be obtained that relates the various velocity functions without the need to specify these functions. The solutions then proceed for each of the models by making an assumption for one velocity component and solving for the others.

Two existing and two new models are considered. If the solutions for the various models are then normalised as for the solutions to the Navier-Stokes equations, the circumferential velocity components are again invariant, whereas the radial and vertical velocities are inversely proportional to a swirl ratio type parameter – the ratio of the maximum circumferential to radial velocities. For three of the four models considered, all the velocity components are bounded in both radial and vertical directions. In allowing the velocity components to fall to zero at the ground, all the models in some way aim to represent the tornado boundary layer near the ground. The main disadvantage of the Euler equation based models is that there is no variation in pressure at ground level. This will be discussed further below.

### 5.4 One-cell and two-cell vortex forms

Most of the models considered are representations of single-cell vortices. Two however model two-cell vortices. The first of these, the Sullivan method based on the Navier-Stokes equations, is specifically described, both by its author and by others, as a two-cell solution. However a detailed examination of its derivation reveals that the approach taken by Sullivan has a much greater generality than described in his short paper, and, through variations of the parameters in the model can describe both single- and two-cell vortices and indeed the transition between them. The second of the two cell models is the newly derived Model B that again describes both types of vortex and the transition between them. Its advantage over that of Sullivan is that the velocity components are bounded in all directions. Its disadvantage is that, as well as predicting the reversal of radial and vertical velocity components, it also predicts the reversal of the circumferential velocity component, which is perhaps not wholly realistic.

A further point emerges from these considerations. It is clear from the analysis for solutions of the Euler equations, that the solutions that have been presented are just four of many possible solutions. Equation (4.18) relates the functions $v_r$ and $u_r$ by a simple algebraic relationship, and equation (4.20) similarly relates $v_z$ and $u_z$. Equations (4.10) and (4.11) relate $u_r$ and $w_r$, and $u_z$ and $w_z$ respectively through very simple differential and integral forms. Thus the only criteria needed for choosing forms for (say) the radial velocity function is that they and their integrals / differential should be suitably bounded at large radial and vertical distances, and they should be simple enough in form to allow easy differentiation and integration. This implies that a very wide range of self-consistent models could be developed that fit the Euler equations and have the correct asymptotic behavior.

### 5.5 Limitations and possible developments

There are a number of limitations to the models discussed in this note.

- All rely on the basic assumption that the velocity components are products of functions of radius and height. This carries the implication that the radius of the vortex core is invariant with height. A recent data collation by Honerkamp et al (2020) shows that this is not the case in reality, and for some tornadoes vortex radius increases quite significantly with height. Any move away from this assumption would require a completely new analytical solution procedure for both the Navier-Stokes and Euler equations.

- Some of the models have either radial or vertical velocities (or both) that are unbound at large radii or heights. This seems to be an issue with the Navier-Stokes solutions in particular, where assumptions have to be made to allow solutions to be obtained that make such unbound velocities inevitable. Solutions of the Euler equations do not necessarily suffer from this, and with a suitable choice of form of the velocity component that initiates the calculation, unbound velocities can be avoided.
- The main disadvantage of Euler methods is that they do not give a pressure variation at ground level. This is as a result of the omission of the viscous terms in the Navier-Stokes solutions. It nonetheless imposes a severe restriction on the practical utility of such methods. To cope with this in loading calculations, Baker (2018a,b) use the pressure variation at $\bar{z} = 1$, which corresponds to the height of the maximum circumferential velocity and is thus taken as the edge of the boundary layer, and the assumption made that the pressure is constant across the layer. This is a very significant, and not terribly well founded, assumption. An alternative way forward might be to model the inner flow using a Navier-Stokes solution, with a Reynolds number based on an eddy viscosity scaled on boundary layer parameters, and to model the outer flow using Euler solutions. The point of transition would give the boundary layer thickness, at which the pressure could be calculated and assumed constant between there and the ground. Because of the deficiencies in the Navier-Stokes methods this implies that the circumferential and radial velocities in the inner region would be constant and would not fall to zero at the wall. Here the formulation of equation (3.17) may be of use, if $\gamma$ is allowed to take a value other than zero, which would result in a power law variation of circumferential velocity. This would complicate the analysis however. More work is required here.

**References**


Baker C (1978) The laminar horseshoe vortex, Journal of Fluid Mechanics 95, 2, 347-367, https://doi.org/10.1017/S0022112079001506

Baker C and Sterling M (2017) Modelling wind fields and debris flight in tornadoes, Journal of Wind Engineering and Industrial Aerodynamics, 168, 312-321, https://doi.org/10.1016/j.jweia.2017.06.017

Baker C and Sterling M (2018a) A conceptual model for wind and debris impact loading of structures due to tornadoes Journal of Wind Engineering and Industrial Aerodynamics, 175, 283-291, https://doi.org/10.1016/j.jweia.2017.11.029

Baker C and Sterling M (2018b) The calculation of train stability in tornado winds, Journal of Wind Engineering and Industrial Aerodynamics, 176, 158-165, https://doi.org/10.1016/j.jweia.2018.03.022

Baker C, Sterling M, Jesson M (2020) The lodging of crops by tornadoes, accepted for publication in the Journal of Theoretical Biology

Bjerknes V (1921). On the dynamics of the circular vortex: with applications to the atmosphere and atmospheric vortex and wave motions, Kristiana (Oslo), Norway: Grøndahl & Søns Boktrykkeri.

Burgers J M (1948) A mathematical model illustrating the theory of turbulence. Advances in Applied Mechanics 1, 171–199, https://doi.org/10.1016/S0065-2156(08)70100-5

Fujita T (1978) Workbook of Tornadoes and High Winds for Engineering Applications, SMRP Research Paper No. 165, https://www.nrc.gov/docs/ML0526/ML052650410.pdf

Honerkamp R, Yan G, J Snyder J (2020) A review of the characteristics of tornadic wind fields through observations and simulations, Journal of Wind Engineering and Industrial Aerodynamics 202, 104195, https://doi.org/10.1016/j.jweia.2020.104195

Kim Y-C and Matsui M (2017) Analytical and empirical models of tornado vortices: A comparative study, Journal of Wind Engineering and Industrial Aerodynamics 171, 230-247, https://doi.org/10.1016/j.jweia.2017.10.009

Kuo H (1971) Axisymmetric flows in the boundary layer of a maintained vortex, Journal of Atmospheric Science28 (1), 20–40.

Rankine W (1858) A Manual of Applied Physics, ninth edition. Charles Griffin and Co., London

Rott N (1958) On the viscous core of a line vortex, Zeitschrift für angewandte Mathematik und Physik, 9, 543–553, https://doi.org/10.1007/BF02424773

Sullivan R (1959) A two-cell vortex solution of the Navier– Stokes equations, Journal of Aerospace Science, 46, 767–768, https://doi.org/10.2514/8.8303

G. H. Vatistas, V. Kozel & W. C. Mih (1991) A simpler model for concentrated vortices, Experiments in Fluids 11, 73–76, https://doi.org/10.1007/BF00198434

Wen Y-K (1975) Dynamic tornadic wind loads on tall buildings, Journal of the Structural Division. 101 (ST1), 169–185, https://cedb.asce.org/CEDBsearch/record.jsp?dockey=0005744

Wood V T, White L W, Willoughby H, Jorgensen D (2013) A new parametric tropical cyclone tangential wind profile model, Monthly Weather Review 141, 1884–1908.

Xu, Z. and Hangan, H (2009) An inviscid solution for modeling of tornado-like vortices, ASME Journal of Mechanics, 76, 031011, https://doi.org/10.1115/1.3063632

| | $u_r$ | $u_z$ | $v_r$ | $v_z$ | $w_r$ | $w_z$ |
|---|---|---|---|---|---|---|
| **Burgers - Rott** | $-\frac{5.02}{R}\bar{r}$ | 1 | $\frac{1.4\left(1-e^{-1.256\bar{r}^2}\right)}{\bar{r}}$ | 1 | $\delta\frac{10.04}{R}$ | $\bar{z}$ |
| **Sullivan** | $-\frac{2\beta\kappa_3\bar{r}}{R\left(1-\frac{\alpha\left(1-e^{-\kappa_3\bar{r}^2}\right)}{\beta\kappa_3\bar{r}^2}\right)}$ | 1 | $\frac{\kappa_4}{\bar{r}}\frac{H(\kappa_3\bar{r}^2)}{H(\infty)}$ | 1 | $\delta\left(\frac{4\beta\kappa_3}{s}\right)\left(1-\frac{\alpha}{\beta}e^{-\kappa_3\bar{r}^2}\right)$ | $\bar{z}$ |
| **Vasistos** | $-\frac{2^{1+1/n}(n+1)}{R\frac{(\bar{r}^{2n-1})}{1+\bar{r}^{2n}}}$ | 1 | $\frac{2^{1/n}\bar{r}}{(1+\bar{r}^{2n})^{1/n}}$ | 1 | $-\delta\frac{2^{2+1/n}n(n+1)}{\frac{R}{\bar{r}^{2n-2}}(1+\bar{r}^{2n})^2}$ | $\bar{z}$ |
| **Baker and Sterling (2017)** | $-\frac{2}{\kappa_1}\frac{\bar{r}}{(1+\bar{r}^2)}$ | $\frac{2.88}{\kappa_2}\frac{\bar{z}}{(1+\bar{z}^2)}$ | $\frac{2\bar{r}}{(1+\bar{r}^2)}$ | $1.44ln(1+\bar{z}^2)$ | $\frac{4\delta}{\kappa_1}\frac{1}{(1+\bar{r}^2)^2}$ | $\frac{1.44}{\kappa_2}ln(1+\bar{z}^2)$ |
| **Baker and Sterling (2020)** | $-\frac{2}{\kappa_1}\frac{\bar{r}}{(1+\bar{r}^2)}$ | $\frac{2}{\kappa_2}\frac{(1-\bar{z}^2)}{(1+\bar{z}^2)^2}$ | $\frac{2\bar{r}}{(1+\bar{r}^2)}$ | $\frac{2\bar{z}}{(1+\bar{z}^2)}$ | $\frac{4\delta}{\kappa_1}\frac{1}{(1+\bar{r}^2)^2}$ | $\frac{2}{\kappa_2}\frac{\bar{z}}{(1+\bar{z}^2)}$ |
| **Model A** | $-\frac{1.398}{\kappa_1\bar{r}}\left(1-e^{-1.256\bar{r}^2}\right)$ | $\frac{1.4}{\kappa_2\bar{z}^2}(e^{-1.256\bar{r}^2}(1+2.512\bar{z}^2)-1)$ | $\frac{1.398}{\bar{r}}\left(1-e^{-1.256\bar{r}^2}\right)$ | $\frac{1.398}{\bar{z}}\left(1-e^{-1.256\bar{z}^2}\right)$ | $-\frac{3.511\delta}{\kappa_1}e^{-1.256\bar{r}^2}$ | $\frac{1.398}{\kappa_2\bar{z}}\left(1-e^{-1.256\bar{z}^2}\right)$ |
| **Model B** | $-\frac{2g}{\kappa_1}\left(\frac{f\bar{r}(f^2\bar{r}^2+\alpha)}{(1+f^2\bar{r}^2)^2}\right)$ | $\frac{2}{\kappa_2}\frac{(1-\bar{z}^2)}{(1+\bar{z}^2)^2}$ | $2g\frac{f\bar{r}(f^2\bar{r}^2+\alpha)}{(1+f^2\bar{r}^2)^2}$ | $v_z=\frac{2\bar{z}}{(1+\bar{z}^2)}$ | $-\frac{\delta}{\kappa_1}\left(\frac{4(f^2\bar{r}^2(2-\alpha)+\alpha)}{(1+f^2\bar{r}^2)^3}\right)$ | $\frac{1}{\kappa_2}\left(\frac{2\bar{z}}{1+\bar{z}^2}\right)$ |

**Table 1 Model Summary**

# Appendix 3 Pollutants, pathogens and public transport - ventilation, dispersion and dose

# Pollutants, pathogens and public transport - ventilation, dispersion and dose

**Chris Baker**

**November 2021**

## 1. Introduction

The ventilation of buses and trains has come to be of some significance to the travelling public in recent years for a number of reasons. On the one hand, such vehicles can travel through highly polluted environments, such as urban highways or railway tunnels, with high levels of the oxides of nitrogen, carbon monoxide, hydrocarbons and particulate matter that can be drawn into the passenger compartments with potentially both short- and long-term health effects on passengers. On the other, the covid-19 pandemic has raised very significant concerns about the aerosol spread of pathogens within the enclosed spaces of trains and buses. There is a basic dichotomy here - to minimise the intake of external pollutants into vehicles, the intake of external air needs to be kept low, whilst to keep pathogen risk low, then high levels of air exchange between the outside environment and the internal space are desirable. This paper addresses this issue by developing a common analytical framework for pollutant and pathogen dispersion in public transport vehicles, and then utilises this framework to investigate specific scenarios, with a range of different ventilation strategies.

In the next section, we present some of the relevant background literature and identify the major pollutant pathways. Section 3 sets out a basic analytical model, that considers both externally and internally generated pollutants and pathogens to be considered in a common ventilation framework, whist making no assumptions about the ventilation mechanisms. This of itself offers some useful insights into the differences between externally and internally generated pollutants. Section 4 then considers the nature of the ventilation of public transport vehicles and identifies the important parameters that govern ventilation rate. The basic model is utilised to study a number of specific scenarios in section 5. Some broad conclusions are drawn in section 6.

## 2. Background

Since the 1980s many investigations have been carried out of pollutant levels in traffic environment - see for example the work of Hicks et al (2021) at a heavily congested roadside site in London, and that of Hickman et al (2018) and Font et al (2020) for enclosed railway stations. More recently, a number of investigators have measured pollutant levels within the passenger compartments of trains and buses, in a variety of different environments. These include metro and commuter rail systems in Czechia (Branis, 2006), South Korea (Park et al, 2008), Taiwan (Cheng et al, 2012), Greece (Maggos et al, 2016), Canada (Heong et al, 2017), Sweden (Cha et al, 2018a,b), Denmark (Anderson et al 2019a,b), the Philippines (Batutay et al, 2020) and Portugal (Buitrago et al, 2021), with measurements made on both underground and overground trains. Measurements made on urban buses are reported from China by Li et al (2017) and from India by Chaudhry and Elumalai (2020).

From these investigations the following major points emerge.

- The main concern is with pollutants that arise from diesel engines, whether in trains or buses. These include the oxides of nitrogen, carbon monoxide, a range of hydrocarbons and particulate matter over a large size range, all of which can cause respiratory problems at elevated concentrations or can be toxic at higher concentrations.
- Diesel trains have much higher levels of all pollutants than electric trains.
- Particulate matter can also be the result of brake wear or road or rail wear.
- For diesel trains, the roof mounted engine exhausts can be in close proximity to the inlets to HVAC systems, with regular plume impingement and thus pollutant can be ingested into the passenger cabin.
- Pollutant levels varied significantly with position within trains, the train consist and whether or not the locomotive was leading or trailing.
- For road vehicles in congested urban areas, the pollutants of concern can arise from all the traffic on the road, dispersed by the vehicle wakes, forming a cloud of pollutant over the highway that can again be ingested into the air conditioning systems or through open windows.
- Similarly in enclosed railway stations, concentrations of diesel pollutants can be significantly above ambient levels.
- Less directly, particulate matter from vehicles and other sources, can be deposited in road or rail environments, particularly enclosed tunnels, resuspended by vehicle movement and then ingested into passenger compartments. In such cases interior concentration of pollutants can be very high.

Pollutants can also be generated internally within vehicles. Carbon dioxide from passenger respiration, which, if allowed to build up, can cause drowsiness and headaches, or more severe symptoms. In addition, pathogens, such as flu or covid-19, can be generated within passenger compartments by infected individuals and have the potential to infect others. This latter aspect has not been extensively studied, although there is some recent CFD based work reported in Zhang et al, (2012), Wang et al (2014) and Peng et al (2020). It is now generally recognised that pathogen transmission is primarily by aerosols, with transmission by larger droplets only occurring between individuals in close proximity - see the recent review by Wang et al (2021), which shows that the evidence for transmission by surface contamination is surprisingly weak.

Finally, there is an emerging body of evidence that high levels of pollutant can increase the risk of pathogen infection. Long term exposure to particulate pollutants in particular can results in a weakened respiratory system that makes individuals more prone to infection and serious illness (Mein et al, 2020; Comunian et al, 2020, Travaglio et al, 2021). There are also indications (although not strong) that particulates in the atmosphere can act as foci for pathogens that increase the local risk of transmission (Nor et al, 2021).

## 3. Analysis

### 3.1 Formulation of concentration equation

In the analysis that follows, we consider the build-up of both pollutants or pathogens in a public transport vehicle using a unified approach based on simple conservation arguments. This approach is not novel and has been used by others (eg Miller et al, 2021), but here we aim to treat the issues in a unified way within a common framework. We assume that the vehicle is ventilated either naturally through openings, or through a number of HVAC systems. There may or may not be the facility for air recirculation and cleaning. The equation of conservation of pollutant or pathogen mass is given in words as follows

*Rate of change of mass of species inside the vehicle = inlet mass flow rate of species + mass generation rate of species within the vehicle - outlet mass flow rate of species– mass flow rate of species removed through cleaning, deposition on surfaces or decay.*

"Mass" here is defined differently for pollutants and pathogens - in the standard way as kilograms for chemical pollutants, and as quanta for pathogens. Concentrations are similarly defined in two ways - as kilograms of pollutant per kilogram of air, or as quanta of pollutant per kilogram of air.

In symbols this conservation equation can be written

$$\rho V \frac{dC}{dt} = \sum \dot{m}_i C_i + g - C \sum \dot{m}_i - \dot{m}_c C\epsilon - \rho V C\gamma - \rho V C\delta \quad (1)$$

Here $\rho$ is the density of air (kg/m³); $V$ is the internal volume of the vehicle (m³); $C$ is the internal concentration in the vehicle (kg/kg or quanta/kg); $t$ is time (h); $\dot{m}_i$ is the mass flow rate of air at ventilation inlet $i$ (kg/h); $C_i$ is the concentration of species at inlet $i$ (kg/kg or quanta/kg); $g$ is the internal generation term in (kg/h or quanta/h); $\dot{m}_c$ is the recirculated mass flow of air (kg/h); $\epsilon$ is the cleaning efficiency of the recirculation system; $\gamma$ is the rate of deposition to surfaces (1/h) and $\delta$ is the decay rate of the pollutant or pathogen (1/h) .

The mass flow rates will depend upon the type of opening and for non-airconditioned vehicles will be a function of vehicle speed. At this stage we make no specific assumptions about the nature of the ventilation system, other than it draws in air through a number of inlets and may or may not offer the facility for recirculating and cleaning a portion of that air.

We now define equivalent mass flow rates and concentrations.

$$\dot{m}_e = \sum \dot{m}_i \quad (2)$$

$$C_e = \frac{\sum \dot{m}_i C_i}{\sum \dot{m}_i} \quad (3)$$

The conservation equation becomes

$$\rho V \frac{dC}{dt} = \dot{m}_e C_e + g - \dot{m}_e C - \dot{m}_c C\epsilon - \rho V C\gamma - \rho V C\delta$$

After some manipulation this becomes

$$\frac{dC}{dt} = \alpha C_e + \frac{g}{\rho V} - (\alpha + \beta + \gamma + \delta)C$$

where $\alpha$ is the number of air changes through the vehicle ventilation system per hour and is given by

$$\alpha = \frac{\dot{m}_e}{\rho V} \quad (4)$$

and $\beta$ is the rate of recirculation of clean air per hour given by

$$\beta = \frac{\dot{m}_c \epsilon}{\rho V} \quad (5)$$

### 3.2 Solutions of concentration equations

This equation is very straightforward and applies to both pollutants and pathogens, provided the terms are appropriately defined. We now consider two cases - the concentrations from external sources (for example, external sources of the oxides of nitrogen or particulate matter); and the concentrations due to internal pollutant or pathogen generation (for example, carbon dioxide or Covid-19).

For external pollutants, the internal generation term is zero. The concentration equation then becomes

$$\frac{dC}{dt} = \alpha C_e - (\alpha + \beta + \gamma + \delta)C \quad (6)$$

This can be straightforwardly solved for internal concentrations for arbitrary time histories of external concentration and also various air recirculation strategies (such as turning HVAC systems on and off, or closing and opening windows). If $C_e$, $\alpha$, $\beta$, $\gamma$ and $\delta$ are constant and the initial concentration is zero, we have the very simple solution

$$C = \frac{\alpha C_e}{(\alpha+\beta+\gamma+\delta)}\left(1 - e^{-T(\alpha+\beta+\gamma+\delta)}\right) \quad (7)$$

where $T$ is the journey time. For large values of $T$ this becomes

$$C_\infty = \frac{\alpha C_e}{(\alpha+\beta+\gamma+\delta+\delta)} \quad (8)$$

and one can thus write

$$C = C_\infty\left(1 - e^{-T(\alpha+\beta+\gamma+\delta)}\right) \quad (9)$$

For internal pollutants, we assume that the internal source is the passenger load, and we write

$$g = Nq_o \quad (10)$$

where $N$ is the total number of passengers when pollutants such as carbon dioxide are being considered, or the number of infected passengers when pathogens are being considered. $q_o$ is the output of pollution per person in kg/h or of pathogen in quanta/h. The conservation equation becomes

$$\frac{dC}{dt} = \frac{Nq_o}{\rho V} - (\alpha + \beta + \gamma + \delta)C \quad (11)$$

Here concentrations are expressed as kg of pollutant / kg of air or quanta of pathogen / kg of air. Again, this can be readily solved numerically for variable values of $C_e$, $q_o$, $\alpha$ etc. As in the external pollutant case, it has a simple solution for $C_e$, $q_o$, $\alpha$, $\epsilon$ and $r$ are constant and an initial concentration of zero.,

$$C = \frac{Nq_o}{\rho V(\alpha+\beta+\gamma+\delta)}\left(1 - e^{-T(\alpha+\beta+\gamma+\delta)}\right) \quad (12)$$

with the solution for large time as

$$C_\infty = \frac{Nq_o}{\rho V(\alpha+\beta+\gamma+\delta)} \quad (13)$$

and again

$$C = C_\infty\left(1 - e^{-T(\alpha+\beta+\gamma+\delta)}\right) \quad (14)$$

Now let us consider the implications of the above equations. For externally or internally produced gaseous pollutants the sum $(\alpha + \beta + \gamma + \delta)$ that appears in the above analysis simplifies to $(\alpha + \beta)$ since there is no deposition and no pollutant decay. For particulate pollutants this term becomes $(\alpha + \beta + \gamma)$ whilst for pathogens all the terms are important. If there is no air recirculation with $\beta = 0$, then for gaseous pollutants the sum simply becomes equal to $\alpha$ and for particulates to $\alpha + \gamma$

At this point it is worth considering the relative magnitudes of $\alpha$, $\beta$, $\gamma$ and $\delta$. It will be shown in the next section that $\alpha$ for most ventilation mechanisms is of the order of 10/h. Jimenez and Peng gives values of $\beta$, $\gamma$ and $\delta$ for a range of ventilation systems of around 3, 0.2 and 1.6. The value for $\gamma$ is quite general and applies to PM2.5 to PM10 particles and also for pathogens, whilst the value for $\delta$ is specifically for covid-19. Thus for both gaseous and particulate pollutants with no recirculation the sum $(\alpha + \beta + \gamma + \delta)$ is dominated by $\alpha$. Now equations (7) to (9) therefore suggest that the internal concentrations of pollutants that are generated outside the vehicle, in the absence of recirculation of air within the vehicle, deposition or decay, tend in the long term to the weighted average of the concentrations at the inlets, be they HVAC systems or windows and doors. These long-term values are (2021) independent of air exchange rates. The air exchange rates do however affect the rate at which the concentrations approach the long-term values. In contrast for internally generated pollutants of pathogens, equations (12) to (14) suggest the long-term values are very dependent upon air exchange rates even when there is no recirculation, decay or deposition, and low rates of air exchange can lead to high internal concentrations. Again, the air exchange rates affect the speed with which the long-term values are reached. For both external pollutants and internally generated pollutants, the concentrations can be significantly reduced by recirculation and cleaning of the air.

In the above equations $T = 1/(\alpha + \beta + \gamma + \delta)$ is effectively the time for one air change. Equations (9) and (14) indicate that after one air change the concentration is 63% of its long-term value, and this rises to 98% after 4 air changes.

### 3.3 Dose calculations

The dose of pollutant or pathogen received can then be calculated from

$$d = q_i T \bar{C} \quad (15)$$

where $q_i$ is the rate of breathing in, $T$ is the journey time and $\bar{C}$ is the average concentration over the course of the journey.

For external pollutants the average concentration for a journey where the initial concentration is zero

$$\bar{C} = \frac{\alpha C_e}{(\alpha+\beta+\gamma+\delta)}\left(1 - \frac{\left(1-e^{-T(\alpha+\beta+\gamma+\delta)}\right)}{T(\alpha+\beta+\gamma+\delta)}\right) \quad (16)$$

which gives a dose of

$$d = \frac{q_i T \alpha C_e}{(\alpha+\beta+\gamma+\delta)}\left(1 - \frac{\left(1-e^{-T(\alpha+\beta+\gamma+\delta)}\right)}{T(\alpha+\beta+\gamma+\delta)}\right) \quad (17)$$

and a dose for a long journey of

$$d_\infty = \frac{q_i T \alpha C_e}{(\alpha+\beta+\gamma+\delta)} \quad (18)$$

For Internal pollutant or pathogen generation the average concentration is

$$\bar{C} = \frac{Nq_o}{\rho V(\alpha+\beta+\gamma+\delta)}\left(1 - \frac{\left(1-e^{-T(\alpha+\beta+\gamma+\delta)}\right)}{T(\alpha+\beta+\gamma+\delta)}\right) \quad (19)$$

and the dose becomes

$$d = \frac{q_i T N q_o}{V(\alpha+\beta+\gamma+\delta)}\left(1 - \frac{\left(1-e^{-T(\alpha+\beta+\gamma+\delta)}\right)}{T(\alpha+\beta+\gamma+\delta)}\right) \quad (20)$$

with the asymptotic dose given by

$$d_\infty = \frac{q_i T N q_o}{V(\alpha+\beta+\gamma+\delta)} \quad (21)$$

In health terms the dose of pollutant or pathogen is an important parameter. This is not well specified, with standards for pollutants usually taking the form as the average concentration allowed over a certain period (usually one or twenty-four hours). For example, the EU limits for Nitrogen Dioxide are 200 μg/m³ over a one-hour period, which must not be exceeded more than 18 times in any one year (EU, 2021). Similarly, the limit for PM10 is 50 μg/m³ over a twenty-four-hour period. Carbon Dioxide by contrast simply has a maximum concentration level specified in CDC (2021) of 5000 ppm. By contrast pathogen dose is utilised in the determination of infection probabilities, and it is that issue to which we now turn.

### 3.4 Infection probabilities

We now consider in more detail the infection probability due to pathogen dose. We follow the methodology of Jimenez and Peng (2021) but adopt a simplified analytical form that throws considerable light on the problems. Note that what follows implicitly assumes complete mixing of the pathogen across the passenger compartment, which is clearly an idealisation, and does not take into account the greatly elevated concentrations around infected individuals. We discuss how this might be allowed for in the future below.

The probability of infection with the pathogen $P$ is given by

$$P = \left(1 - \left(1 - p\left(1 - e^{-d}\right)\right)^{N-1}\right) K\,(1 - f_I)(1 - f_m\epsilon_i)(1 - f_m\epsilon_o) \quad (22)$$

Here $p$ is the population probability of infection; $K$ is a factor that allows for pathogen variants; $f_I$ is the fraction of people who are immune due to vaccination or previous infection; $f_m$ is the fraction of people wearing masks; $\epsilon_o$ is the mask efficiency for breathing out; and $\epsilon_i$ is the mask efficiency for breathing in. For small values of $d$ and $p$ this can be approximated by

$$P = dp(N-1)K\,(1 - f_I)(1 - f_m\epsilon_i)(1 - f_m\epsilon_o) \quad (23)$$

For the general case equations (15) and (26) give

$$P = q_i T\bar{C}\,p(N-1)K\,(1 - f_I)(1 - f_m\epsilon_i)(1 - f_m\epsilon_o) \quad (24)$$

For the case of zero initial concentration, we assume firstly that the number of infected passengers is one and thus equation (20) becomes

$$d = \frac{q_i T q_o}{V(\alpha+\beta+\gamma+\delta)}\left(1 - \frac{\left(1-e^{-T(\alpha+\beta+\gamma+\delta)}\right)}{T(\alpha+\beta+\gamma+\delta)}\right) \quad (25)$$

Now let

$$R = \frac{q_i}{q_{i,ref}}\frac{q_o}{q_{o,ref}} \quad (26)$$

where $q_{i,ref}$ and $q_{o,ref}$ are reference values of $q_i$ and $q_o$ for a person at rest, and not speaking. $R$ allows for the effect of exercise and intensity of speaking / singing. The equation for dose becomes

$$d = \frac{q_{i,ref} T q_{o,ref}}{V(\alpha+\beta+\gamma+\delta)}\left(1 - \frac{\left(1-e^{-T(\alpha+\beta+\gamma+\delta)}\right)}{T(\alpha+\beta+\gamma+\delta)}\right) R \qquad (27)$$

Values of $R$, calculated from the data given in Jimenez and Peng are given in table 1. There can be seen to be very large variations in this parameter depending on physical and oral activity.

Equations (23) and (27) give

$$P = \frac{q_{i,ref} T q_{o,ref}}{V(\alpha+\beta+\gamma+\delta)}\left(1 - \frac{\left(1-e^{-T(\alpha+\beta+\gamma+\delta)}\right)}{T(\alpha+\beta+\gamma+\delta)}\right) R\, p(N-1)K(1-f_I)(1-f_m\epsilon_o)(1-f_m\epsilon_i) \qquad (28)$$

For long journeys this becomes

$$P_\infty = \frac{q_{i,ref} T q_{o,ref}}{V(\alpha+\beta+\gamma+\delta)}\, R(1-f_m\epsilon_o)(1-f_m\epsilon_i)(N-1)\, pK\,(1-f_I) \qquad (29)$$

| Values of R | | Speaking or singing | | |
|---|---|---|---|---|
| | | Not speaking | Speaking quietly | Speaking loudly or singing |
| Exercise type | At rest | 1 | 5 | 30 |
| | Light intensity | 2.5 | 12.5 | 70 |
| | Moderate intensity | 14 | 70 | 420 |
| | High intensity | 70 | 350 | 2100 |

**Table 1 Values of the parameter R**

Now the simple algebraic formulation of equation (29) allows the interplay between the important parameters to be well appreciated. It shows that infection risk is linearly proportional to exposure time, prevailing infection rate, and inversely proportional to volume of the ventilated space and air exchange rate. It is also proportional to the parameter $R$, which can be seen to vary very substantially with activity and can increase the infection rate by two or three orders of magnitude. The effect of mask-wearing and population immunity is also clear. Whilst Jimenez and Peng (2021) would acknowledge the approximations made in the model, and also noting that further approximations have been made in deriving equation ((20), the expression seems to be a very useful one to aid in an understanding of the infection problem.

The main issue with this infection model is that it assumes complete mixing of the pathogen throughout the cabin space and does not take account of the elevated concentrations around an infected individual. A possible way to deal with this is set out in Appendix 1. Further work is required in this area.

## 4. Ventilation of public transport vehicles

### 4.1 Types of ventilation

Up to this point, the precise nature of vehicle ventilation has not been considered. In this section we look at the different types of ventilation that can occur in different vehicles and how the flow rates through these systems can be determined.

There are three basic types of vehicle ventilation for buses and trains - mechanical ventilation through HVAC systems, ventilation through openings such as windows and doors, and ventilation due to leakage. We consider these in turn below.

### 4.2 Mechanical ventilation

Mechanical ventilation is through the use of HVAC systems. These are usually commercially designed and supplied, to provide a specific flow rate of air into the vehicle $\dot{m}_{i,HVAC}$. Some systems include the facility for recirculating and cleaning the ingested air, through the use of filters of different types. They tend to have inlets on vehicle roofs as a rule, where the pressures are close to the undisturbed value, but depending on the precise nature of the geometry the flow rates may be to some degree affected by flow induced pressure variations. Some HVAC systems have the facility for a degree of control i.e. varying the flow rate. See Li et al (2019) for a useful overview, albeit in the context of CFD calculations. The air exchange rate from this ventilation mechanism is given by

$$a_{HVAC} = \frac{\sum \dot{m}_{i,HVAC}}{\rho V} \tag{30}$$

$\dot{m}_{i,HVAC}$ for such systems are of the order of 1200 kg/h. giving values $a_{HVAC}$ in a typical train passenger compartment of volume 200m³ with two HVAC units of 10/h. This is equivalent to a well-ventilated building but somewhat below the 20 to 30/h found in aeroplanes.

### 4.3 Ventilation through windows and doors

Passenger compartment ventilation through openings is of necessity much more variable than mechanical ventilation. The most common type of ventilation is through windows on the side of vehicles and is obviously a function of vehicle speed. To specify this mode of ventilation, we use the analysis of Straw et al (2000) who defined what they termed the shear layer ventilation due to flow across an opening. Using experimental data from a large cube in the atmospheric boundary layer, they were able to show that the mass flow rate could be approximated by $k\rho Au$ where $k$ is a constant (of the order of 0.1), $\rho$ is the density of air, $A$ is the overall opening area, and $u$ is the wind speed across the opening. Applying this to the vehicle case, we write the following expression for ventilation rate due to open windows $\dot{m}_{i,w}$ as

$$\dot{m}_{i,w} = 3600 k \rho v A_{i,w} \tag{31}$$

$A_{i,w}$ is the area of a window opening in m² and $v$ is the vehicle speed in m/s. $\dot{m}_{i,w}$ is the mass flow rate in kg/h. The ventilation rate is thus a function of vehicle speed, which matches with experience. The air exchange rate due to windows is thus

$$a_w = \frac{3600\, kv \sum A_{i,w}}{V} \tag{32}$$

This approach is confirmed to some degree by the CFD work of Li et al (2017) who looked at ventilation rates into a school bus. The linear dependence of ventilation flow rates with bus speed was clear, and, although precise opening areas are not given, values of $k$ between 0.03 and 0.15 could be calculated making reasonable assumptions. These values varied with the window opening configuration. We will use a value of 0.1 in what follows. Putting in typical values of the parameters for a train carriage of internal volume of 200m$^3$, a speed of 25m/s and four open windows of 0.05m$^2$ each gives an air exchange rate $a_w$ of around 9/h which seems reasonable. Increasing the number of open windows to ten gives a high value of $a_w$ of 22.5/h. This high value is consistent with the author's personal (and subjective) experience of travelling on such trains with many windows open. Note however that the air exchange rate can reduce to zero as the speed falls, or if the windows are closed due to low external temperatures.

Some ventilation can also take place through open doors at stations or bus stops. This is difficult to quantify, but in what follows we use expressions analogous to the ones for window ventilation.

$$\dot{m}_{i,d} = 3600 k \rho A_{i,d} u \tag{33}$$

$$a_d = \frac{3600 k u \sum A_{i,d}}{V} \tag{34}$$

Here $A_{i,d}$ is the area of one door, and $u$ is a nominal wind speed across the door opening, that will be taken as 1m/s in what follows. For the train carriage above, with two door openings of 3m$^2$ each, this gives $a_d$ as 10.8/h, although as doors will only be open for a small proportion of the time, the average value over a journey will be much less.

## 4.4 Ventilation by leakage

The third potential source of ventilation is through leakage in the vehicle envelope. This can be conveniently divided into two types. The first, applicable to buses and coaches, is ventilation driven by the relatively large pressure difference between the front and the back of the vehicle, and the second, of more relevance to sealed trains, is due to the pressure difference between the pressure along the sides of the train, and the internal pressure. We consider them in turn.

The first type of leakage can be specified by the orifice type analysis used in building ventilation. The leakage mass flow rate in kg/h is given by the following equation.

$$\dot{m}_l = 3600 \rho A_l v C_d \left(\Delta C_p\right)^{0.5} \tag{35}$$

Here $A_l$ is the leakage area, $C_d$ is the discharge coefficient and $\Delta C_p$ is the difference in the pressure coefficient between the front and rear of the vehicle. This gives an air exchange rate due to leakage of

$$\alpha_l = \frac{3600 A_l v C_d \left(\Delta C_p\right)^{0.5}}{V} \tag{36}$$

For a bus travelling at a speed of 20m/s, with a volume of 100m$^3$, a discharge coefficient of 0.6, a front to back pressure coefficient difference of 1.0, and a leakage area of 0.01m$^2$, this gives a value of $\alpha_l$ of 4.3, a not insubstantial value. This is of course very dependent upon vehicle speed.

An analysis of leakage effects along the side of trains is presented in Appendix 2. It is shown there that the leakage through the envelope results in an air exchange rate given by

$$\alpha_l = \frac{3600}{\tau}\frac{\Delta p}{r p_e} \quad (37)$$

Here $\Delta p$ is the difference between internal and external pressure (usually around 100 Pa); $\tau$ is the leakage time constant obtained from full scale tests (around 30 s); $p_e$ is the ambient pressure ($10^5$ Pa) and $r$ is the ratio of specific heats (=1.4). These figures give the very low value of $\alpha_l$ of 0.1 air changes / hour. Such values are typical, and this type of leakage ventilation will not be considered further in this analysis. See the appendix for further details.

## 5. Scenario analysis

In this section, we present the results of a simple scenario analysis that investigates the application of the above analysis for different types of vehicle with a range different ventilation systems, running through different transport environments. We consider the following vehicle and ventilation types.

- An air-conditioned diesel train, with controllable HVAC systems.
- A window and door ventilated diesel train.
- A bus ventilated by windows, doors, and externally pressure generated leakage.

Two journey environments are considered.

- For the trains, a one-hour commuter journey as shown in figure 1, beginning in an inner-city enclosed station, running through an urban area with two stations and two tunnels, and then through a rural area with three stations (figure 1).
- For buses, a one-hour commuter journey, with regular stops, through city centre, suburban and rural environments (figure 2).

Results are presented for the following scenarios.

- Scenario 1. Air-conditioned train on the rail route, with HVACs operating at full capacity throughout.
- Scenario 2. As scenario 1, but with the HVACs turned to low flow rates in tunnels and enclosed stations, where there are high levels of pollutants.
- Scenario 3. Window ventilated train on rail route with windows open throughout and doors opened at stations.
- Scenario 4. As scenario 3, but with windows closed.
- Scenario 5. Window, door and leakage ventilated bus on bus route with windows open throughout and doors opened at bus stops.
- Scenario 6. As scenario 5, but with windows closed.

Details of the different environments and scenarios are given in tables 2 and 3. Realistic, if somewhat arbitrary levels of environmental and exhaust pollutants are specified for the different environments - high concentrations in cities and enclosed railway and bus stations and lower concentrations in rural areas. The air exchange rates from different mechanisms are also specified, with the values given from the analysis of section 4, specifically using equation (32) for window ventilation, equation (34) for door ventilation an equation (36) for leakage ventilation. Note that, in any development of this methodology, more detailed models of the exhaust emissions could be used that relate concentrations at the HVAC systems and window openings to concentrations at the stack, which would allow more complex speed profiles to be investigated, with acceleration and deceleration phases.

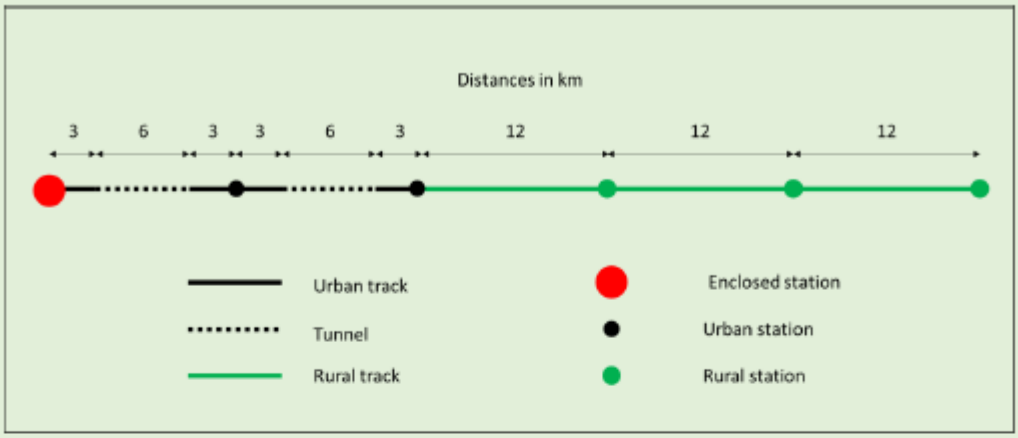


Figure 1. The rail route


Figure 2. The bus route

| | Time (min) | Concentrations | | | | | | Air exchange rates / h | | | | | |
|---|---|---|---|---|---|---|---|---|---|---|---|---|---|
| | | $NO_2$ (µg/m³) | | PM10 (µg/m³) | | $CO_2$ (ppm) | | Scenario 1 | Scenario 2 | Scenario 3 | | Scenario 4 | |
| | | Environment | Exhaust | Environment | Exhaust | Environment | Exhaust | Full HVAC | Controlled HVAC | Window | Door | Window | Door |
| Enclosed station | 0-10 | 300 | 0 | 50 | 0 | 600 | 0 | 10 | 1 | 0 | 10.8 | 0 | 10.8 |
| Urban track | 10-12 | 100 | 200 | 30 | 100 | 300 | 500 | 10 | 10 | 9 | 0 | 0 | 0 |
| Tunnel | 12-16 | 100 | 200 | 100 | 100 | 300 | 500 | 10 | 1 | 9 | 0 | 0 | 0 |
| Urban track | 16-18 | 100 | 200 | 30 | 100 | 300 | 500 | 10 | 10 | 9 | 0 | 0 | 0 |
| Urban station | 18-20 | 100 | 0 | 30 | 0 | 300 | 0 | 10 | 10 | 0 | 10.8 | 0 | 10.8 |
| Urban track | 20-22 | 100 | 200 | 30 | 100 | 300 | 500 | 10 | 10 | 9 | 0 | 0 | 0 |
| Tunnel | 22-26 | 100 | 200 | 100 | 100 | 300 | 500 | 10 | 1 | 9 | 0 | 0 | 0 |
| Urban track | 26-28 | 100 | 200 | 30 | 100 | 300 | 500 | 10 | 10 | 9 | 0 | 0 | 0 |
| Urban station | 28-30 | 100 | 0 | 30 | 0 | 300 | 0 | 10 | 10 | 0 | 10.8 | 0 | 10.8 |
| Rural track | 30-38 | 50 | 200 | 20 | 100 | 300 | 500 | 10 | 10 | 9 | 0 | 0 | 0 |
| Rural station | 38-40 | 50 | 0 | 20 | 0 | 300 | 0 | 10 | 10 | 0 | 10.8 | 0 | 10.8 |
| Rural track | 40-48 | 50 | 200 | 20 | 100 | 300 | 500 | 10 | 10 | 9 | 0 | 0 | 0 |
| Rural station | 48-50 | 50 | 0 | 20 | 0 | 300 | 0 | 10 | 10 | 0 | 10.8 | 0 | 10.8 |
| Rural track | 50-58 | 50 | 200 | 20 | 100 | 300 | 500 | 10 | 10 | 9 | 0 | 0 | 0 |
| Rural station | 58-60 | 50 | 0 | 20 | 0 | 300 | 0 | 10 | 10 | 0 | 10.8 | 0 | 10.8 |

Operating speed on open track and in tunnel 25m/s; Cabin volume 200; Number of passengers 60; Number of infected passengers 1; Carbon Dioxide emitted per passenger 0.0216$m^3$/h; Pathogen quanta emitted per infected passenger 10; Recirculation air exchange rate (Scenarios 1 and 2) 3/h; window opening area (Scenario 3) 0.2$m^2$; door opening area (Scenario 4) 6$m^2$; particulate and pathogen deposition rate 3.3/h; pathogen decay rate 1.6/h.

**Table 2. The rail journey parameters**

| | Time (min) | Concentrations | | | Air exchange rates / h | | | | | |
|---|---|---|---|---|---|---|---|---|---|---|
| | | $NO_2$ | PM10 | $CO_2$ | Scenario 5 | | | Scenario 6 | | |
| | | Environment | Environment | Environment | Window | Door | Leakage | Window | Door | Leakage |
| Bus station | 0-5 | 300 | 50 | 600 | 0 | 10.8 | 0 | 0 | 10.8 | 0 |
| City road | 5-9 | 200 | 40 | 500 | 7.2 | 0 | 2.16 | 0 | 0 | 2.16 |
| City bus stop | 9-10 | 200 | 40 | 500 | 0 | 10.8 | 0 | 0 | 10.8 | 0 |
| City road | 10-14 | 200 | 40 | 500 | 7.2 | 0 | 2.16 | 0 | 0 | 2.16 |
| City bus stop | 14-15 | 200 | 40 | 500 | 0 | 10.8 | 0 | 0 | 10.8 | 0 |
| City road | 15-19 | 200 | 40 | 500 | 7.2 | 0 | 2.16 | 0 | 0 | 2.16 |
| City bus stop | 19-20 | 200 | 40 | 500 | 0 | 10.8 | 0 | 0 | 10.8 | 0 |
| Suburban road | 20-24 | 100 | 30 | 300 | 10.8 | 0 | 3.24 | 0 | 0 | 3.24 |
| Suburban bus stop | 24-25 | 100 | 30 | 300 | 0 | 10.8 | 0 | 0 | 10.8 | 0 |
| Suburban road | 25-29 | 100 | 30 | 300 | 10.8 | 0 | 3.24 | 0 | 0 | 3.24 |
| Suburban bus stop | 29-30 | 100 | 30 | 300 | 0 | 10.8 | 0 | 0 | 10.8 | 0 |
| Suburban road | 30-34 | 100 | 30 | 300 | 10.8 | 0 | 3.24 | 0 | 0 | 3.24 |
| Suburban bus stop | 34-35 | 100 | 30 | 300 | 0 | 10.8 | 0 | 0 | 10.8 | 0 |
| Suburban road | 35-39 | 100 | 30 | 300 | 10.8 | 0 | 3.24 | 0 | 0 | 3.24 |
| Suburban bus stop | 39-40 | 100 | 30 | 300 | 0 | 10.8 | 0 | 0 | 10.8 | 0 |
| Rural road | 40-44 | 50 | 20 | 300 | 14.4 | 0 | 4.32 | 0 | 0 | 4.32 |
| Rural bus stop | 44-45 | 50 | 20 | 300 | 0 | 10.8 | 0 | 0 | 10.8 | 0 |
| Rural road | 45-49 | 50 | 20 | 300 | 14.4 | 0 | 4.32 | 0 | 0 | 4.32 |
| Rural bus stop | 49-50 | 50 | 20 | 300 | 0 | 10.8 | 0 | 0 | 10.8 | 0 |
| Rural road | 50-54 | 50 | 20 | 300 | 14.4 | 0 | 4.32 | 0 | 0 | 4.32 |
| Rural bus stop | 54-55 | 50 | 20 | 300 | 0 | 10.8 | 0 | 0 | 10.8 | 0 |
| Rural road | 55-59 | 50 | 20 | 300 | 14.4 | 0 | 4.32 | 0 | 0 | 4.32 |
| Rural bus stop | 59-60 | 50 | 20 | 300 | 0 | 10.8 | 0 | 0 | 10.8 | 0 |

Operating speed on rural roads, suburban roads and city roads 20m/s, 15m/s and 10m/s respectively; Cabin volume 100 $m^3$; Number of passengers 30; Number of infected passengers 1; Carbon Dioxide emitted per passenger 0.0216$m^3$/h; Pathogen quanta emitted per infected passenger 10; Recirculation air exchange rate (Scenarios 1 and 2) 3/h; window opening area (Scenario 5) 0.2$m^2$; door opening area (Scenario 4) 3$m^2$; leakage area 0.1$m^2$; particulate and pathogen deposition rate 3.3/h; pathogen decay rate 1.6/h.

Table 3. Bus journey parameters

The results of the analysis are shown in figures 3 and 4 below for the train and bus scenarios respectively. Both figures show time histories of concentrations for NO2, PM2.5, CO2 and Covid-19, together with the external concentrations of the pollutants.

For Scenario 1, with constant air conditioning, all species tend to an equilibrium value that is the external value in the case of NO2 and PM2.5, slightly higher than the external value for CO2 due to the internal generation and a value fixed by the emission rate for Covid 19.

For Scenario 2, with low levels of ventilation in the enclosed station and in the tunnels, NO2 and PM2.5 values are lower than scenario 1 at the start of the journey where the lower ventilation rates are used, but CO2 and Covd-19 concentrations are considerably elevated. When the ventilation rates are increased in the second half of the journey all concentrations approach those of Scenario 1.

The concentration values for scenario 3, with open windows, match those of Scenario 1 quite closely as the specified ventilation rates are similar. However, for Scenario 4, with windows shut and only door ventilation at stations, such as might be the case in inclement weather, the situation is very different, with steadily falling levels of NO2 and PM2.5, but significantly higher values of CO2 and Covid-19. The latter clearly show the effect of door openings at stations.

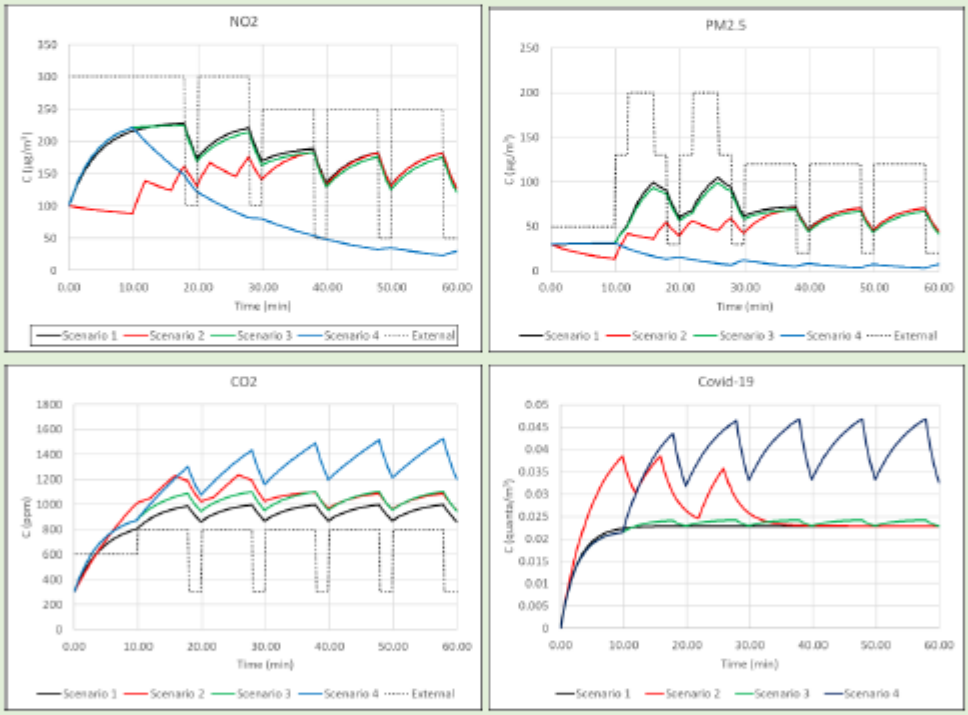


**Figure 3. Train scenarios 1 to 4**

Now consider the bus scenarios in figure 4. For both Scenario 5 with open windows and doors, and Scenario 6 with closed windows and open doors, the NO2 and PM2.5 values tend towards the ambient concentrations and thus fall throughout the journey as the air becomes cleaner in rural areas. The internally generated CO2 and Covid-19 concentrations for CO2 and Covid-19 are however very much higher for Scenario 6 than for Scenario 5.

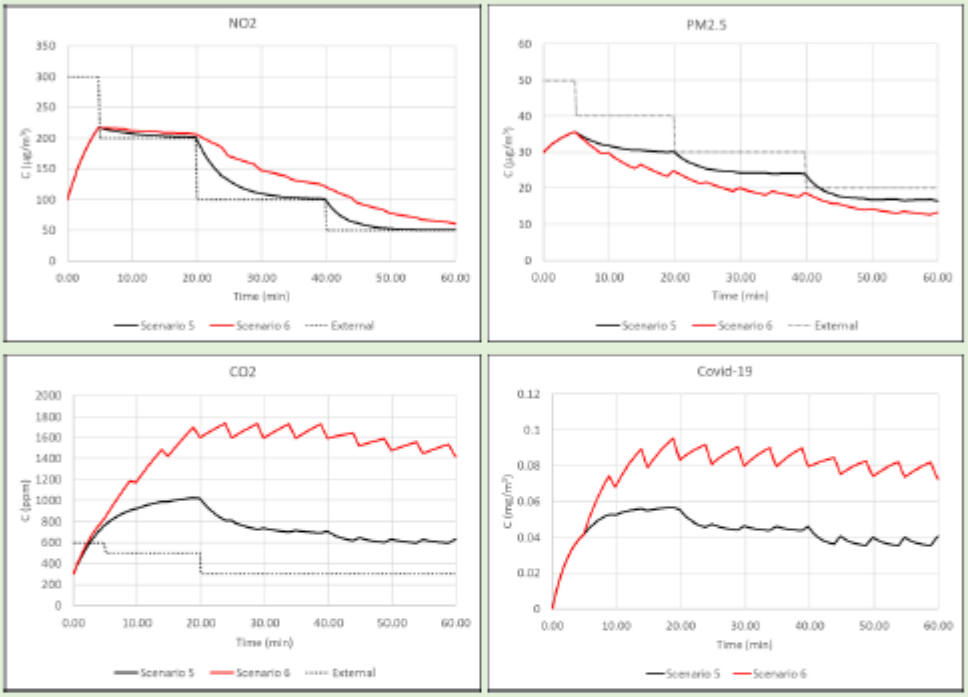


**Figure 4. Bus scenarios 5 and 6**

The average values of concentration for all the scenarios is given in Table 4. The dose and, for Covid-19, the infection probability, are proportional to these concentrations. For NO2 and PM10 the average concentrations reflect the average external concentrations, and, with the exception of Scenario 4, where there is low air exchange with the external environment for part of the journey. The average concentrations for CO2 and Covid-19 for the less ventilated Scenarios 4 and 6 are significantly higher than the other. For Covid-19, the effect of closing windows on window ventilated trains and buses raises the concentrations, and thus the infection probabilities, by 60% and 76% respectively.

| | NO2 (μg/m³) | PM2.5 (μg/m³) | CO2 (ppm) | Covid-19 (quanta/m³) |
|---|---|---|---|---|
| Scenario 1 | 183 | 63 | 890 | 0.022 |
| Scenario 2 | 145 | 49 | 1015 | 0.026 |
| Scenario 3 | 179 | 60 | 978 | 0.022 |
| Scenario 4 | 96 | 13 | 1193 | 0.036 |
| Scenario 5 | 125 | 25 | 745 | 0.043 |
| Scenario 6 | 146 | 21 | 1452 | 0.076 |

**Table 4. Average concentrations**

## 6. Closing comments

The major strength of the methodology described above is its ability, in a simple and straightforward way, to model pollutant and pathogen concentrations for complete journeys, and to investigate the efficacy of various operational and design changes on these concentrations. It could thus be used, for example, to develop HVAC operational strategies for a range of different journey types. That being said, there is much more that needs to be done - for example linking the methodology with calculations of exhaust dispersion around vehicles, with models of particulate resuspension or with models of wind speed and direction variability. It has also been pointed out above that the main limitation of the infection model is the assumption of complete mixing, and a possible way forward has been proposed that might overcome this. Nonetheless the model has the potential to be of some utility to public transport operators in their consideration of pollutant and pathogen concentrations and dispersion within their vehicles.

## References


Anderson, M. H. G., Johannesson, S., Fonseca, A. S., Clausen, P. A., Saber, A. T., Roursgaard, M., Loeschner, K., Koponen, I. K., Loft, S. and VogeL, U. 2019. Exposure to air pollution inside electric and diesel-powered passenger trains. Environmental science and technology, 53, 4579-4587. https://doi.org/10.1021/acs.est.8b06980

Andersen, M.H.G., Frederiksen, M., Saber, A.T., Wils, R.S., Fonseca, A.S., Koponen, I.K., Johannesson, S., Roursgaard, M., Loft, S., Møller, P., Vogel, U., 2019. Health effects of exposure to diesel exhaust in diesel-powered trains. Part. Fibre Toxicol. 16, 1–14. https://doi.org/10.1186/s12989-019-0306-4

J. T. G Batutay, Cabanban, H. S. Serate, F P. S. Quito J. D. and Umali R. D. 2020 Quantitative and Qualitative Analysis of Indoor Air Quality inside the MRT 3 Train Cabins, Proceedings of the 5th NA International Conference on Industrial Engineering and Operations Management, Detroit, Michigan, USA, http://www.ieomsociety.org/detroit2020/papers/29.pdf

Braniš M, m. 2006. the contribution of ambient sources to particulate pollution in spaces and trains of the Prague underground transport system. Atmospheric Environment, 40, 348-356. https://doi.org/10.1016/j.atmosenv.2005.09.060

Buitrago, N., Savdie, J., Almeida, S. and Verde, S. C. 2021. Factors affecting the exposure to physicochemical and microbiological pollutants in vehicle cabins while commuting in Lisbon. Environmental Pollution, 270, 116062. https://doi.org/10.1016/j.envpol.2020.116062

CDC, 2021 https://www.cdc.gov/niosh/idlh/124389.html

Cha, Y., Abbasi, S. and Olofsson, U. 2018a. Indoor and outdoor measurement of airborne particulates on a commuter train running partly in tunnels. Proceedings of the Institution of Mechanical Engineers, Part F: Journal of Rail and Rapid Transit, 232, 3-13. https://doi.org/10.1177/0954409716642492

Cha, Y., Tu, M., Elmgren, M., Silvergren, S. andOlofsson, U. 2018b. Factors affecting the exposure of passengers, service staff and train drivers inside trains to airborne particles. Environmental research, 166, 16-24. https://doi.org/10.1016/j.envres.2018.05.026

Chaudhry S K, Elumalai S P, 2020, The influence of school bus ventilation scenarios over in-cabin PM number concentration and air exchange rates, Atmospheric Pollution Research, 11, 8, 1396-1407, ISSN 1309-1042, https://doi.org/10.1016/j.apr.2020.05.021

Cheng, Y.-H., Liu, Z.-S. and Yan, J.-W. 2012. Comparisons of PM10, PM2. 5, particle number, and CO2 levels inside metro trains between traveling in underground tunnels and on elevated tracks. Aerosol and Air Quality Research, 12, 879-891. https://doi.org/10.4209/aaqr.2012.05.0127

Comunian S, Dario Dongo D, Milani C, Paola Palestini P, 2020, Air Pollution and COVID-19: The Role of Particulate Matter in the Spread and Increase of COVID-19's Morbidity and Mortality, International Journal of Environmental Research for Public Health, 17, 12, 4487, https://doi.org/10.3390/ijerph17124487

EU, 2021 https://ec.europa.eu/environment/air/quality/standards.htm

Font A, Tremper A, Lin C, Priestman M, Marsh D, Woods M, Heal M, Green D, 2020, Air quality in enclosed railway stations: Quantifying the impact of diesel trains through deployment of multi-site measurement and random forest modelling, Environmental Pollution, 262, 114284, ISSN 0269-7491, https://doi.org/10.1016/j.envpol.2020.114284

Hickman A, Baker C, Cai X, Delgado-Saborit J, Thornes J, 2018, Air Quality Evaluation at Birmingham New Street Railway Station, Proceedings of the Institution of Mechanical Engineers, Part F: Journal of Rail and Rapid Transit, http://dx.doi.org/10.1177/0954409717752180

Hicks W, Beevers S, Tremper A, Stewart G, Priestman M, Kelly F, Lanoisellé M, Lowry D, Green Det al., 2021, Quantification of non-exhaust particulate matter traffic emissions and the impact of COVID-19 lockdown at London Marylebone Road, Atmosphere, 12, 1-19, ISSN: 2073-4433, https://doi.org/10.3390/atmos12020190

Jeong, C.-H., Traub, A. and Evans, G. J. 2017. Exposure to ultrafine particles and black carbon in diesel-powered commuter trains. Atmospheric Environment, 155, 46-52. https://doi.org/10.1016/j.atmosenv.2017.02.015

Jimenez J, Peng Z 2021, COVID-19 Aerosol Transmission Estimator, https://tinyurl.com/covid-estimator

Li F, Lee E S, Zhou B, Liu J, Zhu Y, 2017, Effects of the window openings on the micro-environmental condition in a school bus, Atmospheric Environment, 167, 434-443, ISSN 1352-2310, https://doi.org/10.1016/j.atmosenv.2017.08.053

Li X, Wu F, Tao Y, Yang M, Newman R, Vainchtein D, 2019 Numerical study of the air flow through an air-conditioning unit on high-speed trains, Journal of Wind Engineering and Industrial Aerodynamics, 187, 26-35, https://doi.org/10.1016/j.jweia.2019.01.015

Maggos, T., Saraga, D., Bairachtarl, K., Tzagkaroulaki, I., Pateraki, S., Vasilakos, C., Makarounis, C., Stavdaris, A., Danias, G. & Anagnostopoulos, G. 2016. Air quality assessment in passenger trains: the impact of smokestack emissions. Air Quality, Atmosphere and Health, 9, 391-401. https://doi.org/10.1007/s11869-015-0348-1

Mein S A, Annesi-Maesano I, Rice M B, 2020, COVID-19 Pandemic: A Wake-Up Call for Clean Air, Annals of the American Thoracic Society, 18, 9 https://doi.org/10.1513/AnnalsATS.202012-1542VP PubMed: 33821776

Miller S L, Nazaroff W W, Jimenez J L, Boerstra A, Buonanno G, Dancer S J, Kurnitski J, Marr L C, Morawska L, Noakes C, 2021, Transmission of SARS-CoV-2 by inhalation of respiratory aerosol in the Skagit Valley Chorale superspreading event, Indoor Air, 31, 314–323, https://doi.org/10.1111/ina.12751

Nor, N.S.M., Yip, C.W., Ibrahim, N. et al, 2021, Particulate matter (PM2.5) as a potential SARS-CoV-2 carrier. Science Report 11, 2508 https://doi.org/10.1038/s41598-021-81935-9

Park, D.-U. and Ha, K.-C. 2008. Characteristics of PM10, PM2. 5, CO2 and CO monitored in interiors and platforms of subway train in Seoul, Korea. Environment International, 34, 629-634. https://doi.org/10.1016/j.envint.2007.12.007

Peng S, Chen Q, Liu E, 2020 The role of computational fluid dynamics tools on investigation of pathogen transmission: Prevention and control, Science of The Total Environment, 746, 142090, ISSN 0048-9697, https://doi.org/10.1016/j.scitotenv.2020.142090

Travaglio M, Yu Y, Popovic R, Selley L, Leal N S, Martins L M, 2021, Links between air pollution and COVID-19 in England, Environmental Pollution, 268, A, 115859, ISSN 0269-7491, https://doi.org/10.1016/j.envpol.2020.115859

Straw M, Baker C, Robertson A 2000, Experimental measurements and computations of the wind induced ventilation of a cubic structure, Journal of Wind Engineering and Industrial Aerodynamics 88, 213-230, http://dx.doi.org/10.1016/S0167-6105(00)00050-7

Wang C, Prathe K, Sznitman, Jimenez J, Lakdawala S, Tufekci Z, Marr L, 2021, Airborne transmission of respiratory viruses, Science, 373, 6558, https://doi.org/10.1126/science.abd9149

Wang H, Lin M, Chen Y, 2014, Performance evaluation of air distribution systems in three different China railway high-speed train cabins using numerical simulation, Building Simulation, 7, 6, 629-638, https://doi.org/10.1007/s12273-014-0168-5

Zhang, L. and Li, Y. 2012. Dispersion of coughed droplets in a fully occupied high-speed rail cabin. Building and Environment, 47, 58-66. https://doi.org/10.1016/j.buildenv.2011.03.015

## Appendix 1. A possible method for allowing for non-spatially uniform passenger cabin concentrations

The analytical method in the main text gives the approximate probability of an infection occurring amongst *N* passengers, where one is infected, assumed complete mixing of the pathogen in the cabin (equation (24)). In this short appendix we propose a way in which spatially uneven concentrations of pathogen could be allowed for.

If we assume that there are just two passengers where one is infected, we obtain from equation (24) the following for the probability of a passenger in seat *i* being infected by a passenger in seat *j*.

$$P_{i,j} = q_i T \bar{C}_{i,j}\, p\, K\, (1 - f_I)(1 - f_m \epsilon_i)(1 - f_m \epsilon_o)$$

Here $\bar{C}_{i,j}$ is the time average concentration of pathogen in seat *i* due to an infected passenger in seat *j*. The total infection probability for *N* passengers is obtained by finding the average probability for all possible non-infected passenger and infected passenger positions ($s$) and multiplying by $(N-1)$.

$$P = (N-1)\frac{(\sum_{i=1 to\, s, j=1\, to\, s} P_{i,j})}{s^2}$$

This gives

$$P = q_i T\, \frac{(\sum_{i=1 to\, s, j=1\, to\, s} \bar{C}_{i,j})}{s^2}\, p(N-1)K\, (1 - f_I)(1 - f_m \epsilon_i)(1 - f_m \epsilon_o)$$

We define a factor *F*

$$F = \frac{\sum_{i=1 to\, s, j=1\, to\, s} \bar{C}_{i,j}}{s^2 \bar{C}}$$

The overall infection probability thus becomes

$$P = q_i T\, F\, \bar{C}\, p(N-1)K\, (1 - f_I)(1 - f_m \epsilon_i)(1 - f_m \epsilon_o)$$

This is of course identical to equation (24) with the addition of the parameter $F$. In principle, this parameter could be found by a CFD calculation of the internal flow in a specific vehicle and tracking the concentration of (say) carbon dioxide from each person throughout the cabin to find the resulting concentration at every other passenger position, to give the function $\bar{C}_{i,j}$ and thus $F$. $\bar{C}_{i,j}$ can be expected to be well above unity when the seats *i* and *j* are close, and well below unity for all other cases. Whether or not it will be above or below 1.0 will depend upon the vehicle, the seating arrangement etc. Thus, a CFD calculation of the internal flow within a vehicle could be used to calibrate the simple model outlined here for predicting infection risk during specific journeys, with specific ventilation strategies and searing arrangements.

## Appendix 2. Leakage through the vehicle envelope

The leakage into a train cabin can be modelled in one of two ways - either as a large number of small pipes, or as a number of orifices. The basics of the two methods are shown in table A2 below. They begin in row 1 with the conservation of mass where the leakage mass flow rate is equal to the rate of change of internal mass and specified by either the pipe flow energy loss equation of the orifice discharge equation. Here $\rho$ is the external air density, $A$ is the total leakage area, $w$ is the leakage velocity, $V$ is the cabin volume, $\rho_i$ is the internal density, $d_1$ is the leakage pipe diameter, $l_1$ is the leakage pipe length, $f$ is the Darcy friction factor, $C$ is the orifice coefficient and $\Delta p$ is the difference between the internal and external pressure $(p_i - p_e)$. Assumptions are then made for the Darcy friction factor and orifice coefficient (row 2). Both are given in their low Reynolds number form. Here $k_1$ and $k_2$ are constants, $\mu$ is the dynamic viscosity of air and $d_2$ is the leakage orifice diameter. The adiabatic gas law is then used to relate the rate of change of internal pressure to that of internal density (row 3). Here $r$ is the ratio of specific heats. The equations in rows 1 to 3 are then use to derive a relationship between the leakage velocity and the pressure difference (row 4) and between the rate of change of internal pressure and the pressure difference (row 5). Leakage time constants are then defined in row 6, and these are then used to rewrite the leakage velocity and pressure rate of change equations in much simpler form in rows 7 and 8. Written in this form the two methods are actually equivalent. The pressure rate of change equation in row 8 is the form used in calculating train leakage from pressure decay in full scale tests, where the internal pressure is raised to a high value and then allowed to decay. In these experiments the time constant $\tau$ is measured. For sealed trains this parameter has values of around 20 to 60 seconds. Finally in row 9 the expression for air exchange rate is given, which is again identical for both methods. Substituting typical values for $\tau$ = 30 s (=0.0083 h); $\Delta p$ = 100 Pa; $p_e$ = $10^5$ Pa and $\gamma$ =1.4 gives a value of air changes per hour of less than 0.1. Higher values of $\Delta p$ are possible when trains experience pressure transients passing through tunnels (perhaps as high as 2000 Pa, but these will be very transitory and the briefly increased air exchange rates will not greatly contribute to cabin ventilation. The use of such formulae in the calculation of internal pressures as trains pass through tunnels is however important when passenger aural comfort is being considered.

| | Pipe model | Orifice model |
|---|---|---|
| 1. Conservation of mass for internal flow | $\rho A w = V\frac{d\rho_i}{dt} = -A\left(\frac{d_1}{f l_1}\right)^{0.5}(2\rho\Delta p)^{0.5}$ | $\rho A w = V\frac{d\rho_i}{dt} = -AC(2\rho\Delta p)^{0.5}$ |
| 2. Friction factors | $f = \frac{k_1\mu}{\rho w d_1}$ | $C = k_2\left(\frac{\rho w d_2}{\mu}\right)^{0.5}$ |
| 3. Adiabatic gas law | $\frac{dp_i}{dt} = rp_e\frac{d\rho_i}{dt}$ | |
| 4. Leakage velocity and pressure difference | $w = \frac{2{d_1}^2}{l_1 k_1 \mu}\Delta p$ | $w = \frac{2 d_2 {k_2}^2}{\mu}\Delta p$ |
| 5. Leakage pressure rate of change and pressure difference | $\frac{dp_i}{dt} = -\frac{2A{d_1}^2 rp_e}{l_1 k_1 \mu V}\Delta p$ | $\frac{dp_i}{dt} = -\frac{2A d_2 {k_2}^2 rp_e}{\mu V}\Delta p$ |
| 6. Leakage time constant | $\tau = \frac{l_1 k_1 \mu V}{2A{d_1}^2 rp_e}$ | $\tau = \frac{\mu V}{2A d_2 {k_2}^2 rp_e}$ |
| 7. Leakage velocity and pressure difference | $w = \frac{V}{A rp_e}\frac{\Delta p}{\tau}$ | |
| 8. Leakage pressure rate of change and pressure difference | $\frac{dp_i}{dt} = -\frac{\Delta p}{\tau}$ | |
| 9. Air changes per hour | $a = \frac{1}{\tau}\frac{\Delta p}{rp_e} = \frac{Aw}{V}$ | |

Table A2. Leakage calculations